12-2021

Evapotranspiration in Mid-South Rice Production

Colby Wade Reavis
University of Arkansas, Fayetteville

Evapotranspiration in Mid-South Rice Production

A dissertation submitted in partial fulfillment
of the requirements for the degree of
Doctor of Philosophy in Engineering with a concentration in Biological Engineering

by

Colby W. Reavis
University of Arkansas
Bachelor of Science in Biological Engineering, 2014
University of Arkansas
Master of Science in Biological Engineering, 2017

December 2021
University of Arkansas

This dissertation is approved for recommendation to the Graduate Council.

_____
Benjamin R.K. Runkle, Ph.D.
Committee Chair

_____   _____
Brian E. Haggard, Ph.D.   Michele L. Reba, Ph.D.
Committee Member   Committee Member

_____
Kusum Naithani, Ph.D.
Committee Member

Abstract

Rice provides much needed sustenance to a large portion of the global population, particularly in the developing world. With stress placed on food production systems under the reality of climate change and an increasing global population, rice production systems require solutions to a number of issues, including a limited water supply. As producers explore new strategies for conserving local water resources to continue to maintain yields, new irrigation strategies and technologies are being developed and validated for use at commercial production scales. Alternate wetting and drying (AWD) is an irrigation practice that provides water savings through the capture of rainfall during periodic drying events during the growing season. The AWD practice also has relevance as a climate change mitigation measure as the periodic drying disrupts and reduces methane production commonly associated with continuously flooded rice. With drying introduced during the growing season, there is potential for AWD to cause drought stress that is harmful to the plant and may reduce yields. To validate AWD as a safe practice, the following work is focused on estimating and characterizing canopy water use as evapotranspiration (ET). In each chapter, ET is presented as a means to understand how drying may affect canopy water use. Furthermore, ET also has operational value in that accurate estimates of ET can be used to better inform irrigation management decisions for producers. To that end, we also explore ET estimation methods of varying complexity that can be used to assess the impacts of drying while also providing accurate estimates of ET throughout the growing season. Ultimately, our work provided validation for AWD as a safe irrigation practice that can be applied at the commercial scale.

Dedication

      I dedicate this dissertation to my late grandfather, Carroll Craig, who instilled the curiosity and passion I exercise daily. He provided my first exposure to agriculture while working on the farm, and he made sure I always had the opportunity to learn something new when we were together. I hope to continue his legacy as an individual who pursues life and opportunity while exercising compassion and care for those around me.

List of published works

Chapter One

Reavis, C.W., Suvočarev, K., Reba, M.L., Runkle, B.R.K., 2021. Impacts of alternate wetting and drying and delayed flood rice irrigation on growing season evapotranspiration. Journal of Hydrology 596, 126080. https://doi.org/10.1016/j.jhydrol.2021.126080

Table of Contents

Introduction

Rice is a staple food for a large portion of the global population and plays a major role in the economics of the developing world (Maclean et al., 2013). Given the continued aspects of climate change, rice production faces several challenges in the form of increasing temperatures, increasing demand to feed a growing population, and limited water resources to support elevated production (Ahmed and Ahmad, 2017; Boazar et al., 2020; Ye et al., 2015). In order to maintain and promote the sustainable production of rice globally, solutions to these challenges will likely require combinations of both scientific innovation as well as adaptation of current growing practices (Chhetri et al., 2012; Foley et al., 2011; Jovanovic et al., 2020; Spangenberg et al., 2018). To reduce water demand associated with growing rice, alternative irrigation practices have been proposed that can improve the irrigation efficiency and potentially reduce the amount of water applied during the growing season (Horst et al., 2005; Massey et al., 2018; Massey et al., 2017; Wang et al., 2020; Zhuang et al., 2019). Alternate wetting and drying (AWD) is an irrigation practice that introduces periodic drying instead of maintaining a constant flood throughout the growing season to increase water savings while maintaining yields (Ishfaq et al., 2020; Yao et al., 2012). The drying events provide water savings through potential rainfall capture, which offsets the amount of pumping required to maintain inundation (Henry et al., 2013). Current research has indicated that AWD can reduce irrigation water use by up to 20% (Carrijo et al., 2017; Lampayan et al., 2015). Additional benefits of AWD include reduced methane emissions normally associated with rice, which aid in curbing the effects of climate change (Feng et al., 2021; Liao et al., 2020). One of the primary challenges with AWD is the potential for drought stress introduced by allowing the field to dry while rice is growing, which

could result in decreased yields and lower quality grain at harvest (Graham-Acquaah et al., 2019; Norton et al., 2017).

The impacts of stress can be reflected in ET and primary production, where drought stress can result in decreased production and inefficient use of water (Shekhar et al., 2020). Accurate estimates of primary production and canopy water use are then needed to observe the impacts of drying at the canopy scale (Hsiao et al., 2007; Liu et al., 2009). Canopy water use and production are reflected in evapotranspiration (ET) and photosynthesis, which can both be measured or modeled using advanced instrumentation and measurements of the local microclimate. Eddy covariance (EC) is a technique which uses advanced instrumentation to directly measure water and carbon dioxide fluxes at the canopy scale. The carbon dioxide fluxes can be partitioned further into ecosystem respiration (R_{eco}) and gross primary production (GPP), where GPP is the amount of carbon fixed during photosynthesis. The water fluxes can also be partitioned in contributing portions of transpiration (T) and evaporation (E), where transpiration represents plant mediated water use that is tied to photosynthetic activity. When formulating representations of canopy water use, ecosystem water use efficiency (eWUE) is the most common and represents the ratio of GPP to ET (Ito and Inatomi, 2012). In addition to eWUE, canopy water use can also be represented as the ratio of GPP to T as both fluxes share common pathways that are mediated by the plant (Molden et al., 2010; Tanner and Sinclair, 1983). Understanding how GPP, ET, and T change during drying and throughout the growing season is beneficial when evaluating AWD as a suitable alternative to conventional flooded irrigation. In addition to understanding how different practices affect canopy water use, ET has operational value for producers when deciding how much water needs to be applied during irrigation events (Earl D. Vories and Phil L. Tacker, 2006; Martin et al., 1990; Vories et al., 2017).

Given the importance of ET in irrigation planning and understanding canopy water use, there is a growing number of methods and applications used to estimate ET (Amatya et al., 2016; Subedi and Chávez, 2015). Many models use measured microclimactic variables in empirical or mechanistic frameworks to determine ET across a given surface, occasionally including specific parameters for a specific crop (Allen, 2000; Drexler et al., 2004; Subedi and Chávez, 2015; Zhang et al., 2014). In addition to localized models, developments in remote sensing have made it possible to estimate both ET and GPP across a greater area using satellite observations, which reduces the need and cost for widely distributed instrumentation (Balch et al., 1989; Carlson et al., 1995; Chen et al., 2014; Courault et al., 2005; Jiang and Ryu, 2016; Ryu et al., 2012). The estimates of GPP and ET can be used in similar fashion to models driven by field scale data when estimating canopy water use and understanding water use efficiency dynamics and responses to disturbances such as drought (Huang et al., 2018; Jiang et al., 2020; Zhao et al., 2020). Additionally, some products estimate ET use at fine spatial scales (~70 m), meaning the estimates can be used to inform management decisions during the growing season (Melton et al., 2012; Savoca et al., 2013; Senay, 2018). In the case of products such as ECOSTRESS, ET can also be partitioned into contributing portions of evaporation (E) and T without the need for sites specific parameterization (Anderson et al., 2021; Fisher et al., 2008).

The following chapters of this dissertation will highlight ET in Mid-South rice production with emphasis on estimation and modeling throughout each chapter. The first chapter provides estimates of ET across three growing seasons in two commercial rice fields. Included in the analysis is a direct comparison of the impact of AWD on ET as well as a comparison of common ET estimation methods. This chapter was published in the Journal of Hydrology, where I, Colby Reavis, served as the primary and corresponding author who was responsible for processing and

analyzing data, creating the document, assimilating feedback from coauthors and reviewers throughout the submission process, and guiding and submitting the document to final approval by the publisher.

The second chapter provides a detailed look at canopy water use during the growing season. Using the same growing season data as Chapter 1, we provide a further look at the impacts of drying with respect to ET and GPP, and we apply a new method for estimating T using EC flux data at our field sites. To provide a constrained estimate on T as well as T:ET, we also compare the EC-derived T to two other common methods for estimating transpiration, the Priestley-Taylor Equation developed by NASA's Jet Propulsion Laboratory (PT-JPL) and the FAO56 Penman Monteith dual crop coefficient (PM56Dual) approach. We also observe the dynamics of WUE with respect to canopy development during the growing season using field observations of LAI.

In the third chapter, we expand our assessment of the PT-JPL method by comparing ET across the EC towers, the PT-JPL model using local microclimate measurements, and the ECOSTRESS remote sensing product, which is based entirely on the PT-JPL framework utilizing remotely sensed information. We test the viability of the parameterless approach of the PT-JPL model to estimate ET as compared to ECOSTRESS, which uses remotely sensed data in the same modeling framework. The analysis includes an examination of the ECOSTRESS product to estimate both daily ET and instantaneous ET rates measured at different times of day. In addition to comparing modeled and observed ET, we estimate ET across different periods of the growing season marked by both phenological development and irrigation management.

Across all three chapters, we reduce the uncertainty of growing season ET for rice in commercial production within the Mid-South. We test the impacts of drying in AWD treatment

on observed fluxes during the growing season, and we provide a comprehensive view of water use across different fields, growing seasons, and irrigation treatments. We employ EC as an advanced technique to provide the most accurate estimate of ET while testing the ability of other ET estimation methods. The selected methods differ in complexity with varying degrees of input data required. We also provide an evaluation of the same framework supported by either remote sensing or field level data. The outcomes of this work provide the best estimates for ET in Mid-South rice, detailed information regarding the pros and cons of different methods used to estimate ET, and support for the adoption of AWD as a safe irrigation practice with potential for water savings.

Introduction References

Ahmed, M., Ahmad, S., 2017. Climate variability impact on rice production: Adaptation and mitigation strategies, in: Quantification of Climate Variability, Adaptation and Mitigation for Agricultural Sustainability. Springer, pp. 91–111.

Allen, R.G., 2000. Using the FAO-56 dual crop coefficient method over an irrigated region as part of an evapotranspiration intercomparison study. J. Hydrol. 229, 27–41. https://doi.org/10.1016/S0022-1694(99)00194-8

Amatya, D.M., Irmak, S., Gowda, P., Sun, G., Nettles, J.E., Douglas-Mankin, K.R., 2016. Ecosystem evapotranspiration: challenges in measurements, estimates, and modeling. Trans. ASABE 59, 555–560.

Anderson, M.C., Yang, Yang, Xue, J., Knipper, K.R., Yang, Yun, Gao, F., Hain, C.R., Kustas, W.P., Cawse-Nicholson, K., Hulley, G., Fisher, J.B., Alfieri, J.G., Meyers, T.P., Prueger, J., Baldocchi, D.D., Rey-Sanchez, C., 2021. Interoperability of ECOSTRESS and Landsat for mapping evapotranspiration time series at sub-field scales. Remote Sens. Environ. 252, 112189. https://doi.org/10.1016/j.rse.2020.112189

Balch, W.M., Abbott, M.R., Eppley, R.W., 1989. Remote sensing of primary production—I. A comparison of empirical and semi-analytical algorithms. Deep Sea Res. Part Oceanogr. Res. Pap. 36, 281–295. https://doi.org/10.1016/0198-0149(89)90139-8

Boazar, M., Abdeshahi, A., Yazdanpanah, M., 2020. Changing rice cropping patterns among farmers as a preventive policy to protect water resources. J. Environ. Plan. Manag. 63, 2484–2500.

Carlson, T.N., Capehart, W.J., Gillies, R.R., 1995. A new look at the simplified method for remote sensing of daily evapotranspiration. Remote Sens. Environ. 54, 161–167. https://doi.org/10.1016/0034-4257(95)00139-R

Carrijo, D.R., Lundy, M.E., Linquist, B.A., 2017. Rice yields and water use under alternate wetting and drying irrigation: A meta-analysis. Field Crops Res. 203, 173–180. https://doi.org/10.1016/j.fcr.2016.12.002

Chen, Y., Xia, J., Liang, S., Feng, J., Fisher, J.B., Li, Xin, Li, Xianglan, Liu, S., Ma, Z., Miyata, A., Mu, Q., Sun, L., Tang, J., Wang, K., Wen, J., Xue, Y., Yu, G., Zha, T., Zhang, L., Zhang, Q., Zhao, T., Zhao, L., Yuan, W., 2014. Comparison of satellite-based evapotranspiration models over terrestrial ecosystems in China. Remote Sens. Environ. 140, 279–293. https://doi.org/10.1016/j.rse.2013.08.045

Chhetri, N., Chaudhary, P., Tiwari, P.R., Yadaw, R.B., 2012. Institutional and technological innovation: Understanding agricultural adaptation to climate change in Nepal. Appl. Geogr., The Health Impacts of Global Climate Change: A Geographic Perspective 33, 142–150. https://doi.org/10.1016/j.apgeog.2011.10.006

Courault, D., Seguin, B., Olioso, A., 2005. Review on estimation of evapotranspiration from remote sensing data: From empirical to numerical modeling approaches. Irrig. Drain. Syst. 19, 223–249. https://doi.org/10.1007/s10795-005-5186-0

Drexler, J.Z., Snyder, R.L., Spano, D., U, K.T.P., 2004. A review of models and micrometeorological methods used to estimate wetland evapotranspiration. Hydrol. Process. 18, 2071–2101. https://doi.org/10.1002/hyp.1462

Earl D. Vories, Phil L. Tacker, 2006. Effect of ET Calculation Method on Irrigation Scheduling in Midsouth, in: 2006 Portland, Oregon, July 9-12, 2006. Presented at the 2006 Portland, Oregon, July 9-12, 2006, American Society of Agricultural and Biological Engineers. https://doi.org/10.13031/2013.20753

Feng, Z.Y., Qin, T., Du, X.Z., Sheng, F., Li, C.F., 2021. Effects of irrigation regime and rice variety on greenhouse gas emissions and grain yields from paddy fields in central China. Agric. Water Manag. 250, 106830. https://doi.org/10.1016/j.agwat.2021.106830

Fisher, J.B., Tu, K.P., Baldocchi, D.D., 2008. Global estimates of the land–atmosphere water flux based on monthly AVHRR and ISLSCP-II data, validated at 16 FLUXNET sites. Remote Sens. Environ. 112, 901–919. https://doi.org/10.1016/j.rse.2007.06.025

Foley, J.A., Ramankutty, N., Brauman, K.A., Cassidy, E.S., Gerber, J.S., Johnston, M., Mueller, N.D., O'Connell, C., Ray, D.K., West, P.C., Balzer, C., Bennett, E.M., Carpenter, S.R., Hill, J., Monfreda, C., Polasky, S., Rockström, J., Sheehan, J., Siebert, S., Tilman, D., Zaks, D.P.M., 2011. Solutions for a cultivated planet. Nature 478, 337–342. https://doi.org/10.1038/nature10452

Graham-Acquaah, S., Siebenmorgen, T.J., Reba, M.L., Massey, J.H., Mauromoustakos, A., Adviento-Borbe, A., January, R., Burgos, R., Baltz-Gray, J., 2019. Impact of alternative irrigation practices on rice quality. Cereal Chem. 96, 815–823. https://doi.org/10.1002/cche.10182

Henry, C.G., Daniels, M., Hamilton, M., Hardke, J.T., 2013. Water Management, in: Arkansas Rice Production Handbook. University of Arkansas Extension Service, pp. 103–128.

Horst, M.G., Shamutalov, S.S., Pereira, L.S., Gonçalves, J.M., 2005. Field assessment of the water saving potential with furrow irrigation in Fergana, Aral Sea basin. Agric. Water Manag., Special Issue on Land and Water Use: Environmental Management Tools and Practices 77, 210–231. https://doi.org/10.1016/j.agwat.2004.09.041

Hsiao, T.C., Steduto, P., Fereres, E., 2007. A systematic and quantitative approach to improve water use efficiency in agriculture. Irrig. Sci. 25, 209–231. https://doi.org/10.1007/s00271-007-0063-2

Huang, Y., Ryu, Y., Jiang, C., Kimm, H., Kim, S., Kang, M., Shim, K., 2018. BESS-Rice: A remote sensing derived and biophysical process-based rice productivity simulation model. Agric. For. Meteorol. 256–257, 253–269. https://doi.org/10.1016/j.agrformet.2018.03.014

Ishfaq, M., Farooq, M., Zulfiqar, U., Hussain, S., Akbar, N., Nawaz, A., Anjum, S.A., 2020. Alternate wetting and drying: A water-saving and ecofriendly rice production system. Agric. Water Manag. 241, 106363. https://doi.org/10.1016/j.agwat.2020.106363

Ito, A., Inatomi, M., 2012. Water-Use Efficiency of the Terrestrial Biosphere: A Model Analysis Focusing on Interactions between the Global Carbon and Water Cycles. J. Hydrometeorol. 13, 681–694. https://doi.org/10.1175/JHM-D-10-05034.1

Jiang, C., Guan, K., Pan, M., Ryu, Y., Peng, B., Wang, S., 2020. BESS-STAIR: a framework to estimate daily, 30 m, and all-weather crop evapotranspiration using multi-source satellite data for the US Corn Belt. Hydrol. Earth Syst. Sci. 24, 1251–1273. https://doi.org/10.5194/hess-24-1251-2020

Jiang, C., Ryu, Y., 2016. Multi-scale evaluation of global gross primary productivity and evapotranspiration products derived from Breathing Earth System Simulator (BESS). Remote Sens. Environ. 186, 528–547. https://doi.org/10.1016/j.rse.2016.08.030

Jovanovic, N., Pereira, L.S., Paredes, P., Pôças, I., Cantore, V., Todorovic, M., 2020. A review of strategies, methods and technologies to reduce non-beneficial consumptive water use on farms considering the FAO56 methods. Agric. Water Manag. 239, 106267. https://doi.org/10.1016/j.agwat.2020.106267

Lampayan, R.M., Rejesus, R.M., Singleton, G.R., Bouman, B.A.M., 2015. Adoption and economics of alternate wetting and drying water management for irrigated lowland rice. Field Crops Res. 170, 95–108. https://doi.org/10.1016/j.fcr.2014.10.013

Liao, B., Wu, X., Yu, Y., Luo, S., Hu, R., Lu, G., 2020. Effects of mild alternate wetting and drying irrigation and mid-season drainage on CH4 and N2O emissions in rice cultivation. Sci. Total Environ. 698, 134212. https://doi.org/10.1016/j.scitotenv.2019.134212

Liu, J., Zehnder, A.J.B., Yang, H., 2009. Global consumptive water use for crop production: The importance of green water and virtual water. Water Resour. Res. 45. https://doi.org/10.1029/2007WR006051

Maclean, J., Hardy, B., Hettel, G., 2013. Rice Almanac: Source book for one of the most important economic activities on earth. IRRI.

Martin, D.L., Stegman, E.C., Fereres, E., 1990. Irrigation scheduling principles. Manag. Farm Irrig. Syst. Am. Soc. Agric. Eng. St Joseph MI 1990 P 155-203 19 Fig 9 Tab 81 Ref.

Massey J. H., Smith M. C., Vieira D. A. N., Adviento-Borbe M. A., Reba M. L., Vories E. D., 2018. Expected Irrigation Reductions Using Multiple-Inlet Rice Irrigation under Rainfall Conditions of the Lower Mississippi River Valley. J. Irrig. Drain. Eng. 144, 04018016. https://doi.org/10.1061/(ASCE)IR.1943-4774.0001303

Massey, J.H., Mark Stiles, C., Epting, J.W., Shane Powers, R., Kelly, D.B., Bowling, T.H., Leighton Janes, C., Pennington, D.A., 2017. Long-term measurements of agronomic crop irrigation made in the Mississippi delta portion of the lower Mississippi River Valley. Irrig. Sci. 35, 297–313. https://doi.org/10.1007/s00271-017-0543-y

Melton, F.S., Johnson, L.F., Lund, C.P., Pierce, L.L., Michaelis, A.R., Hiatt, S.H., Guzman, A., Adhikari, D.D., Purdy, A.J., Rosevelt, C., Votava, P., Trout, T.J., Temesgen, B., Frame, K., Sheffner, E.J., Nemani, R.R., 2012. Satellite Irrigation Management Support With the Terrestrial Observation and Prediction System: A Framework for Integration of Satellite and Surface Observations to Support Improvements in Agricultural Water Resource Management. IEEE J. Sel. Top. Appl. Earth Obs. Remote Sens. 5, 1709–1721. https://doi.org/10.1109/JSTARS.2012.2214474

Molden, D., Oweis, T., Steduto, P., Bindraban, P., Hanjra, M.A., Kijne, J., 2010. Improving agricultural water productivity: Between optimism and caution. Agric. Water Manag., Comprehensive Assessment of Water Management in Agriculture 97, 528–535. https://doi.org/10.1016/j.agwat.2009.03.023

Norton, G.J., Shafaei, M., Travis, A.J., Deacon, C.M., Danku, J., Pond, D., Cochrane, N., Lockhart, K., Salt, D., Zhang, H., Dodd, I.C., Hossain, M., Islam, M.R., Price, A.H., 2017. Impact of alternate wetting and drying on rice physiology, grain production, and grain quality. Field Crops Res. 205, 1–13. https://doi.org/10.1016/j.fcr.2017.01.016

Ryu, Y., Baldocchi, D.D., Black, T.A., Detto, M., Law, B.E., Leuning, R., Miyata, A., Reichstein, M., Vargas, R., Ammann, C., Beringer, J., Flanagan, L.B., Gu, L., Hutley, L.B., Kim, J., McCaughey, H., Moors, E.J., Rambal, S., Vesala, T., 2012. On the temporal upscaling of evapotranspiration from instantaneous remote sensing measurements to 8-day mean daily-sums. Agric. For. Meteorol. 152, 212–222. https://doi.org/10.1016/j.agrformet.2011.09.010

Savoca, M.E., Senay, G.B., Maupin, M.A., Kenny, J.F., Perry, C.A., 2013. Actual evapotranspiration modeling using the operational Simplified Surface Energy Balance (SSEBop) approach. US Department of the Interior, US Geological Survey.

Senay, G.B., 2018. Satellite psychrometric formulation of the Operational Simplified Surface Energy Balance (SSEBop) model for quantifying and mapping evapotranspiration. Appl. Eng. Agric. 34, 555–566.

Shekhar, S., Tamilarasan, R., Mailapalli, D.R., Raghuwanshi, N.S., 2020. Estimation of evapotranspiration for paddy under alternate wetting and drying irrigation practice*. Irrig. Drain. n/a. https://doi.org/10.1002/ird.2536

Spangenberg, J.H., Beaurepaire, A.L., Bergmeier, E., Burkhard, B., Van Chien, H., Cuong, L.Q., Görg, C., Grescho, V., Hai, L.H., Heong, K.L., Horgan, F.G., Hotes, S., Klotzbücher, A., Klotzbücher, T., Kühn, I., Langerwisch, F., Marion, G., Moritz, R.F.A., Nguyen, Q.A., Ott, J., Sann, C., Sattler, C., Schädler, M., Schmidt, A., Tekken, V., Thanh, T.D., Thonicke, K., Türke, M., Václavík, T., Vetterlein, D., Westphal, C., Wiemers, M., Settele, J., 2018. The LEGATO cross-disciplinary integrated ecosystem service research framework: an example of integrating research results from the analysis of global change impacts and the social, cultural and economic system dynamics of irrigated rice production. Paddy Water Environ. 16, 287–319. https://doi.org/10.1007/s10333-017-0628-5

Subedi, A., Chávez, J.L., 2015. Crop evapotranspiration (ET) estimation models: a review and discussion of the applicability and limitations of ET methods. J. Agric. Sci. 7, 50.

Tanner, C., Sinclair, T., 1983. Efficient water use in crop production: Research or re-search? Limit. Effic. Water Use Crop Prod. 1–27.

Vories, E., Stevens, W. (Gene), Rhine, M., Straatmann, Z., 2017. Investigating irrigation scheduling for rice using variable rate irrigation. Agric. Water Manag., Special Issue on Improving Agricultural Water Productivity to Ensure Food Security under Changing Environments Overseen by: Brent Clothier 179, 314–323. https://doi.org/10.1016/j.agwat.2016.05.032

Wang, H., Zhang, Yan, Zhang, Yaojun, McDaniel, M.D., Sun, L., Su, W., Fan, X., Liu, S., Xiao, X., 2020. Water-saving irrigation is a 'win-win' management strategy in rice paddies – With both reduced greenhouse gas emissions and enhanced water use efficiency. Agric. Water Manag. 228, 105889. https://doi.org/10.1016/j.agwat.2019.105889

Yao, F., Huang, J., Cui, K., Nie, L., Xiang, J., Liu, X., Wu, W., Chen, M., Peng, S., 2012. Agronomic performance of high-yielding rice variety grown under alternate wetting and drying irrigation. Field Crops Res. 126, 16–22. https://doi.org/10.1016/j.fcr.2011.09.018

Ye, Q., Yang, X., Dai, S., Chen, G., Li, Y., Zhang, C., 2015. Effects of climate change on suitable rice cropping areas, cropping systems and crop water requirements in southern China. Agric. Water Manag. 159, 35–44.

Zhang, Z., Tian, F., Hu, H., Yang, P., 2014. A comparison of methods for determining field evapotranspiration: photosynthesis system, sap flow, and eddy covariance. Hydrol. Earth Syst. Sci. 18, 1053–1072. https://doi.org/10.5194/hess-18-1053-2014

Zhao, J., Xu, T., Xiao, J., Liu, S., Mao, K., Song, L., Yao, Y., He, X., Feng, H., 2020. Responses of water use efficiency to drought in southwest China. Remote Sens. 12, 199.

Zhuang, Y., Zhang, L., Li, S., Liu, H., Zhai, L., Zhou, F., Ye, Y., Ruan, S., Wen, W., 2019. Effects and potential of water-saving irrigation for rice production in China. Agric. Water Manag. 217, 374–382. https://doi.org/10.1016/j.agwat.2019.03.010

Chapter 1: Impacts of Alternate Wetting and Drying and Delayed Flood Rice Irrigation on Growing Season Evapotranspiration

Authors: Colby W. Reavis[1], Kosana Suvočarev[3], Michele L. Reba[2], Benjamin R.K. Runkle[1]

[1] Department of Biological and Agricultural Engineering, University of Arkansas, Fayetteville, AR, USA

[2] USDA ARS Delta Water Management Research Unit, Jonesboro, AR, USA

[3] Department of Land, Air, and Water Resources, University of California–Davis, CA, USA

1. Introduction

Water resources are currently consumed at unsustainable rates within the Lower Mississippi River Basin, where a majority of rice is grown in the United States (Reba et al., 2013; Kresse et al., 2014). Due to this depletion, the region is increasing efforts to conserve water and quantify water use, particularly by agricultural irrigation for its sustainable future management (ANRC, 2014; Reba et al., 2017). To promote sustainable water use in rice production, various methods and technologies are being applied, such as field levelling to zero–grade, which can reduce irrigation water use by up to 40% (Henry et al., 2016), and multiple inlet irrigation, which can reduce water use by up to 24% (Massey et al., 2014, 2018). Alternate wetting and drying (AWD) is a practice that can potentially reduce irrigation water use by up to 20% by capturing rain during the growing season, offsetting pumping costs for the producer (Carrijo et al., 2017; Pan et al., 2017; Lampayan et al., 2015). Prior to the onset of the initial flood in both AWD and delayed flood (DF) practices, the rice germinates and establishes in non–

flooded soils (Hardke, 2013). The recommended AWD practice allows periodic paddy drying, which lasts approximately 5 days, to occur at least 3 weeks after the first flooding. The conventional DF practice maintains a constant flood once the first flood is established until the fields are drained for harvest. However, the level and timing of drying induced in AWD are management decisions based on irrigation infrastructure, precipitation forecasting, soil type, plant variety, growth stage, and water supply. While AWD conserves water, there are concerns regarding plant health, grain quality, and decreases in yield compared to conventional growing practices (Norton et al., 2017a, 2017b; Sudhir–Yadav et al., 2012, Graham-Acquaah et al., 2019); therefore, the timing and duration of the dry periods needs careful management. AWD is also expanding in use because of its potential to reduce greenhouse gas emissions associated with rice production (Linquist et al., 2014, 2018; Runkle et al., 2019).

Fields managed with AWD have the potential to reduce evapotranspiration (ET) when compared to conventionally managed fields due to the decline of available water at the soil surface and alteration of land surface radiative properties, which may reduce the amount of open water or soil water evaporation (Norman et al., 1995; Liu et al., 2019). However, ET is typically dominated by the plant–mediated release of water (transpiration), especially during the later portion of the growing season when the rice canopy is fully developed (Wei et al., 2015; Wei et al., 2017). The water savings for AWD are primarily seen in the capturing of rain events during drying periods. Ideally, the amount of rainfall captured during these events should offset the amount of pumped water required to replace water lost through ET (Kima et al., 2015). In rice water budgets and irrigation schedulers, producers use ET to estimate the amount of water required to sustain crop production without incurring stress (Li and Cui, 1996; Smith, 1996). Understanding how ET changes throughout the growing season also provides an indication of

canopy health (Moran et al., 1995). ET is tied to primary production of plant biomass as water

release from the plant is regulated by stomatal control, which helps dictate assimilation of carbon

dioxide within the plant during the daytime (Roel et al., 1999; Ikawa et al., 2018; Lieu et al.,

2020). Because AWD has the potential to conserve water resources and provide economic

benefits to the producer (Nalley et al., 2015), uncertainty within the terms of the water balance

(including ET) must be reduced through careful measurement.

In agricultural settings, ET is typically estimated using approaches such as the

Hargreaves or Penman–Monteith equations, which rely on meteorological data and basic

estimates of phenology (Allen et al., 1998; Hargreaves & Allen, 2003; Pereira et al, 2015).

However, studies conducted in rice have indicated sizeable differences when comparing

measured ET, using micrometeorological approaches such as the eddy covariance method, and

ET estimated with variations of the Penman–Monteith equation (Ikawa et al., 2017; Wang et al.,

2017). These approaches include the Penman–Monteith method for actual ET (PM–AET) and

the Penman–Monteith method as outlined in FAO Document 56 (PM–FAO56) (Penman, 1948;

Monteith, 1965; Allen et al., 1998). Methods such as the PM–AET are of interest as their

improvement would provide a platform for relating associated changes in measured ET to

physically derived relationships between ET and multiple meteorological and phenological

variables contained within the PM–AET. Many studies have identified areas of improvement for

different implementations of the Penman–Monteith equation by focusing on different

components, including canopy conductance and variable crop coefficients (Lecina et al., 2003;

Alberto et al., 2014; Yan et al., 2018).

A common application of conductance is the "big leaf" approach that treats conductance

as a bulk value across all leaves in the canopy, where its parameterization can be completed

using only observations of local meteorological variables, LAI, and ET observations. However, single layer conductance models typically underperform in periods of sparse (LAI<2) vegetation (Xu et al., 2018; Lafleur & Rouse, 1990). Dual-layer conductance approaches that address canopy and soil as separate contributors to ET have been recommended to address the poor performance of the PM-AET under sparse vegetation, including rice (Shuttleworth and Wallace, 1985; Facchi et al., 2013). Studies utilizing both the dual-layer and single layer conductance frameworks in rice have shown comparable performance between each approach during the growing season (Gharsallah et al., 2013; Liu et al., 2020).

Here, we quantify ET rates from within two fields in the humid U.S. Mid–South and compare AWD and DF irrigation management practices. The primary aim of this study is to better characterize half-hourly and seasonal ET in this region and identify associated impacts of altering the conventional irrigation regime with respect to ET. For this aim, we test whether fields with AWD irrigation show reduced ET relative to the DF field due to the lack of a free water surface during drying events by quantifying ET using different methods across multiple growing seasons. We then examine how ET changes during drying events to observe the effects drying has on plant activity. We assume that during drying events, if the plants undergoing AWD remain unstressed, the differences in transpiration should be negligible. Because transpiration makes up a large portion of ET during the growing season, we hypothesize that canopies with similar transpiration rates will show little differences in ET once the canopy is established. The second aim is to evaluate the performance of two accepted estimation methods in comparison to eddy covariance observations within both DF and AWD fields across the 2015–17 growing seasons. Finally, we seek to compare crop coefficients derived from local estimates of reference ET and eddy covariance to the crop coefficients for rice recommended in the FAO 56 document.

2. Materials and Methods

2.1. Site Description

The study site is composed of two adjacent commercial fields (~24 ha each) located in eastern Arkansas, USA (34° 35' 8.6" N, 91° 45' 05" W). The fields have been used to grow rice in continuous rotation since 2004 and are zero–graded with no slope within the planted area of the field. For this study, the fields are identified as North Field (NF) and South Field (SF). The soil within the fields is primarily characterized as poorly drained Perry silty clay (USDA classification: very-fine, smectitic, thermic Chromic Epiaquerts), which represents 100% of NF and 93.2% of SF (Runkle et al., 2019; Soil Survey Staff, 2018). The remaining portion of SF soil (~2 ha) is a Herbert silt loam (fine-silty, mixed, superactive, mesic Udollic Epiaqualfs). The composition of the soil varied between NF and SF where NF had greater clay content (62% vs. 43%). The fields are connected in a series of five similarly-sized fields where irrigation water is delivered across each field, moving north to south, before arriving at the desired field.

The rice was drill seeded and the growers apply the first flood approximately 47 days after planting (DAP). Rice grown within the fields in each study year was a hybrid variety (Clearfield XL745, RiceTec, Inc., Alvin, TX, USA) and followed the typical growing season for rice in Arkansas from early April to September. The 2015–2017 growing seasons for NF and SF ranged 133–143 days from planting to harvest (Runkle et al., 2019). Irrigation during the growing season relies primarily on surface water, which travels between fields by gravity flow through pipes and ditches. Irrigation routes are set up so that water must flow through each field as a series running north to south. The irrigation treatments were altered between the three growing seasons (Table 1). In 2016, seeding was delayed due to wet field conditions, and, thus,

the first flood was established later in the summer compared to 2015 and 2017 (i.e., 14 Jun vs.

14-17 May).

Table 1. Seasonal Irrigation and first flooding dates for NF and SF during the 2015-2017
growing seasons.

Field	Year	Irrigation Treatment	Planting Date	First Flooding Date	DAP	Harvest Date
NF	2015	DF	8-Apr	14-May	40	19-Aug
	2016	AWD	23-Apr	14-Jun	52	13-Sep
	2017	DF	10-Apr	17-May	37	26-Aug
SF	2015	AWD	8-Apr	15-May	41	19-Aug
	2016	AWD	23-Apr	16-Jun	54	13-Sep
	2017	DF	9-Apr	18-May	38	27-Aug

Instrumentation consisted of eddy covariance and biometeorological sensors (Runkle et

al., 2019) and was identically installed in both fields. These measurements contribute to the

Ameriflux Management Project (NF:US–HRC and SF:US–HRA) and its subnetwork Delta–Flux

for responding to questions on sustainable practices in agriculture (Runkle et al., 2017). Due

to the homogeneous fetch requirements for the eddy covariance technique, the equipment was

installed on the northern edge of each field at approximately half the distance of the northern

border to capture the dominant southern winds during the growing season, and fluxes north of

each field were discarded. Equipment was installed approximately 15 m from the north edge of

each field after drill–seeding and removed immediately prior to harvest. Deployment during the

growing season normally occurred within 4 days post-planting, and removal of equipment

occurred 2 days prior to harvest. Fluxes collected at the towers using eddy covariance were

screened to include only wind directions between 95 and 265 degrees to ensure measurement

footprints were limited to their respective fields. Gaps within the observed fluxes for all three

years were empirically filled using an artificial neural networks approach (Knox et al., 2015, 2016). This method used the following explanatory variables: days since the start of the study period, leaf area index (LAI), plant height, friction velocity (u*), air temperature (T), incoming solar radiation ($R_{g,in}$), vapor pressure deficit (VPD), water depth (WD), and fuzzy transformation sets representing seasonality and time of day (see Runkle et al., 2019 for more details). The turbulent energy flux models correlated with observations with R^2 values greater than 0.90.

2.2. Measurement of fluxes, microclimate, and plant parameters

The eddy covariance (EC) system provided measurements of sensible heat (H) and latent heat (LE) flux through the net exchange of the scalars, temperature and H_2O, respectively. The EC system included a 3D sonic anemometer (CSAT3, Campbell Scientific, Inc., Logan, UT, USA) and an open–path infrared CO_2/H_2O analyzer (LI–7500A, LI–COR, Inc., Lincoln, NE, USA). The EC system was mounted on a tripod, with the sensor height measuring 2.2 m above the surface of the rice field. Separation for the EC sensors was approximately 0.1 m and was accounted for with frequency correction factors and signal lagging, including flow distortion by transducer shadowing (Horst et al., 2015), described in Runkle et al. (2019) and Suvočarev et al. (2019). The EC components used a designated analyzer interface unit (LI–7550, LI–COR, Inc., Lincoln, NE, USA) with outputs recorded at 20 Hz and half-hourly fluxes calculated with EddyPro v. 6.2 software with the output including calculated flux, quality flags, and an analysis of the flux footprint throughout the growing season. Fluxes were screened based on multiple factors, including turbulence, dominant wind direction (southern winds), footprint size, and availability based on power failures. The flux footprint was used to only include periods where 90% of the data was measured within 350 m of the tower to remove the effects of measurement drift across adjacent fields (Runkle et al., 2019). The resulting data coverage for half-hourly

sensible and latent heat fluxes after filtering ranged between 23% to 34% across the growing periods.

The four components of net radiation (RN) were measured (CNR4, Kipp & Zonen, Inc., Delft, NL) at a height of 2.0 m. Incoming and outgoing photosynthetically active radiation (PAR) was also measured using quantum sensors (LI–190SB, LI–COR, Inc., Lincoln, NE, USA) at 1.85 m. Air temperature (T) and relative humidity (RH) were measured using a shielded probe (HMP155A, Vaisala, Helsinki, FI). In addition to the sonic anemometer, wind speed and direction were also measured using a 2-D anemometer mounted at 3.2 m (05103−5 propeller wind monitor, R.M. Young, Traverse City, MI, USA). Soil heat flux (G) measurements were collected using two soil heat flux plates (HFP01, Hukseflux, Delft, NL) placed at different depths in each year: 8 cm, 5 cm, and 4 cm below the soil surface for the 2015, 2016, and 2017 growing seasons, respectively. Soil heat flux plate measurements were corrected for the stored energy in both soil and water column, using soil surface temperature and water temperature thermistor measurements (CS–107 (BetaTherm 100K6A1IA), Campbell Scientific, Inc., Logan, UT, USA). Thermistors were placed directly at the soil surface, 2 cm above each soil heat flux plate, and on a flotation device to capture the temperature of the changing flood level. The energy balance closure (EBC), as reported in Runkle et al. (2019), was calculated using sensible and latent heat flux from the EC towers, RN, and storage-corrected G at the half-hourly time step. For the 2015-2017 growing seasons, the EBC for NF was 0.73, 0.75, and 0.69, respectively, and 0.89, 0.69, and 0.82 for SF, respectively.

Volumetric water content measurements were collected using soil moisture Time Domain Transmissometer probes (SDI–12, Acclima, Sydney, AU) at 8 cm and 15 cm for all fields during all growing seasons. Measurements of WD were collected continuously using a

piezometric sensor (Series 46x, Keller USA Inc., Fort Mill, SC, USA), vented for automatic compensation for barometric pressure changes, installed 30 cm from the tower in a perforated tube reaching approximately 30 cm below the soil surface. Other field parameters including plant density and soil bulk density were collected manually at different times during the growing season (Runkle et al., 2019). Bulk density and soil temperature above the soil heat flux plate were used in conjunction with WD measurements to correct for changes in heat storage in the water and saturated soil matrix above the plate during flooded and dry conditions (Fuchs and Tanner, 1968; Runkle et al., 2019).

2.3 Leaf area index (LAI) and canopy height model

To characterize changing canopy conditions and provide necessary inputs for the Penman–Monteith approach and EC processing, canopy height measurements were collected throughout the growing season and averaged across 10–measurements during each field excursion (approx. twice monthly, but less frequently in 2016; see below). Because of high crop uniformity, canopy height measurements were taken only within 30 m of the EC station, and represented the height from the soil surface to the height of the canopy top at eye level, ignoring flag leaves. LAI was measured at similar intervals using a plant canopy analyzer (LAI–2200C, LI–COR, Inc., Lincoln, NE, USA), averaging three samples taken within 30 m of the EC tower, per measurement period. Typically, sampling for LAI did not begin until the canopy had achieved a measurable level of growth, usually 50–60 DAP when the canopy height was approximately 0.5 m. We estimated LAI and canopy height throughout the growing season with a growing–degree–day (GDD) model (Yang et al., 1995). This approach uses GDD as the cumulative sum of the differences between the mean daily temperature ($T_{mean,daily}$) and a base

temperature (T_{base}). In this setting, T_{base} was set as 10 ºC to represent the minimum temperature for growth and development in rice (Keisling et al., 1984).

LAI and canopy height data were collected through field measurements during the 2015–2017 growing seasons in both the NF and SF. LAI observations were complemented with MODIS Terra (AM) satellite LAI (MOD15A2H; Myneni et al., 2015) to remedy gaps in field measurements and improve model timing regarding canopy development. The MODIS data provided information about rice canopy dynamics, most notably the transition to a phase of rapid growth (approximately 45 DAP) as the rice canopy transitioned from the vegetative to reproductive stages. The 1–km MODIS pixel encompassed vegetation from both studied fields (Figure 1). The area surrounding the experimental fields are also rice paddies with similar phenological development.
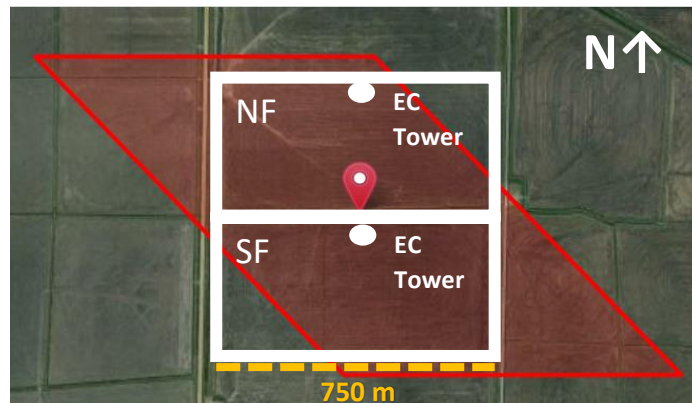
Figure 1. MODIS pixel (1–km) in red used for both NF and SF fields also known as US–HRC and US–HRA, respectively, in the Ameriflux Management Project. Pixel taken from ORNL MODIS Web Interface (ORNL, 2017); Background image from Google Earth (imagery date, 14 October 2015). Towers include eddy covariance equipment.

For the 2015 and 2017 growing seasons, field observations collected with the LAI-2200C (n=8 and n=13, respectively) were necessary to model LAI as a linear and quadratic function of GDD during the early and rapid growth stages, respectively. In contrast, only two field

observations (n=2) of LAI were collected during the 2016 growing season in the early growth period. To compensate for lack of data in 2016, in that year the MODI5AH2 LAI product was used to estimate LAI (Myneni et al., 2015). To correct for the MODIS LAI product's consistent under–estimation bias (up to 20%) determined in 2015 and 2017, the MODIS data points used to model LAI during the 2016 growing season were adjusted using a scaling factor. This factor was estimated using a regression slope between measured data points and the MODIS data at the same time period for each field across the 2015–2017 growing seasons. The scaling factors (slopes) for each field were then applied to their respective MODIS data to generate a sufficient (n > 5) set of LAI data that could be used to identify linear and quadratic growth periods with respect to GDD during the 2016 growing season. A similar approach was applied to canopy height, where field data were collected and modeled based on the period of the growing season. Canopy height measurements were collected during the 2015–2017 growing seasons for each field within the study (NF and SF). The same approach used to model LAI before and after the transition from vegetative to reproductive stages was applied to canopy height, where the growth patterns before and after this transition were considered to be linear and quadratic, respectively, in relation to GDD.

2.4 Methods for modeling ET

The PM–AET is based on meteorological data and information about plant development. The combination equation (1) is based on the latent energy requirement for evaporating water and the deficit of vapor pressure necessary for removing water. It also accounts for the resistances for transpiring the water from plant tissue and transporting it away from the crop canopy. It was used to evaluate data collected in real time from both fields at the 30–min time step.

$$\lambda ET = \frac{\Delta(RN - G) + c_p \rho_a VPD / r_a}{\Delta + \gamma(1 + r_s / r_a)} \qquad (1)$$

Where λ is the latent heat of vaporization (2.45 MJ kg^{-1}), ET is evapotranspiration (mm day^{-1}), c_p is specific heat of air (J kg^{-1} °C^{-1}), ρ_a is mean air density (kg m^{-3}), r_s is bulk surface resistance (s m^{-1}), r_a is aerodynamic resistance (s m^{-1}) derived from wind speed, canopy height, and measurement height of wind speed (see Appendix A), Δ is the slope of vapor pressure–temperature relationship (kPa °C^{-1}), and γ is the psychrometric constant (kPa °C^{-1}) determined as $6.65*10^{-3}$ P_{atm} (Atm). The PM–AET can be used to estimate stomatal conductance using EC data through inversion and is also one of the few methods that can generate an ET estimate at the half–hourly time scale using only meteorological data.

The PM–FAO56 method (Equation 2) generates daily estimates of reference ET (ETo, mm day^{-1}) from a reference crop, a short, well-watered grass, and the crop ET (mm day^{-1}) is calculated using dimensionless crop coefficients:

$$ET_c = ET_0 * K_c = \frac{0.408\Delta(R_n - G) + \gamma\left(\frac{C_n}{T + 273}\right)(VPD)u_{2m}}{\Delta + \gamma(1 + C_d u_{2m})} * K_c \qquad (2)$$

where ET_c is crop evapotranspiration (mm day^{-1}), ET_0 is reference evapotranspiration (mm day^{-1}), T is mean daily air temperature at 2.0 m height (°C), u_{2m} is wind speed at 2.0 m height (m s^{-1}), C_d and C_n are coefficients based on canopy development for a theoretical crop at 0.12 m in height, and K_c is the crop coefficient for converting ET_0 to rice canopy ET.

Each rice development stage has corresponding crop coefficient that is changing. According to tabulated FAO56 values the crop coefficients for rice grown in a humid

environment with moderately high wind speed (>2 m s^{-1}) are equal to 1.05, 1.20, and 0.9 for the initial, mid–season, and late–season periods of the growing season, respectively. The lengths of time used to define the initial, developmental, mid–season, and late season stages of rice crop growth are 30, 30, 80, and 40 days, respectively. The tabulated rice crop coefficients given were also derived from the water-seeded rice practice, where rice was deposited directly into pre-flooded paddies, based on the identical recommended values (1.05) for coefficient $K_{c,ini}$ and open water surfaces. For this method, several assumptions were made in relation to the reference evapotranspiration and G. Reference evapotranspiration requires measurements taken from a representative plot that adheres to FAO 56 standards so that all other assumptions inherent to the model hold for representativeness of the evaporative demand of the atmosphere. The local USDA weather station in Stuttgart, AR (~20 km to east of site surrounded by similar agricultural fields) provided measurements of T, RH, u_{3m}, and $R_{g,in}$. The wind speed measurements from the weather station were corrected to u_{2m} using the logarithmic wind speed profile approach outlined in FAO56. Additional components of RN were estimated using "missing climate data methods" outlined in FAO 56 based on the location of the site as well as the day of year. Daily ground heat flux G is assumed by FAO 56 to average to zero at the daily time step. The crop coefficient was also adjusted using modeled canopy height and relative humidity as outlined in FAO 56, Chapter 6 to account for differences between the field site and the sites used to derive the recommended crop coefficients (Allen et al., 1998). Both the recommended and adjusted crop coefficients were compared to the observed crop coefficients at our field site.

2.5 Estimating and modeling canopy conductance

Canopy conductance, g_c, is a key term within the PM–AET model that reflects biological mediation of the exchange of gases between the rice canopy and the surrounding atmosphere. To

23

estimate g_c within each experimental field site, the PM–AET model was inverted (Equation 3) to

solve for g_c using observed (non–gap–filled) EC measurements of ET (ET_{EC}) for the

evapotranspiration term:

$$g_c = \frac{\lambda ET_{EC} * \gamma * g_a}{\Delta(R_n - G) + c_p p_a(e_s - e_a)g_a - \lambda ET_{EC}(\Delta + \gamma)} \tag{3}$$

Values of estimated g_c were limited to periods with positive ET_{EC}. The estimated g_c in these

half–hour intervals was used to parameterize a model (Equations 4–8), which utilized both

meteorological and biological inputs to predict estimates of g_c in a Jarvis–style approach (Jarvis,

et al., 1976; Xu et al., 2017; Ershadi, 2015; Gardiol et al., 2003). Surface conductance, g_s, was

determined through $g_s = g_c \, LAI_{active}^{-1}$ where LAI_{active}, determined with Equation 8, represents the

active fraction of LAI ($m^2 \, m^{-2}$) available for transpiration.

$$g_c = g_{s,max} * f(R_{g,in}) * f(VPD) * f(T) * LAI_{active} \tag{4}$$

$$f(R_{g,in}) = 1 - e^{\left(\frac{-R_{g,in}}{a_1}\right)} \tag{5}$$

$$f(VPD) = 1 - a_2 * VPD \tag{6}$$

$$f(T) = 1 - a_3 * (25 - T)^2 \tag{7}$$

$$LAI_{active} = \begin{cases} 1 & LAI < 1 \\ LAI & 1 \leq LAI < 2 \\ 2 & 2 \leq LAI < 4 \\ 0.5 \, LAI & 4 \leq LAI \end{cases} \tag{8}$$

where a_1, a_2, a_3 are fitted parameters and $g_{s,max}$ is the maximum surface conductance. The

LAI_{active} scales from g_s to g_c, to incorporate the effects of canopy development and associated

driving forces on surface conductance across the rice canopy (Collatz et al., 1991; Leuning et al.,

1995). The use of LAI_{active} follows the "big leaf" approach for modeling conductance across

landscapes (Zhang et al., 2008; Li et al., 2016; Xu et al., 2017). To prevent uneven weighting of

LAI and contributing plant transpiration, the LAI_{active} parameter was assigned to have a value of

unity during the early growing season when surface evaporation would be most pronounced in

ET. Maximum surface conductance ($g_{s,max}$) was determined as the maximum g_s observation in a

7–day moving window across the entire growing season. Negative and pseudo–infinite values (g_s

$> 10^4$ mm s^{-1}) were removed as well as values when incoming $R_{g,in}$ radiation was less than 30

W m^{-2}.

For calibration and validation of the model, we conducted a random selection of the data

across all six site years for each step. The calibration dataset represented 70% of the total dataset

while the model and parameters were validated using the remaining 30%. The parameters for the

conductance model were optimized using nonlinear regression of measured and modeled ET, and

assessed by the slope, R^2, and RMSE of the regression. The parameters were calculated using

nonlinear least squares regression between measured ET and modeled ET while fitting g_c with

parameters a_1, a_2, and a_3; thus, any uncertainty in the biometeorological inputs (in addition to

measured ET) was also transmitted to the conductance term. Conductance parameterization only

utilized data taken from 40 DAP and during the daytime period (8 AM to 6 PM, local time) to

ensure that conductance terms were not estimated with influence from periods when the rice

canopy was less likely to impact ET.

2.6 Comparison and analysis of ET observations

To better understand impacts related to differences in irrigation treatment, we directly

compared simultaneous ET observations (non–gap–filled) to other biometeorological factors.

The variables tested included meteorological drivers in the Penman–Monteith equation, such as

available energy and VPD, and variables tied to the soil conditions in each field, including

volumetric water content (VWC) and WD. Modeled canopy height and LAI were included in this analysis to account for canopy differences. Ratios of H to RN were analyzed over the growing season to better understand how shifts in ET and canopy development affect the partitioning of available energy within the field energy balance. Cumulative estimates of ET were compared across growing seasons and irrigation treatments. The number of days missed due to the instrument deployment and pre-harvest removal averaged 6, 5, and 2 days across both fields for the 2015, 2016, and 2017 growing seasons, respectively. The estimates of cumulative ET were also normalized by DAP to calculate a seasonal ET rate absent of bias incurred by differences in growing season length.

The 2015 growing season was the only growing season where the effects of drying could be compared using simultaneous observations between both fields throughout the entire growing season. In 2016 and 2017, both fields were kept under the same irrigation management, making it impossible to directly compare simultaneous ET observations during drying events occurring in a single field. Instead, comparisons for the 2016 and 2017 growing season provided an opportunity to observe the effects of drying by comparing periods where both fields were either wet or dry to determine the relative impacts of drying events during each month of the growing season. To assess the impacts of drying events on ET, analysis of covariance (ANCOVA) was used to determine if ET was significantly different between fields when one was wet and the other was dry using WD measured in both fields. The comparison was conducted on a monthly basis where "Wet" ($WD_{DF} > 0$ & $WD_{AWD} > 0$) and "Dry" ($WD_{DF} > 0$ & $WD_{AWD} < 0$) categories served as the groupings for ET, where the subscripts indicate the respective field. To remain consistent with other comparisons between fields, this analysis was limited to measurements taken during the daytime (8 AM – 6 PM, local time). For the purposes of this paper, we define a

26

drying event as any period after initial flooding where WD in a field falls below the soil surface for at least 24 hours. The analysis was also limited to AWD drying periods, meaning any data prior to initial flooding and after the beginning of final drainage was not included.

Comparisons between the modeled and observed ET were used to evaluate model performance using residuals analysis. Residuals from regressions between modeled and observed ET were compared to both meteorological and phenological variables within the respective fields to identify periods of higher and lower model performance. The approach would also determine what input variables are critical in determining ET in the U.S. Mid–South production setting as well as identifying variables that could be associated with differences between observed and modeled ET. Moreover, comparing performance across both PM methods allows a test of which methods are better suited for estimating ET and understanding dynamics of ET with respect to the local biometeorology. For the PM–FAO56 method, comparisons between modeled and observed values were limited to days where less than 40% of the original EC data between 8 AM and 6 PM were missing before gap filling using the ANN procedure. This measure was taken to limit the impact of completely gap–filled days while preventing uneven weighting within the non–gap–filled dataset due to quality control based on turbulence and instrumentation limits.

3. Results

3.1 Meteorological observations

Across all growing seasons, the NF and SF sites maintained a mean daily temperature of 24.5 °C with values ranging between 10 °C (early April) and 36 °C (mid–July). Mean daily relative humidity was 80% with values ranging 22–100% during the early growing season (April and May) and 40–100% during the mid–late growing season (June–August) after the flood was applied. The mean daily VPD ranged between 0.5 and 1.7 kPa with maximum values exceeding

27

2.5 kPa during the daytime period (8 AM – 6 PM, local time) with peak values typically

occurring between 4 PM and 6 PM. Wind speed averaged 2.06 m s^{-1} with maximum speeds

exceeding 10 m s^{-1}. Mean incoming solar radiation was 248 W m^{-2} across all growing seasons

with maximum measured values greater than 1000 W m^{-2} occurring between mid-June and early

July, and maximum values typically occurred between 12h and 14h. Comparisons to the 30-year

(1981–2010) average showed that monthly mean temperatures were always within 2 °C of

normal (Runkle et al., 2019). Comparison of precipitation during the growing season months of

April to August showed that all three growing seasons were wetter than the 30–year normal of

492 mm, with 505 mm in 2015, 627 mm in 2016, and 868 mm in 2017. For all three

measurement seasons, 40–60% of the growing season precipitation occurred in April and May.

3.2 Canopy height and LAI

By comparing MODIS data to collected LAI data, we were able to determine a shift from

slow to rapid canopy growth, after emergence and the initial vegetative growth stages (Figure 2).

Due to different planting dates, this transition date varied among growing seasons, occurring

between 40 and 50 DAP. Maximum LAI was achieved in the SF at 103, 89, and 99 DAP and

103, 89, and 94 DAP in the NF during the 2015–2017 growing seasons, respectively. Maximum

LAI for the three respective growing seasons was 5.4, 6.5, and 5.6 for the SF and 4.5, 5.5, and

4.5 for the NF, respectively. Relative to other years, MODIS data for 2016 indicated a more

rapid early growth and higher peak in LAI; while we do not have LAI-2200C measurements in

this year, the canopy height measurements also show higher values.
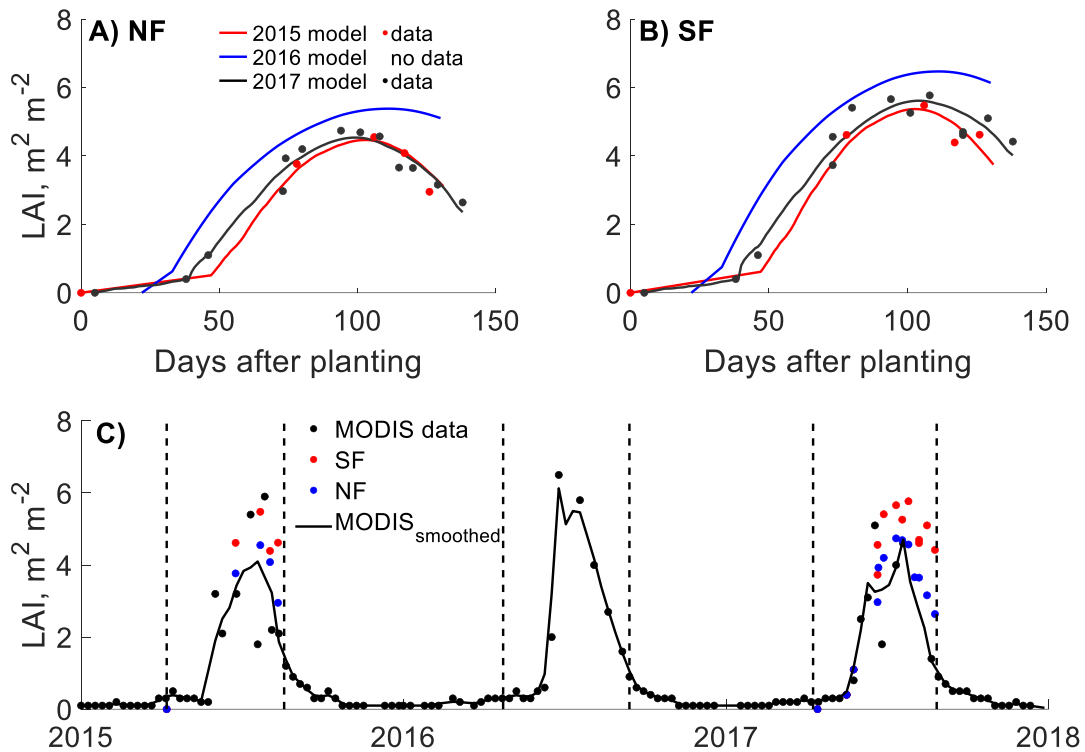
Figure 2. Comparison between measured, GDD–modeled, and remote sensing LAI throughout the 2015–2017 growing seasons at: (A) the North Field (NF) and (B) South Field (SF), including the model in 2016 where LAI was directly scaled from MODIS without using direct measurements. Points displayed represent field observations made by the LAI-2200C; (C) smoothed (n=5) and 8–day unscaled MODIS LAI time series from 2015 through 2017 with measured LAI points from the LAI-2200C for comparison, where black points represent MODIS data points, and dashed lines mark the planting and harvest dates for each year. The standard deviation of individual points ranged between 0.24 and 0.73 m^2 m^{-2} throughout the growing season.

For the 2015–2017 growing seasons, maximum canopy height was reached between 111 and 124 DAP for SF and between 109 and 130 days for NF (Figure 3). Maximum canopy height for NF and SF ranged between 0.95–1.32 m and 0.93—1.24 m, respectively. Similar to observed LAI, the 2016 growing season had a taller canopy during the latter portion of the growing season when the canopy was fully developed. The timing of peak canopy height varied as well, occurring between 105 and 118 DAP across NF and SF, respectively. Based on our estimates of

29

phenological development, both peak LAI and peak canopy height occurred near the end of the

R4 reproductive growth stage and the beginning of grain filling.
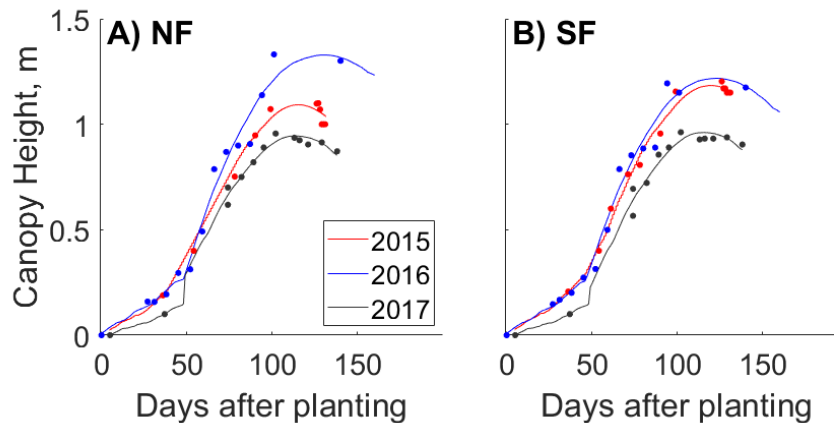
Figure 3. Comparison between measured and GDD–modeled daily canopy height for the 2015, 2016, and 2017 growing seasons for NF (a) and SF (b) using DAP for inter-year comparison. Solid lines are the GDD–derived modeled values, while the dots represent measured values.

3.3 Growing Season ET Estimates and Dynamics in 2015-2017

 The observed and gap–filled growing season ET ranged from 560 to 636 mm across the three

growing seasons in both fields (Table 2). The 2015 growing season showed the lowest

cumulative ET across both fields. From planting to harvest, the lengths of the growing season

were comparable between the fields (i.e., from 0-2 days difference). WD varied throughout each

growing season, especially in the 2015 and 2016 growing seasons where AWD was applied to at

least one field (Figure 4).
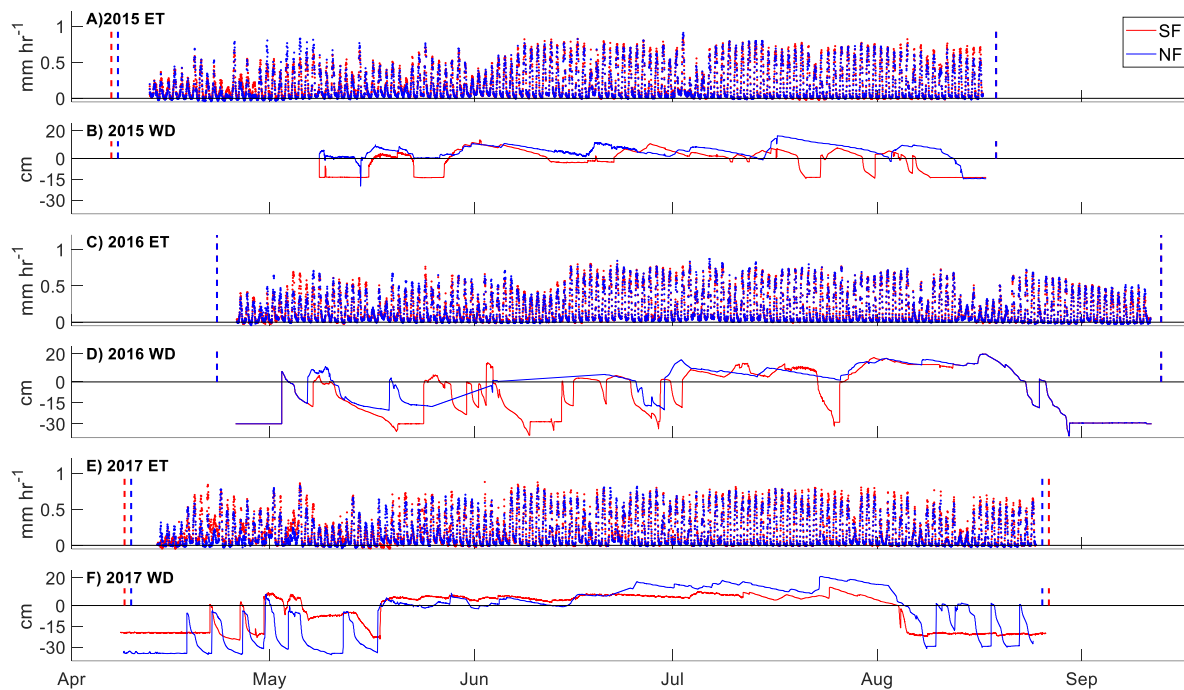
Figure 4. Half-hourly ANN gap–filled eddy covariance ET and water depth (WD) time series for the 2015–2017 growing seasons for NF (blue) and SF (red). Dashed lines mark planting and harvest for NF (blue) and SF (red) (NOTE: The planting date was the same in 2016 for both fields, and harvest dates were the same in 2015 and 2016 for both fields).

For the 2015 and 2016 growing seasons, drying events lasted between 2 to 7 days when irrigation was interrupted, and the flood water was evaporated. The minimum WD during drying events ranged between 2–30 cm below the soil surface prior to re–flooding. The soil moisture sensors at 15 cm below the soil surface indicated up to a 33 percentage-point reduction (saturation to minimum VWC) in VWC during drying events. Volumetric water content measured during drying events in both fields during the 2015 and 2016 growing seasons did not fall below 20% compared to 58% soil moisture at saturation during inundation. The producers reestablished the flood based on presumed soil dryness and observed decline in the water depth, corresponding to a WD of between 25 and 30 cm below the soil surface measured at the EC tower.

Using the gap–filled eddy covariance observations, cumulative growing season ET was calculated for NF and SF for the 2015–2017 growing seasons (Table 2). There were no clear relationships between irrigation treatment and estimated daily ET rate, as AWD and DF fields produced overlapping ranges of estimated daily ET rates during the 2015–2017 growing seasons. There were also no distinguishing patterns when only looking at the daytime ET, therefore irrigation regime did not seem to play a major factor in determining growing season ET for NF and SF during the 2015–2017 growing seasons. Fields under AWD management averaged 609 mm while fields under DF management averaged 595 mm, which were not significantly different. In relation to cumulative seasonal precipitation across both fields during the growing season, ET exceeded growing season precipitation in 2015 and 2016 by as much as 20% while only accounting for up to 78% of growing season precipitation in 2017, when precipitation events were unusually frequent. However, the precipitation event dynamics did not match the crop water requirements and some irrigation applications were necessary to regulate the flood levels.

Table 2. Estimated growing season (GS) ET from gap–filled EC observations, seasonal Daily ET rate, and Daytime ET for NF and SF during the 2015–2017 growing seasons.

Field	Year	Irrigation Treatment	Growing Season ET [mm]	Growing Season Length [days]	Avg. Daily ET Rate [mm day^{-1}]	Growing Season Precipitation [mm]
	2015	DF	551 ± 7.1	133	4.14	500
NF	2016	AWD	601 ± 10.5	143	4.20	556
	2017	DF	628 ± 6.9	138	4.55	795
	2015	AWD	598 ± 14.0	134	4.46	500
SF	2016	AWD	604 ± 9.7	143	4.22	556
	2017	DF	579 ± 13.4	140	4.13	795

Next, we compared treatments at the half hourly time step to test the effects of AWD and DF on ET across both fields for the 2015–2017 growing seasons using ANN gap–filled half–hourly ET. The period of observation was limited to daytime values between 8 AM and 6 PM to prevent uneven weighting from nighttime periods. This comparison also confirms, despite having different irrigation regimes, there were no significant differences in ET during the 2015 growing season (Figure 5). Comparisons of ET measured in 2016 and 2017, when both fields were in the same irrigation treatment, showed similar results as well. In addition, these results did not change significantly when only observed values (i.e., not gap–filled data) were used for comparison.
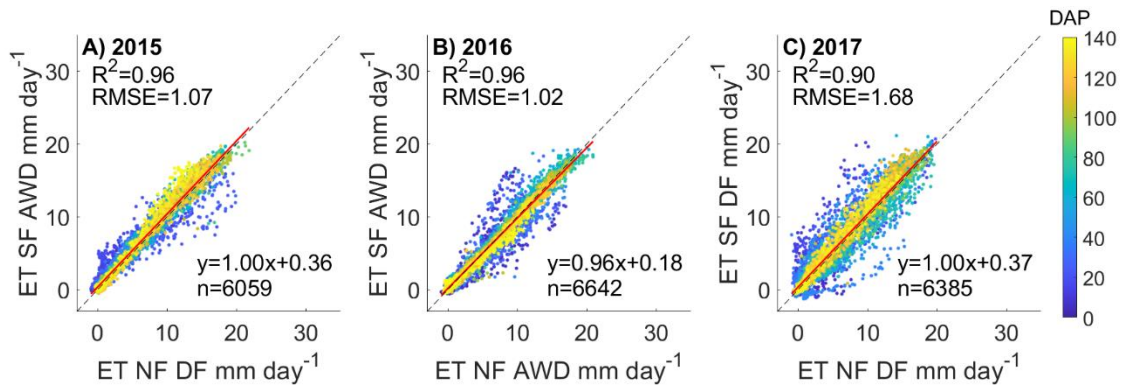
Figure 5. Comparison of half-hourly ANN gap–filled eddy covariance evapotranspiration (ET) between the South Field (SF) and North Field (NF) during the 2015–2017 growing seasons, where the irrigation treatments are indicated (Alternate wetting and drying, AWD; Delayed Flood, DF). Points are colored by days after planting (DAP) (Note: In 2017, SF was planted a day earlier than NF, but the coloring represents DAP for SF only).

NF showed consistently similar LE compared to SF. In 2016, NF had slightly higher ET based on a linear regression slope of 0.96. The slopes of each regression were significant with the slope standard error across all three comparisons, never exceeding 0.00042. For comparisons between NF and SF across 2015–2017, RMSE ranged between 1.02 to 1.68 mm day^{-1} with a majority of the divergence occurring earlier in the growing season. The divergence in ET during

the early growing season, when the soil water or water evaporation components dominate the ET process, was due to different planting and flooding schedules for each field. Events where one field was flooded first before the other indicate higher ET, and these events are especially common during the early growing season (e.g., the cluster of points in Figure 5c extending to 16 mm day^{-1} in NF and 8 mm day^{-1} in SF). Typically, once the canopy was established, the fields converged in terms of ET and continued to do so through closure until they were drained for harvest. Based on our observations, development and closure of the rice canopy clearly reduced the impact of factors of change in ET between both fields, including factors related to their respective irrigation treatments such as water level or soil moisture.

There were no significant differences in the measured RN between NF and SF across all three growing seasons. The majority of ET was driven by RN with the ratio of LE to RN throughout the growing seasons ranging between 0.71 and 0.85. For individual months, particularly July and August, LE measured between 55–75% of RN while in early periods of the growing season (April and May), LE ranged between 24 and 51% of RN. The ratio of H to RN consistently decreased from the beginning of the growing season until pre–harvest draining, when the ratio of H to RN increased in most cases. Given that the variation of RN was minimal during the growing season, this decrease in the ratio of H to RN was most likely due to the increase in LE associated with flooding, canopy development, and greater amounts of transpiration.

3.4 Effects of AWD on ET in Eddy Covariance Observations

In order to test the effect of AWD on ET variation due to changing flood water availability for evaporation, parts of the 2015 growing season with drying events in SF and inundation in NF field were used to compare the simultaneous ET values. The length of drying

34

events was consistently around 1 week. Our results indicate that prior to canopy development

and closure, specifically in May 2015 when dry and wet conditions were being compared

directly, there is a significant difference ($p<0.05$) in measured ET (Table 3). While there were

significant differences in ET, these drying events were not carried out as part of an AWD

treatment as the first permanent flood had yet to be established.

Table 3. ANCOVA analysis of NF vs. SF ET observations across different hydrological scenarios throughout the growing season. Values are slopes between a number, n, of simultaneous 30–min ET estimates in each field. "Wet Condition" refers to periods when both fields are wet, defined as having a water level above the soil surface in both fields. "Drying Condition" refers to periods where drying occurred in one or both fields with drying considered as a decline in the WD below the soil surface for given field(s).

Year	Month	Number of AWD drying events		Total duration of drying events, days[1]		Wet Condition slope (n)	Drying Condition slope (n)
		NF	SF	NF	SF		
2015	May	0	1	0	5	1.05 (110)	0.91 (34)*
	June	0	2	0	10	1.01 (124)	1.06 (152)
	July	0	2	0	8	0.96 (286)	0.96 (22)
	August	0	1	0	1	0.91 (18)	
2016	May	0	0	0	0	0.75 (18)	
	June	1	3	4	7	0.85 (63)	0.99 (31) †
	July	0	1	0	3	0.93 (262)	
	August	0	0	0	0	0.93 (161)	
2017	May	1	0	2	0	0.77 (36)	
	June	2	0	4	0	0.99 (170)	
	July	0	0	0	0	1.01 (293)	
	August	0	0	0	0	1.04 (15)	

[1] Total duration of drying event does not include period prior to first flooding or drainage period in late growing season, rounded to the nearest day based on half–hourly WD data.
* Denotes significantly different "Drying Condition" slope compared to "Wet Condition" slope
† Marks comparisons of drying condition where both fields were dry (i.e., not 2015)

In May 2015, the slope of 0.91 indicates that drying period ET was 9% greater in the

inundated NF compared to the non-flooded conditions in SF. During this period, both fields did

not have a developed canopy, and one drying event had occurred. While we do not consider the

significant differences in ET to be a direct result of the AWD treatment in NF, analysis between

the residuals taken from the initial field–to–field regression and the declining WD in SF

indicated that the drying was able to significantly explain only up to 5% of ET residual variance.

All other months during the 2015 growing season indicated no significant difference in observed

ET across all hydrological conditions, and declining WD in the drying field was unable to

explain any significant differences observed in ET between NF and SF. We suspect that

differences occurring early in the growing season are substantially influenced by precipitation as

well in altering the plant canopy response with respect to ET. Additionally, in this farm setting,

precipitation can be managed in a way that water is actively drained between fields along a

designated flow path (NF to SF) to prevent unsuitable growth conditions for the crop during

early growth stages.

The canopy development stages explain the convergence of ET between the two fields

and the inability of changes in WD to explain significant differences in ET during the latter

portion of the growing season. Because both canopies were similar in structure and showed no

decreases in yield associated with drying events in 2015, we can conclude that plant–mediated

transpiration was likely similar in both fields. As the canopy continued to develop, the

contributing portion of transpiration to ET increased, resulting in similar ET rates across both

fields when the canopy was fully closed and developed. Canopy cover also likely exercised

control over open water surface evaporation through shading, meaning the contributing portion

of evaporation to ET likely decreased as well. This would result in insensitivity to ET and

differences between fields with respect to water level.

In 2016 and 2017, there were no periods where only one field was dry since both fields

were treated in AWD and DF, respectively. The columns in Table 3 for these years are therefore

36

during periods when both are dry. During the 2016, slopes from the "All Wet" case did not significantly differ from slopes in the "All Dry" case across the growing season. Under both conditions, NF appeared to always have greater ET compared to SF despite both fields undergoing the same treatment. Measured ET between both fields seemed to agree more during dry periods, but these slopes were not significantly different from their wet counterpart during each individual month. In 2017, when both fields were managed with DF throughout the entire growing season, the comparison indicated no significant differences in slopes from the comparison between wet and dry periods. Flooded conditions made it impossible to perform dry period analysis in June and July of 2017 as well. Based on the observations in 2016–2017, we can infer wetting and drying did not play a significant role in influencing differences in ET across both fields, meaning the field effect based on changing WD does not play a consistent, significant role in our ET comparisons. This finding supports our observation of similar ET between fields regardless of WD management across all growing seasons. The change in slope between NF and SF ET rates also indicated that the fields continued to converge on similar ET as the canopy developed during the growing season as the slope drew nearer to a value of 1 with each successive month. Given that both fields were treated using the same irrigation method in 2016 and 2017, this similarity was expected and supports the concept of decreasing impacts of changing WD and associated soil water evaporation throughout the growing season as canopy transpiration dominates the ET flux.

 3.4 Modeling canopy conductance for the 2015–2017 growing seasons.

Canopy conductance estimated using eddy covariance measurements for LE and the inverted Penman–Monteith equation was estimated using the full 2015–2017 dataset (including both NF and SF). Maximum applied surface conductance from the 7–day moving window ranged

37

between 8 and 70 mm s^{-1} across both fields for the 2015–2017 growing seasons with peak values occurring during periods characterized by increased canopy height and LAI. Parameterization was performed for individual site seasons and across all six site-years combined. The parameters and standard error were estimated for each growing season as well as the combined period of all growing seasons (Table 4).

Table 4. Fitted parameters for the individual and combined growing seasons across NF and SF for 2015–2017. Standard error estimates in parentheses were derived from the MSE for each parameter associated with the regression; RMSE is presented in terms of the LE flux (where 28 W m^{-2} is approx. equivalent to 1 mm ET)

	Year	a_1 [W m^{-2}]	a_2 [kPa^{-1}]	a_3 [°C^{-2}]	Mean $g_{s,max}$ [mm s^{-1}]	RMSE [W m^{-2}]
	2015	2445 (85)	0.14 (0.02)	0.005 (0.0003)	30	23.50
NF	2016	2522 (189)	0.04 (0.06)	0.007 (0.0004)	24	34.48
	2017	1367 (80)	0.26 (0.02)	0.005 (0.0008)	22	32.11
	2015	1542 (63)	0.26 (0.02)	0.006 (0.0005)	32	30.16
SF	2016	2169 (130)	0.33 (0.00)	0.000 (0.0012)	20	40.26
	2017	826 (85)	0.31 (0.04)	0.006 (0.0009)	19	27.77
NF+SF	2015–2017	1659 (30)	0.31 (0.00)	0.003 (0.0003)	28	34.88

3.5 Modeling ET for the 2015–2017 growing seasons using PM–AET

After parameterization with 70% of the data during calibration with data from across all six field–seasons, the calibrated model performed well against the remaining data as a validation set. The parameterized PM equation was able to estimate half–hourly ET with high correlation (R^2=0.84; m=1 ± 0.0015 mm day^{-1}; RMSE=2.12 mm day^{-1}) during daytime periods of the growing season across all six site–years. Within each individual growing season, model performance was varied across each irrigation comparison scenario, but was still able to explain similar amounts of variance (Figure 6).
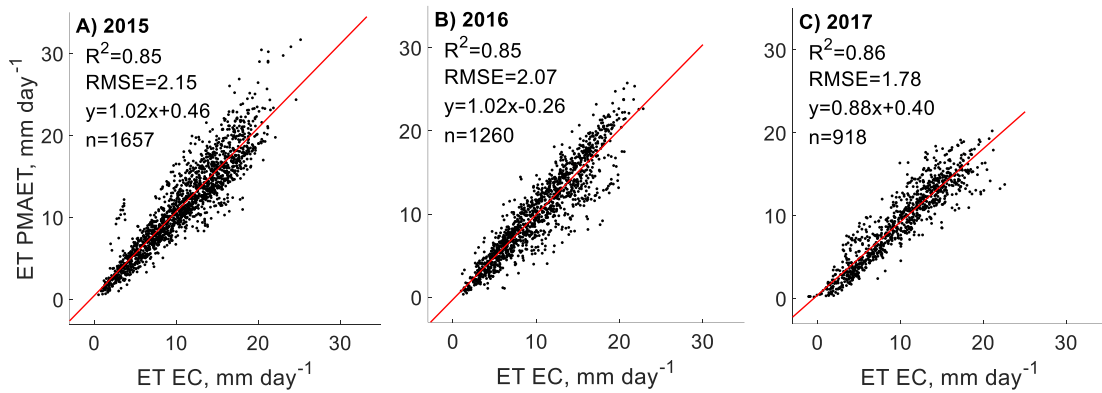
Figure 6. Comparison of half-hourly PM model to non–gap–filled EC observations during the daytime period (8 AM to 6 PM, local time) across the 2015–2017 growing seasons and observations from both fields are plotted together.

Analysis of model performance across the growing season indicated that the largest portion of variance between model and observation was during the early portion of the growing season (<40 DAP) when the active fraction of LAI was the lowest. General performance across all three growing seasons was inconsistent as the model both overestimates ET by 2% in 2015 and 2016 and underestimates ET by 12% in 2017. During the 2017 growing season, there was greater precipitation than 2015 and 2016, which could explain the model's inability to accurately reflect changes in canopy ET in response to rain events and an elevated moisture status. A two–sample t–test indicated that mean $g_{s,max}$ estimated across 2017 was significantly (p<0.05) lower than mean $g_{s,max}$ in 2015 and 2016 by as much as 60%.

3.6 Modeling ET for the 2015–2017 growing seasons using PM–FAO56

The PM–FAO56 method was applied to the 2015–2017 growing season measurements at the daily time scale and compared to daily ET measured using EC. Because we did not observe noticeable differences in ET between NF and SF for all three growing seasons (the average daily difference was only 0.027 mm), an average ET representing both fields was used when comparing to the FAO56 estimates at the daily time step. Estimates from the PM–FAO56

approach were consistently higher than EC estimates with cumulative seasonal ET amounts at 607, 709, and 660 mm for the 2015–2017 growing seasons, respectively. These values were 8, 105, and 81 mm greater than the seasonal ET as directly measured by the EC. Adjusted estimates of ET from the FAO56 method for the 2015–2017 growing seasons were 611, 698, and 651 mm, which are 13, 94, and 72 mm higher from the observed seasonal values, respectively. The estimated crop coefficient curve was shown to vary greatly throughout the growing season when compared to the FAO56 recommended values, including cases where the coefficient was adjusted for nonstandard conditions (Figure 7).
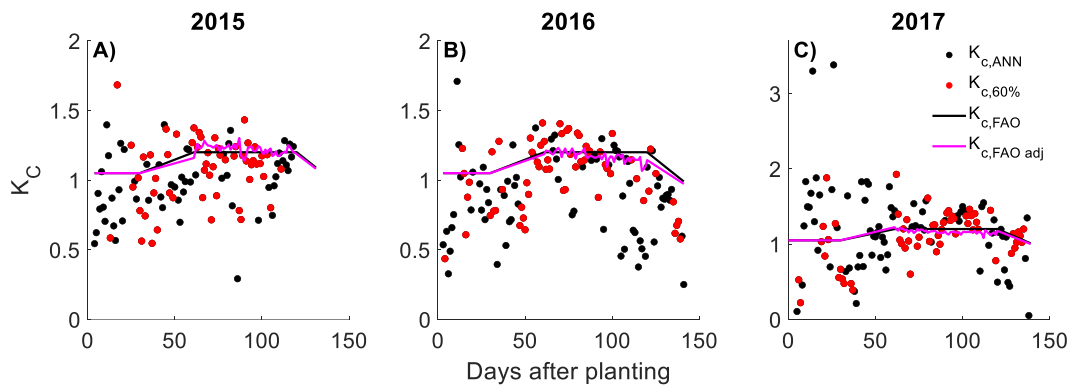
Figure 7. Comparison of FAO56 recommended and adjusted crop coefficient (black and pink lines, respectively) and estimated crop coefficient (K_c) using eddy covariance ET (black data points) for SF and NF during the 2015–2017 growing seasons (note change of scale for 2017). Red data points represent K_c values where more than 60% of the daytime (8 AM to 6 PM, local time) non–gap–filled EC ET data was available to help interpret the impacts of using only gap–filled data (Note y-axis scale change on C)

The agreement between estimated and recommended K_c values was poor throughout the growing season. When comparing values of K_c derived from gap–filled EC data to recommended values, daily values could vary as much as 80% higher or lower than the recommended values. Compared to data points from days containing less gap filling, variance is reduced by 40% in estimated K_c across the growing season, but individual K_c values are still underestimated up to

40

79% and overestimated up to 80% across both the recommended and adjusted K_c values. Using

only the non–gap–filled EC derived K_c (red points in Figure 7) across 2015-2017, we estimate

the $K_{c, ini}$, $K_{c,mid}$, and $K_{c,end}$ to be 0.94 ± 0.03, 1.16 ± 0.02, and 0.95 ± 0.11, respectively.

Variability between the recommended and observed crop coefficients was noticeable in the early

growing season due to the difference in irrigation practices between the FAO recommendation

and our field site as mentioned in the methods, but values were within an acceptable margin of

error for the mid and late growing seasons. When comparing ET rates between the PM-FAO56

method and the EC towers using data, we excluded data points from the initial 60 days to remove

the variance introduced from $K_{c, ini}$. We also limited observation to only include periods where

greater than 60% of the measured daytime (8 AM to 6 PM, local time) ET was present to reduce

the amount of uncertainty introduced by ANN gap-filling (Figure 8).
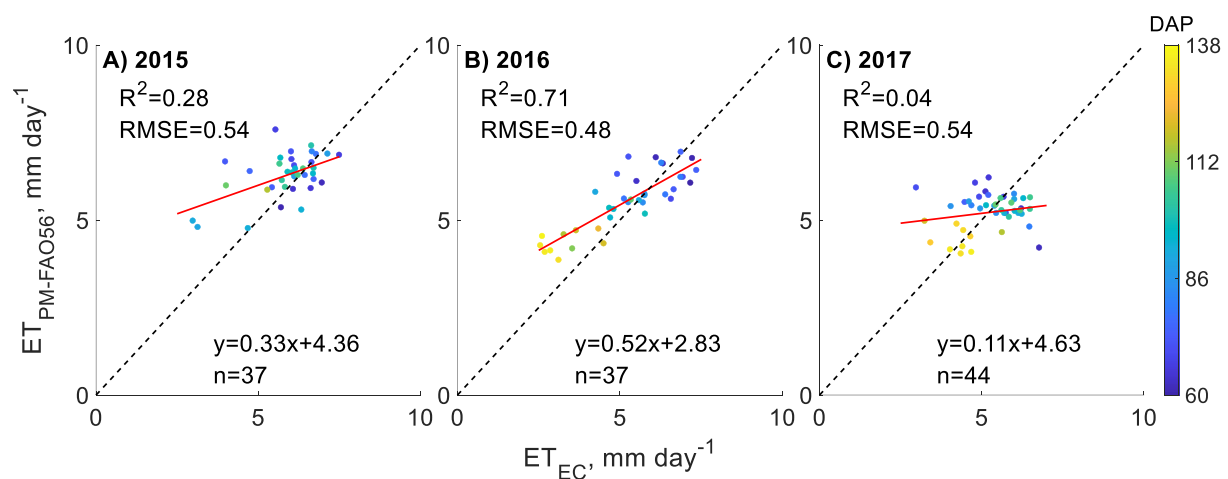
Figure 8. Comparison of PM-FAO56 to EC-derived, gap-filled daily ET during the mid to late growing season across the 2015-2017 growing seasons. Points are colored by DAP.

Our results indicated no clear seasonal pattern to increased performance of the PM-

FAO56 method when considering only the mid and late growing season. Across all growing

seasons, we observed a consisted overestimation of ET during the late season period (DAP>115)

41

in 2015 and 2016, but mid-season performance varied from year to year. The adjusted crop

coefficients (not shown) provided no improvement when compared to the same EC observations.

Similar to the PM-AET approach, we suspect that increased precipitation and regional

differences in growth conditions between our site and the reference site could have resulted in an

irregular canopy response and altered ET from both fields during the growing season. We

observed the best performance of the PM-FAO56 method when both fields were under AWD

treatment and the amount of precipitation was noticeably less than in 2017 (Table 2).

4. Discussion

4.1 Comparing ET across irrigation regimes

Mean growing season ET was estimated to be between 4.14 and 4.55 mm day^{-1} for DF

and between 4.20 and 4.46 mm day^{-1} for AWD using gap–filled eddy covariance estimates.

Thus, this is additional evidence that ET rates do not significantly differ between the different

treatments. Other studies have indicated a similar range of mean growing season ET when

compared to other conventional systems involving continuous flooding and AWD both

domestically and internationally (Table 5). Based on this literature synthesis across methods,

climate conditions, and production settings, estimated growing season ET ranged between 411

and 889 mm with daily ET rates ranging from 3.31 to 7.87 mm day^{-1} (Table 5). When EC was

used to measure ET directly, the range narrowed to 485 mm to 636 mm with measured daily ET

between 3.50 and 4.65 mm day^{-1}. When only comparing studies reporting DAP, the median

growing season ET was 653 mm with an equivalent ET rate of 4.87 mm day^{-1}. Other methods,

including the PM model, showed a much larger range of ET from 499 mm to 762 mm with

estimated daily ET ranging between 4.05 and 4.65 mm day^{-1}. Variation in estimated rates was

likely linked to differences in climate conditions, method, and possibly production practices such

as transplanting, which changes the scope or range of observation compared to direct seeding (Naklang et al., 1996; Tuong & Bhuiyan, 1999). With respect to metrics such as derived daily ET rate, the number of days after transplanting or direct seeding indicate different growth phases that can potentially differ in productivity (Dingkuhn et al., 1991).

Table 5. Cumulative ET estimates and estimated daily ET rate during the growing season for different studies estimating ET in rice agriculture; EC is eddy covariance, PM is Penman–Monteith AET, PM–FAO56 is PM as defined in FAO56).

Seasonal ET (mm)	Growing Season Length (Days)	Equivalent Rate (mm day^{-1})	Location	Transplanted	Method	Study
813	122	6.66	CA–Water Seeded	No		
889	113	7.87		No		
856	115	7.44		No	Energy balance residual	Linquist et al., 2015
873	134	6.51	CA–Dry Seeded	No		
865	112	7.72		No		
875	116	7.54		No		
670	116	5.76	Namibia	Yes	Penman Monteith	Kotani et al., 2017
548	100	5.48	Hyderabad, India	Yes	Pan evaporation	Mote et al., 2018
499	117	4.25	IRRI	No	EC, PM	Alberto et al., 2014
562	132	4.26	Brazil	No	EC	
593	132	4.49	Brazil	No	PM	Timm et al., 2014
596	132	4.52	Brazil	No	PM–FAO56	
411	124	3.31	Japan	Yes	Lysimeter	Shimono et al., 2013
485	113	4.29	IRRI–Flooded	Yes	EC, PM	Alberto et al., 2011
506	133	3.8	IRRI–AWD	Yes		
568	122	4.66	Italy-DF	No		
678	122	5.56	Italy-DF	No	PM	Facchi et al., 2013
691	120	5.76	Italy-AWD	No		
419–534	120	3.5–4.4	Japan	Yes	EC	Ikawa et al., 2017
595	147	4.05		No		
762	164	4.65		No		
677	164	4.13	Brazil	No	EC	Diaz et al., 2019
733	162	4.52		No		
716	154	4.65		No		
693	168	4.13		No		
551	133	4.14		No		NF, 2015
601	143	4.20		No		NF, 2016
628	138	4.55	Arkansas (this study)	No	EC	NF, 2017
598	134	4.46		No		SF, 2015
604	143	4.22		No		SF, 2016
579	140	4.13		No		SF, 2017

4.2 The effects of AWD on ET during the 2015 growing season

In our study, ET rates measured using eddy covariance showed no significant differences across the entire growing season and no significant differences during drying events when ET

44

was expected to change due to the decline in WD. Regarding the drying events, neither field experienced major declines in volumetric water content (<20% VWC) that significantly influenced differences in ET between NF and SF. Studies conducted on field plots containing poorly drained clay soils have also reported similar results. Significant levels of drying relative to the study soils still yielded no significant differences in AWD and control yields (Carrijo et al., 2018; Norton et al., 2017). Because we observed no significant differences in yield quality or quantity between the treatments (Runkle et al., 2019), we assume with confidence that the plants were not significantly inhibited by water stress in grain production and associated transpiration. Thus, a large portion of ET remained unaffected by the AWD treatment. Additionally, the rice grown in both fields (XL745) was a hybrid variety associated with high nutrient efficiency and water–use efficiency to produce comparable yields in water–limited conditions (Lopez et al., 2018). The combination of limited drying and the rice variety likely explained the lack of response in ET to drying events in both fields.

4.3 Modeling conductance using inverted PM

Across the daytime period, the estimated canopy conductance values from the inversion of the Penman–Monteith equation showed values ranging roughly between 3 and 33 mm s^{-1}, which are similar to other studies estimating canopy conductance in rice across a number of studies (Table 6).

Table 6. Comparisons of estimated rice canopy conductance ranges under different production practices reported in studies

Conductance range [mm s^{-1}]	Irrigation Style	Location	Method	Author(s)
4 to 16	Controlled irrigation	Japan	Inverted PM & EC (daily mean over 5–day period in late season)	Harazano et al., 1998
0 to 20	Flooded	Japan (Saito)	Dual–Source Heat transfer model (based on seasonal observations)	Marayuma & Kuwagata, 2008
0 to 20	Flooded	Japan (Saga)		
0 to 30	Flooded	Japan (Aso)		
16.55 ± 8.99	Flooded	Philippines (2008, Dry Season)		
8.85 ± 4.51	Aerobic (AWD)	Philippines (2008, Dry Season)		
12.47 ± 6.39	Flooded	Philippines (2008, Wet Season)		
9.82 ± 4.34	Aerobic (AWD)	Philippines (2008, Wet Season)	Inverted PM & EC (seasonal mean)	Alberto et al., 2011
14.86 ± 7.12	Flooded	Philippines (2009, Dry Season)		
8.91 ± 3.35	Aerobic (AWD)	Philippines (2009, Dry Season)		
18.24 ± 7.98	Flooded	Philippines (2009, Wet Season)		
9.44 ± 3.59	Aerobic (AWD)	Philippines (2009, Wet Season)		
0 to 16.86	DF	NF (2015)		
1.5 to 20.5	AWD	SF (2015)		
0 to 15.56	AWD	NF (2016)	Inverted PM & EC (seasonal mean)	This study
0 to 14.09	AWD	SF (2016)		
0 to 13.53	DF	NF (2017)		
0 to 15.94	DF	SF (2017)		

Canopy conductance estimates from various studies (Table 6) show comparable ranges to the current study, between 0 and 21 mm s^{-1} during the growing season. Daily maximum conductance estimated from half hourly data throughout growing seasons ranged between 24 mm s^{-1} (2016) and 28 mm s^{-1} (2015) for NF and 20 mm s^{-1} (2016) and 33 mm s^{-1} (2017) for SF with peak values occurring between 1 PM and 5 PM for both fields when the canopy is most active. However, based on comparisons between the model and the initial estimates of conductance, the model was not able to accurately estimate conductance at any given time. A comparison of initial

conductance estimates from the inverted PM–AET and known drivers of ET, such as net radiation and VPD, showed no apparent relationships during the daytime period throughout the growing season. While the parameterized model was able to give some definition to the relationships between environmental drivers and conductance across each growing season, our results indicated that the rice canopy faced no apparent limitation based on VPD, available energy, or temperature with respect to conductance. However, the parameterized conductance was still able to generate more consistently accurate estimates of LE when compared to using a static monthly value for canopy conductance in the Penman–Monteith equation.

4.4 Improving PM–AET and PM–FAO56

In this study, the PM–AET approach was able to estimate ET effectively across the growing season at the half–hourly time step. Because the model was constrained based on time of day due to the conductance modeling, ET estimates generated outside of the primary period are considered less reliable and less valuable when describing mechanistic relationships between drivers and associated ET. During the growing season, the canopy consistently experienced elevated levels of humidity (>80%) during the daytime period, reducing the overall atmospheric demand of water. We were also unable to detect significant responses in modeled stomatal conductance to changes in temperature and VPD, meaning the plants were not stressed despite the elevated temperatures and increased VPD. Available energy was the primary driver of ET throughout the growing season as evidenced through both direct observations and the use of the PM–AET, where measured available energy was able to explain a significant amount of the variance in ET residuals between both fields. Regarding our hypotheses, we did not see any significant amount of variance between modeled and observed ET explained using soil moisture or water level across a variety of conditions in each growing season. As mentioned previously

47

when addressing the effects of AWD, the canopy did not experience significant levels of drying below 40% VWC. Thus, while we did not see a significant response, low soil moisture is known to impact canopy health (Carrijo et al., 2018). Additionally, the PM–AET method generated acceptable estimates of ET during the growing season regardless of irrigation regime.

Regarding the PM–FAO56 approach, it was clear that the current methodology was able to produce comparable estimates of ET in 2015, but the model performance was inconsistent across the 2016 and 2017 growing seasons based on the comparison of cumulative ET amounts between the PM-FAO56 approach and the EC measurements. When observing the PM-FAO56 daily ET rates during the mid to late growing season, we saw the best performance in 2016, when both NF and SF were under AWD. Contrastingly, the model performance was poorest in years the precipitation was greater (2017) or the fields were kept under different management strategies (2015). Across the growing season, the estimated K_c and recommended K_c were more similar in the mid to late growing season. The dissimilarity between the estimated and recommended $K_{c,ini}$ was likely due to the difference in production settings over which the coefficients were estimated. Water seeded rice production applies a substantially greater amount of water to the field during the early growing season compared to the drill seeding approach used in our experiments. Under flooded conditions at planting, the resulting ET would be higher compared to dry soil present in drill seeded rice, meaning the ratio of crop ET to reference ET would also be greater in the flooded field. This effect was reduced as the canopy developed in the later portion (DAP>60) of the growing season, where variance was almost 50% less in the regression between EC derived values for $K_{c,mind}$ and $K_{c,end}$ and the recommended FAO56 values.

However, the early growing season does not represent a period of time where producers are actively concerned with irrigation applications as the first flood has not been applied yet.

Producer interest in using ET to schedule irrigation events would likely be tied to the mid and late growing season, when plant water availability is critical to maintaining profitable yields (Hardke, 2013). Local climate likely played a role in differences in crop coefficient as the recommended crop coefficients were generated under climates that are less humid (Doorenbos et al., 1977; Doorenbos and Kassam, 1979). Considering our findings, we recommend that improvements to the method should include regional or site–specific crop coefficient development to better account for differences in production practices, such as water seeding vs. drill seeding. For practical applications, the PM-FAO56 method could still be a viable option for producers to estimate ET and schedule irrigation events.

The PM–AET model was able to perform well as a method for gap filling LE fluxes at the half hourly time step. Based on our results with the PM–AET, capturing the amount of available energy as the difference between the net radiation and G is a critical component of estimating ET as demonstrated in our experiment. Because available energy represents such a large portion of ET in our production settings, less complex ET estimation methods such as the Priestley–Taylor (also a PM derivative) and the Hargreaves equation could prove to be valuable. Other studies based in rice across varying production systems have also identified available energy as the driving factor of ET in rice paddy systems with the ratio of LE to RN ranging from 71 to 74% during the typical growing period under flooded conditions (Hossen et al., 2011; Timm et al., 2014; Liu et al., 2019). While establishing robust methodology and application of tools is complex and multifaceted, development of methods for estimating ET at the canopy scale provides valuable information to better inform producers. Exploration and improved knowledge of modeling limitations and controls at the field scale can serve as a point of

comparison for larger scale applications of ET modeling using remote sensing (Jiang & Ryu, 2016; Fisher et al., 2020).

5. Conclusions

Based on this experiment's findings, the use of AWD as an irrigation treatment showed no significant effect on ET when compared to the conventional DF practice. The treatments showed no significant differences in yields, meaning that there was not significant water stress associated with drying events. If taken as a plant health indicator, ET was not affected and leads us to conclude that the plants did not experience drought stress and could still access sufficient water within the soil as VWC did not fall below 20% during drying events. We were able to use the PM–AET approach and conductance model to estimate half-hourly ET across the growing season. The model has potential to continue to provide mechanistic insight on driving environmental variables during different portions of the growing season with respect to ET. As seen in the comparison of field and recommended Kc, the PM–FAO56 method did not yield strong results. We conclude that site-specific crop coefficient values are necessary to generate accurate crop coefficient values, especially during the early growing season. However, we also recognize that in practical application, ET during the mid-to-late growing season is more valuable for planning irrigation based on field ET estimates.

6. Acknowledgements

Chapter 1: References

Alberto, Ma.C.R., Quilty, J.R., Buresh, R.J., Wassmann, R., Haidar, S., Correa, T.Q., Sandro, J.M., 2014. Actual evapotranspiration and dual crop coefficients for dry–seeded rice and hybrid maize grown with overhead sprinkler irrigation. Agricultural Water Management 136, 1–12. https://doi.org/10.1016/j.agwat.2014.01.005

Alberto, Ma.C.R., Wassmann, R., Hirano, T., Miyata, A., Hatano, R., Kumar, A., Padre, A., Amante, M., 2011. Comparisons of energy balance and evapotranspiration between flooded and aerobic rice fields in the Philippines. Agricultural Water Management 98, 1417–1430. https://doi.org/10.1016/j.agwat.2011.04.011

Allen, R.G., Pereira, L.S., Raes, D., Smith, M., 1998. Crop evapotranspiration – Guidelines for computing crop water requirements – FAO Irrigation and drainage paper 56. FAO, Rome 300, D05109.

Carrijo, D.R., Akbar, N., Reis, A.F.B., Li, C., Gaudin, A.C.M., Parikh, S.J., Green, P.G., Linquist, B.A., 2018. Impacts of variable soil drying in alternate wetting and drying rice systems on yields, grain arsenic concentration and soil moisture dynamics. Field Crops Research 222, 101–110. https://doi.org/10.1016/j.fcr.2018.02.026

Carrijo, D.R., Lundy, M.E., Linquist, B.A., 2017. Rice yields and water use under alternate wetting and drying irrigation: A meta–analysis. Field Crops Research 203, 173–180. https://doi.org/10.1016/j.fcr.2016.12.002

Collatz, G.J., Ball, J.T., Grivet, C., Berry, J.A., 1991. Physiological and environmental regulation of stomatal conductance, photosynthesis and transpiration: a model that includes a laminar boundary layer. Agricultural and Forest Meteorology 54, 107–136. https://doi.org/10.1016/0168–1923(91)90002–8

Diaz, M.B., Roberti, D.R., Carneiro, J.V., Souza, V. de A., de Moraes, O.L.L., 2019. Dynamics of the superficial fluxes over a flooded rice paddy in southern Brazil. Agricultural and Forest Meteorology 276–277, 107650. https://doi.org/10.1016/j.agrformet.2019.107650

Dingkuhn, M., Schnier, H.F., De Datta, S.K., Dorffling, K., Javellana, C., 1991. Relationships between ripening–phase productivity and crop duration, canopy photosynthesis and senescence in transplanted and direct–seeded lowland rice. Field Crops Research 26, 327–345. https://doi.org/10.1016/0378–4290(91)90009–K

Doorenbos, J., Kassam, A., 1979. Yield response to water. Irrigation and Drainage 257, 33.

Doorenbos, J., Pruitt, W.O., 1977. Crop water requirements. FAO irrigation and drainage paper 24. Land and Water Development Division, FAO, Rome 144.

Ershadi, A., McCabe, M.F., Evans, J.P., Wood, E.F., 2015. Impact of model structure and parameterization on Penman–Monteith type evaporation models. Journal of Hydrology 525, 521–535. https://doi.org/10.1016/j.jhydrol.2015.04.008

Facchi, A., Gharsallah, O., Chiaradia, E.A., Bischetti, G.B. and Gandolfi, C., 2013. Monitoring and modelling evapotranspiration in flooded and aerobic rice fields. Procedia Environmental Sciences, 19, pp.794-803.

Fisher, J.B., Lee, B., Purdy, A.J., Halverson, G.H., Dohlen, M.B., Cawse-Nicholson, K., Wang, A., Anderson, R.G., Aragon, B., Arain, M.A., Baldocchi, D.D., Baker, J.M., Barral, H., Bernacchi, C.J., Bernhofer, C., Biraud, S.C., Bohrer, G., Brunsell, N., Cappelaere, B., Castro-Contreras, S., Chun, J., Conrad, B.J., Cremonese, E., Demarty, J., Desai, A.R., Ligne, A.D., Foltýnová, L., Goulden, M.L., Griffis, T.J., Grünwald, T., Johnson, M.S., Kang, M., Kelbe, D., Kowalska, N., Lim, J.-H., Maïnassara, I., McCabe, M.F., Missik, J.E.C., Mohanty, B.P., Moore, C.E., Morillas, L., Morrison, R., Munger, J.W., Posse, G., Richardson, A.D., Russell, E.S., Ryu, Y., Sanchez-Azofeifa, A., Schmidt, M., Schwartz, E., Sharp, I., Šigut, L., Tang, Y., Hulley, G., Anderson, M., Hain, C., French, A., Wood, E., Hook, S., 2020. ECOSTRESS: NASA's Next Generation Mission to Measure Evapotranspiration From the International Space Station. Water Resources Research 56, e2019WR026058. https://doi.org/10.1029/2019WR026058

Fuchs, M., Tanner, C.B., 1968. Calibration and Field Test of Soil Heat Flux Plates. Soil Science Society of America Journal 32, 326–328. https://doi.org/10.2136/sssaj1968.03615995003200030021x

Gardiol, J.M., Serio, L.A., Della Maggiora, A.I., 2003. Modelling evapotranspiration of corn (Zea mays) under different plant densities. Journal of Hydrology 271, 188–196. https://doi.org/10.1016/S0022–1694(02)00347–5

Gharsallah, O., Facchi, A. and Gandolfi, C., 2013. Comparison of six evapotranspiration models for a surface irrigated maize agro-ecosystem in Northern Italy. Agricultural Water Management, 130, 119-130.

Graham-Acquaah, S., Siebenmorgen, T.J., Reba, M.L., Massey, J.H., Mauromoustakos, A., Adviento-Borbe, A., January, R., Burgos, R., Baltz-Gray, J., 2019. Impact of alternative irrigation practices on rice quality. Cereal Chemistry 96, 815–823. https://doi.org/10.1002/cche.10182

Hardke, J., 2013. Arkansas Rice Production Handbook – MP192.

Hargreaves George H., Allen Richard G., 2003. History and Evaluation of Hargreaves Evapotranspiration Equation. Journal of Irrigation and Drainage Engineering 129, 53–63. https://doi.org/10.1061/(ASCE)0733–9437(2003)129:1(53)

Henry C. G., Hirsh S. L., Anders M. M., Vories E. D., Reba M. L., Watkins K. B., Hardke J. T., 2016. Annual Irrigation Water Use for Arkansas Rice Production. Journal of Irrigation and Drainage Engineering 142, 05016006. https://doi.org/10.1061/(ASCE)IR.1943–4774.0001068

Horst, T.W., Semmer, S.R., Maclean, G., 2015. Correction of a Non–orthogonal, Three–Component Sonic Anemometer for Flow Distortion by Transducer Shadowing. Boundary–Layer Meteorology 155, 371–395. https://doi.org/10.1007/s10546–015–0010–3

Hossen, M.S., Mano, M., Miyata, A., Baten, M.A., Hiyama, T., 2012. Surface energy partitioning and evapotranspiration over a double–cropping paddy field in Bangladesh. Hydrological Processes 26, 1311–1320. https://doi.org/10.1002/hyp.8232

Ikawa, H., Chen, C.P., Sikma, M., Yoshimoto, M., Sakai, H., Tokida, T., Usui, Y., Nakamura, H., Ono, K., Maruyama, A., Watanabe, T., Kuwagata, T., Hasegawa, T., 2018. Increasing canopy photosynthesis in rice can be achieved without a large increase in water use—A model based on free–air CO2 enrichment. Global Change Biology 24, 1321–1341. https://doi.org/10.1111/gcb.13981

Ikawa, H., Ono, K., Mano, M., Kobayashi, K., Takimoto, T., Kuwagata, T., Miyata, A., 2017. Evapotranspiration in a rice paddy field over 13 crop years. Journal of Agricultural Meteorology 73. https://doi.org/10.2480/agrmet.D–16–00011

Jarvis, P.G., Monteith, J.L., Weatherley, P.E., 1976. The interpretation of the variations in leaf water potential and stomatal conductance found in canopies in the field. Philosophical Transactions of the Royal Society of London. B, Biological Sciences 273, 593–610. https://doi.org/10.1098/rstb.1976.0035

Jiang, C. and Ryu, Y., 2016. Multi-scale evaluation of global gross primary productivity and evapotranspiration products derived from Breathing Earth System Simulator (BESS). Remote Sensing of Environment, 186, 528-547.

Keisling, T., Wells, B.R., Davis, G.L., 1984. Rice Management Decision Aids Based Upon Thermal Time Base 50˚. Cooperative Extension Service, University of Arkansas, USDA, and county governments cooperating.

Kima, A.S., Chung, W.G., Wang, Y.–M., Traoré, S., 2015. Evaluating water depths for high water productivity in irrigated lowland rice field by employing alternate wetting and drying technique under tropical climate conditions, Southern Taiwan. Paddy Water Environ 13, 379–389. https://doi.org/10.1007/s10333–014–0458–7

Knox, S.H., Matthes, J.H., Sturtevant, C., Oikawa, P.Y., Verfaillie, J., Baldocchi, D., 2016. Biophysical controls on interannual variability in ecosystem–scale CO2 and CH4 exchange in a California rice paddy. Journal of Geophysical Research: Biogeosciences 121, 978–1001. https://doi.org/10.1002/2015JG003247

Knox, S.H., Sturtevant, C., Matthes, J.H., Koteen, L., Verfaillie, J., Baldocchi, D., 2015. Agricultural peatland restoration: effects of land–use change on greenhouse gas (CO2 and CH4) fluxes in the Sacramento–San Joaquin Delta. Global Change Biology 21, 750–765. https://doi.org/10.1111/gcb.12745

Lafleur, P.M. and Rouse, W.R., 1990. Application of an energy combination model for evaporation from sparse canopies. Agricultural and Forest Meteorology, 49, 135-153.

Lampayan, R.M., Rejesus, R.M., Singleton, G.R., Bouman, B.A.M., 2015. Adoption and economics of alternate wetting and drying water management for irrigated lowland rice. Field Crops Research 170, 95–108. https://doi.org/10.1016/j.fcr.2014.10.013

Lecina, S., Martínez–Cob, A., Pérez, P.J., Villalobos, F.J., Baselga, J.J., 2003. Fixed versus variable bulk canopy resistance for reference evapotranspiration estimation using the Penman–Monteith equation under semiarid conditions. Agricultural Water Management 60, 181–198. https://doi.org/10.1016/S0378–3774(02)00174–9

Leuning, R., Kelliher, F.M., Pury, D.G.G.D., Schulze, E.–D., 1995. Leaf nitrogen, photosynthesis, conductance and transpiration: scaling from leaves to canopies. Plant, Cell & Environment 18, 1183–1200. https://doi.org/10.1111/j.1365–3040.1995.tb00628.x

Li, X., Kang, S., Li, F., Jiang, X., Tong, L., Ding, R., Li, S., Du, T., 2016. Applying segmented Jarvis canopy resistance into Penman–Monteith model improves the accuracy of estimated evapotranspiration in maize for seed production with film–mulching in arid area. Agricultural Water Management 178, 314–324. https://doi.org/10.1016/j.agwat.2016.09.016

Li, Y.H., Cui, Y.L., 1996. Real–time forecasting of irrigation water requirements of paddy fields. Agricultural Water Management 31, 185–193. https://doi.org/10.1016/0378–3774(96)01252–8

Linquist, B.A., Anders, M.M., Adviento-Borbe, M.A.A., Chaney, R.L., Nalley, L.L., Rosa, E.F.F. da, Kessel, C. van, 2015. Reducing greenhouse gas emissions, water use, and grain arsenic levels in rice systems. Global Change Biology 21, 407–417. https://doi.org/10.1111/gcb.12701

Linquist, B., Snyder, R., Anderson, F., Espino, L., Inglese, G., Marras, S., Moratiel, R., Mutters, R., Nicolosi, P., Rejmanek, H. and Russo, A., 2015. Water balances and evapotranspiration in water–and dry–seeded rice systems. Irrigation science, 33(5), pp.375–385.

Linquist, B.A., Marcos, M., Adviento-Borbe, M.A., Anders, M., Harrell, D., Linscombe, S., Reba, M.L., Runkle, B.R.K., Tarpley, L., Thomson, A., 2018. Greenhouse Gas Emissions and Management Practices that Affect Emissions in US Rice Systems. Journal of Environmental Quality 47, 395–409. https://doi.org/10.2134/jeq2017.11.0445

Liu, H., Yang, L., Wang, Y., Huang, J., Zhu, J., Yunxia, W., Dong, G., Liu, G., 2008. Yield formation of CO_2–enriched hybrid rice cultivar Shanyou 63 under fully open–air field conditions. Field Crops Research 108, 93–100. https://doi.org/10.1016/j.fcr.2008.03.007

Liu, B., Cui, Y., Luo, Y., Shi, Y., Liu, M., Liu, F., 2019. Energy partitioning and evapotranspiration over a rotated paddy field in Southern China. Agricultural and Forest Meteorology 276–277, 107626. https://doi.org/10.1016/j.agrformet.2019.107626

Liu, X., Xu, J., Yang, S., Lv, Y., 2019. Surface Energy Partitioning and Evaporative Fraction in a Water-Saving Irrigated Rice Field. Atmosphere 10, 51. https://doi.org/10.3390/atmos10020051

Liu, X., Xu, J., Wang, W., Lv, Y., Li, Y., 2020. Modeling rice evapotranspiration under water-saving irrigation condition: Improved canopy-resistance-based. Journal of Hydrology 590, 125435. https://doi.org/10.1016/j.jhydrol.2020.125435

López-López, R., Jiménez-Chong, J.A., Hernández-Aragón, L., Ibarra, M.A.I., 2018. Water Productivity of Rice Genotypes with Irrigation and Drainage. Irrigation and Drainage 67, 508–515. https://doi.org/10.1002/ird.2250

Lv, Y., Xu, J., Yang, S., Liu, X., Zhang, J., Wang, Y., 2018. Inter–seasonal and cross–treatment variability in single–crop coefficients for rice evapotranspiration estimation and their validation under drying–wetting cycle conditions. Agricultural Water Management 196, 154–161. https://doi.org/10.1016/j.agwat.2017.11.006

Massey, J. H., Smith M. C., Vieira D. A. N., Adviento–Borbe M. A., Reba M. L., Vories E. D., 2018. Expected Irrigation Reductions Using Multiple–Inlet Rice Irrigation under Rainfall Conditions of the Lower Mississippi River Valley. Journal of Irrigation and Drainage Engineering 144, 04018016. https://doi.org/10.1061/(ASCE)IR.1943–4774.0001303

Massey, J.H., Mark Stiles, C., Epting, J.W., Shane Powers, R., Kelly, D.B., Bowling, T.H., Leighton Janes, C., Pennington, D.A., 2017. Long–term measurements of agronomic crop irrigation made in the Mississippi delta portion of the lower Mississippi River Valley. Irrig Sci 35, 297–313. https://doi.org/10.1007/s00271–017–0543–y

Moran, M.S., Maas, S.J., Jr, P.J.P., 1995. Combining remote sensing and modeling for estimating surface evaporation and biomass production. Remote Sensing Reviews 12, 335–353. https://doi.org/10.1080/02757259509532290

Mote, K., Rao, V.P., Kumar, K.A., Ramulu, V., 2018. Estimation of crop evapotranspiration and crop coefficients of rice (Oryza sativa L.) under low land condition. Journal of Agrometeorology; Anand 20, 117–121.

Myneni, R., Knyazikhin, Y., Park, T. (2015). MOD15A2H MODIS/Terra Leaf Area Index/FPAR 8–Day L4 Global 500m SIN Grid V006 [Data set]. NASA EOSDIS Land Processes DAAC. Accessed 2020–03–27 from https://doi.org/10.5067/MODIS/MOD15A2H.006

Naklang, K., Shu, F., Nathabut, K., 1996. Growth of rice cultivars by direct seeding and transplanting under upland and lowland conditions. Field Crops Research 48, 115–123. https://doi.org/10.1016/S0378-4290(96)01029-5

Nalley, L., Linquist, B., Kovacs, K., Anders, M., 2015. The Economic Viability of Alternative Wetting and Drying Irrigation in Arkansas Rice Production. Agronomy Journal 107, 579–587. https://doi.org/10.2134/agronj14.0468

Norman, J.M., Kustas, W.P., Humes, K.S., 1995. Source approach for estimating soil and vegetation energy fluxes in observations of directional radiometric surface temperature. Agricultural and Forest Meteorology, Thermal Remote Sensing of the Energy and Water Balance over Vegetation 77, 263–293. https://doi.org/10.1016/0168-1923(95)02265-Y

Norton, G.J., Shafaei, M., Travis, A.J., Deacon, C.M., Danku, J., Pond, D., Cochrane, N., Lockhart, K., Salt, D., Zhang, H., Dodd, I.C., Hossain, M., Islam, M.R., Price, A.H., 2017. Impact of alternate wetting and drying on rice physiology, grain production, and grain quality. Field Crops Research 205, 1–13. https://doi.org/10.1016/j.fcr.2017.01.016

Pan, J., Liu, Y., Zhong, X., Lampayan, R.M., Singleton, G.R., Huang, N., Liang, K., Peng, B., Tian, K., 2017. Grain yield, water productivity and nitrogen use efficiency of rice under different

water management and fertilizer–N inputs in South China. Agricultural Water Management 184, 191–200. https://doi.org/10.1016/j.agwat.2017.01.013

Pereira, L.S., Allen, R.G., Smith, M., Raes, D., 2015. Crop evapotranspiration estimation with FAO56: Past and future. Agricultural Water Management, Agricultural Water Management: Priorities and Challenges 147, 4–20. https://doi.org/10.1016/j.agwat.2014.07.031

Reba, M.L., Daniels, M., Chen, Y., Sharpley, A., Bouldin, J., Teague, T.G., Daniel, P., Henry, C.G., 2013. A statewide network for monitoring agricultural water quality and water quantity in Arkansas. Journal of Soil and Water Conservation 68, 45A–49A. https://doi.org/10.2489/jswc.68.2.45A

Reba, M.L., Massey, J.H., Adviento-Borbe, M.A., Leslie, D., Yaeger, M.A., Anders, M., Farris, J., 2017. Aquifer Depletion in the Lower Mississippi River Basin: Challenges and Solutions. Journal of Contemporary Water Research & Education 162, 128–139. https://doi.org/10.1111/j.1936–704X.2017.03264.x

Roel, A., Heilman, J.L., McCauley, G.N., 1999. Water use and plant response in two rice irrigation methods. Agricultural Water Management 39, 35–46. https://doi.org/10.1016/S0378–3774(98)00087–0

Runkle, B.R.K., Rigby, J.R., Reba, M.L., Anapalli, S.S., Bhattacharjee, J., Krauss, K.W., Liang, L., Locke, M.A., Novick, K.A., Sui, R., Suvočarev, K., White, P.M., 2017. Delta–Flux: An Eddy Covariance Network for a Climate–Smart Lower Mississippi Basin. Agricultural & Environmental Letters 2. https://doi.org/10.2134/ael2017.01.0003

Runkle, B.R.K., Suvočarev, K., Reba, M.L., Reavis, C.W., Smith, S.F., Chiu, Y.–L., Fong, B., 2019. Methane Emission Reductions from the Alternate Wetting and Drying of Rice Fields Detected Using the Eddy Covariance Method. Environ. Sci. Technol. 53, 671–681. https://doi.org/10.1021/acs.est.8b05535

Shuttleworth, W.J. and Wallace, J.S., 1985. Evaporation from sparse crops-an energy combination theory. Quarterly Journal of the Royal Meteorological Society, 111, 839-855.

Smith, M., 1992. CROPWAT: A computer program for irrigation planning and management. Food & Agriculture Org.

Soil Survey Staff, Natural Resources Conservation Service, United States Department of Agriculture, 2018. Web Soil Survey. Available at: https://websoilsurvey.sc.egov.usda.gov (accessed 12.3.18).

Sudhir–Yadav, Humphreys, E., Li, T., Gill, G., Kukal, S.S., 2012. Evaluation of tradeoffs in land and water productivity of dry seeded rice as affected by irrigation schedule. Field Crops Research 128, 180–190. https://doi.org/10.1016/j.fcr.2012.01.005

Suvočarev, K., Castellví, F., Reba, M.L., Runkle, B.R.K., 2019. Surface renewal measurements of H, λE and CO2 fluxes over two different agricultural systems. Agricultural and Forest Meteorology 279, 107763. https://doi.org/10.1016/j.agrformet.2019.107763

Tuong, T.P., Bhuiyan, S.I., 1999. Increasing water-use efficiency in rice production: farm-level perspectives. Agricultural Water Management 40, 117–122. https://doi.org/10.1016/S0378-3774(98)00091-2

Wang, Y., Zhou, L., Jia, Q., Yu, W., 2017. Water use efficiency of a rice paddy field in Liaohe Delta, Northeast China. Agricultural Water Management 187, 222–231. https://doi.org/10.1016/j.agwat.2017.03.029

Wei, Z., Yoshimura, K., Okazaki, A., Kim, W., Liu, Z., Yokoi, M., 2015. Partitioning of evapotranspiration using high–frequency water vapor isotopic measurement over a rice paddy field. Water Resources Research 51, 3716–3729. https://doi.org/10.1002/2014WR016737

Wei, Z., Yoshimura, K., Wang, L., Miralles, D.G., Jasechko, S., Lee, X., 2017. Revisiting the contribution of transpiration to global terrestrial evapotranspiration. Geophysical Research Letters 44, 2792–2801. https://doi.org/10.1002/2016GL072235

Xu, J., Liu, X., Yang, S., Qi, Z., Wang, Y., 2017. Modeling rice evapotranspiration under water–saving irrigation by calibrating canopy resistance model parameters in the Penman–Monteith equation. Agricultural Water Management 182, 55–66. https://doi.org/10.1016/j.agwat.2016.12.010

Xu, J., Wu, B., Yan, N., Tan, S., 2018. Regional Daily ET Estimates Based on the Gap–Filling Method of Surface Conductance. Remote Sensing 10, 554. https://doi.org/10.3390/rs10040554

Yan, H., Zhang, C., Hiroki, O., 2018. Parameterization of canopy resistance for modeling the energy partitioning of a paddy rice field. Paddy Water Environ 16, 109–123. https://doi.org/10.1007/s10333–017–0620–0

Yang, S., Logan, J., Coffey, D.L., 1995. Mathematical formulae for calculating the base temperature for growing degree days. Agricultural and Forest Meteorology 74, 61–74. https://doi.org/10.1016/0168–1923(94)02185–M

Zhang, B., Kang, S., Li, F., Zhang, L., 2008. Comparison of three evapotranspiration models to Bowen ratio–energy balance method for a vineyard in an arid desert region of northwest China. Agricultural and Forest Meteorology 148, 1629–1640. https://doi.org/10.1016/j.agrformet.2008.05.016

Chapter 1: Appendix A

Aerodynamic resistance (r_a)

Aerodynamic resistance was calculated using the following equation presented as a part of FAO 56 document with regards to the Penman–Monteith equation:

$$r_a = \frac{\ln\left(\frac{z_m - d}{z_{om}}\right) * \ln\left(\frac{z_h - d}{z_{oh}}\right)}{k^2 * u_z}$$

$$d = \frac{2}{3} * h$$

$$z_{om} = 0.123 * h$$

$$z_{oh} = 0.1 * z_{om}$$

Where r_a is aerodynamic resistance, s m^{-1}, z_m is height of wind measurements in meters (2.2 m), z_h is height of humidity measurements in meters (2.2 m), d is zero plane displacement height in meters, z_{om} is roughness length governing momentum transfer in meters, z_{oh} is roughness length governing transfer of heat and vapor in meters, k is von Karman's constant, 0.41, u_z is wind speed at height z, m s^{-1}.

Crop Coefficient Adjustments

For the initial crop coefficient, $K_{c,ini}$, FAO56 recommends a value of 1.05 for rice. The document also provides adjustments based on wind speed and humidity. Our site was classified as very humid with moderate to strong winds, meaning the initial value could be between 1.05 and 1.10 based on Table 14 in Chapter 6 of FAO 56. For this study, we used 1.05 as $K_{c,ini}$.

For the mid–season crop coefficient and end crop coefficient, $K_{c,mid}$ and $K_{c,end}$, similar adjustments were made based on relative humidity, wind speed, and canopy height using the equation:

$$K_{c,mid(end)} = K_{c,mid(end),rec} + [0.4 * (u_2 - 2) - 0.004(RH_{min} - 45)] \left(\frac{h}{3}\right)^{0.3}$$

Where $K_{c,mid\ (end),rec}$ is the recommended value for the middle or end of the growing season taken from Table 12 of FAO56 (1.2 and 1.0, respectively), u_2 is the daily wind speed at 2 m during the mid–season or end growth stage, RH_{min} is the daily minimum during the mid–season or end growth stage, respectively, %, and h is mean plant height during the mid–season or end growth stage, respectively, in m.

Chapter 2: Water use efficiency dynamics for improved understanding of carbon and water exchange in rice

Authors: Colby W. Reavis[1], Michele L. Reba[2], Benjamin R.K. Runkle[1]

[1] Department of Biological and Agricultural Engineering, University of Arkansas, Fayetteville, AR, USA

[2] USDA ARS Delta Water Management Research Unit, Jonesboro, AR, USA

Author's Note: This work is currently in internal review with the USDA-ARS. We intend to submit the document to Agricultural and Forest Meteorology where I (Colby) will serve as the corresponding author.

1. Introduction

Carbon assimilated as gross primary production (GPP) and water released as evapotranspiration (ET) are commonly linked as canopy water use efficiency, or WUE (Law et al., 2002). In agriculture, understanding crop water use efficiency is especially important under an environment where changes in crop performance are driven by limited water availability (Zwart and Bastiaanssen, 2004), elevated ambient CO_2 concentration (Kim et al., 2003), increased vapor pressure deficit (VPD) during the daytime (Kobayasi et al., 2010; Massmann et al., 2019), and higher nighttime temperatures (Cheng et al., 2009). Heavily irrigated crops, such as rice, rely on well-timed irrigation events and water availability during key stages in their growth cycle to secure profitable yields (Kato et al., 2009; Pan et al., 2017). Rice has been historically produced in an inundated environment with continuous water cover throughout the year, where the crop is most sensitive to water stress during panicle initiation and anthesis (Moldenhauer et al., 2013). However, new management practices, such as alternate wetting and

61

drying (AWD), provide opportunities for producers to conserve water while maintaining

comparable yields at the commercial scale (Massey et al., 2014; Moreno-García et al., 2021;

Yang et al., 2017). The application of AWD is challenging because it introduces periodic drying

during the growing season, which can stress the crop under severe moisture deficit (Wopereis et

al., 1996; Henry et al., 2011). Because these techniques disrupt the typical application of water in

conventional rice growing practices, additional research is needed to determine the impacts of

different growing methods with respect to canopy water use during the growing season.

In application, ET provides an estimate of water to be replaced in irrigated fields based

on how much water the crop utilizes (Cahoon et al., 1990; Martin et al., 1990; Allen et al., 1998).

Developmentally, crops exhibit different levels of control on water use based on the growth stage

(Tomar and O'Toole, 1980; Yang et al., 2019), cultivar (Yao et al., 2012; Xu et al., 2015) and the

implementation of alternative management practices (Zhang et al., 2008; Sudhir-Yadav et al.,

2012; Kima et al., 2015). In practical settings, rice growers tend to prioritize irrigation during

periods where the plant is most sensitive to water stress, mainly during flowering and grain

filling, to prevent declines in yield (Henry et al., 2013). In commercial production settings, the

conservation of water should not be implemented at the expense of declining yields (Tuong and

Bhuiyan, 1999; Yang et al., 2007; Lampayan et al., 2015a). One of the primary concerns with the

AWD irrigation practice is the introduction of periodic drying events, which can potentially

induce stress and subsequently decrease yield while altering plant water use during the growing

season (Carrijo et al., 2017; Lampayan et al., 2015b; Norton et al., 2017).

Our previous research indicated that the impacts of AWD on growing season ET were

negligible when compared to traditional delayed flood (DF) irrigation (Reavis et al., 2021). In

that study, we observed no significant impacts of drying on measured ET, indicating that plants

were still able to access water in the absence of inundation at our field site. Furthermore, adjacent AWD and DF fields converged in terms of ET rates as the canopy developed, and ET transitioned from being primarily driven by open evaporation to transpiration. However, in wet environments, the combined ET term may mask stress that is expressed disproportionately through canopy water use in transpiration (O'Toole and Baldia, 1982; Bouman et al., 2005). Because transpiration is considered a critical component in multiple areas related to crop productivity, including water use and yield estimation, accurate estimates of transpiration are both relevant and useful in agricultural production settings (Howell, 2001; Hsiao et al., 2007; Paredes et al., 2014).

Partitioning ET throughout the growing season has potential in evaluating individual canopy responses and controls to the environment throughout the growing season. Through partitioning, the isolated impacts of individual management decisions on plant mediated water use can be identified in agricultural settings when irrigation events can introduce sizeable amounts of evaporation from soil, open water surface, and interception compared to transpirative water release (Kool et al., 2014; Zhou et al., 2018). Transpiration is a key component in water use efficiency as it shares the stomatal pathway as carbon assimilation, with similar controls at the leaf level (Wallace, 2000; Haefele et al., 2009). Partitioned ET can be estimated and used to further represent canopy water use efficiency in relation to gross primary productivity (GPP) as ecosystem water use efficiency (eWUE), inherent WUE (iWUE), underlying water use efficiency (uWUE), and transpirative WUE (tWUE) where each metric represents WUE with increasing proximity to canopy level dynamics and controls (Zhou et al., 2016, 2014). The uWUE partitioning method presented in Zhou et al. (2016) has been tested on rice landscapes in

both California, US and Ibaraki, Japan, with T:ET ranging between 0.55 and 0.59 during the growing season (Jiang et al., 2020).

Historically, methods used to estimate and partition ET in agricultural settings have varied significantly under the advent of advanced instrumentation and development of models that take advantage of these data streams. Efforts have been made to combine models and instrumentation to estimate contributing portions of ET individually and a separate estimate of ET to understand changes in canopy water use during the growing season (Kool et al., 2014). Alternatively, models have also employed a variety of frameworks to mechanistically define and quantify transpiration, evaporation, and interception using localized microclimate measurements (Shuttleworth, 1991; Stannard, 1993; Allen, 2000; Allen et al., 2005; Zhao et al., 2015; Qiu et al., 2019). These models can differ based on how phenological input, such as leaf area index (LAI) or canopy height, are incorporated to improve a variety of radiative transfer models (Tanner and Jury, 1976; Shuttleworth and Wallace, 1985; Béziat et al., 2013; Gong et al., 2021). Some methods have also directly incorporated models of GPP to better simulate water use during the growing season given the connected pathway for transpirative water use and canopy production (Collatz et al., 1991; Tian et al., 2010). In an effort to develop accurate estimates of ET that are applicable across greater spatial scales, methods, such as the Priestley-Taylor model developed by NASA's Jet Propulsion Laboratory (PT-JPL), leverage a wealth of remotely sensed information in conjunction with well-defined models for the estimation of ET and its constituent portions (Fisher et al., 2008, 2020). The variety of methods and platforms used to estimate and constrain T and ET is valuable given the uncertainty surrounding global and field scale estimates of T:ET and associated phenological and meteorological controls (Wang et al., 2014; Schlesinger and Jasechko, 2014; Stoy et al., 2019; Nelson et al., 2020).

In this work, we seek to use methods for estimating ET in conjunction with field observations of ET and an observation-driven model of GPP to estimate and describe WUE throughout the growing season in rice fields using conventional delayed-flood (DF) and alternative (AWD) irrigation practices. First, we examine the impacts of drying events and elevated VPD on GPP and calculate WUE throughout the plant life cycle to detect how it changes across key developmental stages (such as flowering, etc.). Next, we employ ET models to partition ET to (1) better understand the direct relationship between canopy transpiration and WUE, and (2) identify plant response under "drier" soil conditions introduced by AWD across different developmental stages. We apply the uWUE method in the humid Mid-South to complement previous rice studies and allow a basis for comparison across major rice production areas. We hypothesize that as the canopy develops during the growing season, vulnerability to drought-induced stress during soil drying is increased and reflected in the transpiration portion of ET as well as the GPP. In characterizing canopy WUE and response to alternative management practices, we aim to contextualize the impacts of AWD with respect to water use throughout the rice developmental cycle to better inform management decisions.

2. Methods

2.1 Site Information

The study site is comprised of two adjacent commercial rice fields located in Arkansas, in the mid-South US rice production region. The fields, labeled as North Field (NF) and South Field (SF), are managed to study the impacts of alternative irrigation practices with respect to irrigation water conservation and greenhouse gas emissions. The fields are zero-graded and have been used to grow rice in continuous rotation for at least 15 years. Both NF and SF were drill seeded across the 2015-2017 growing seasons. Soils in NF and SF are primarily poorly drained

Perry silty clays (USDA classification: very-fine, smectitic, thermic Chromic Epiaquerts) with a small (~2 ha) contributing portion of Herbert silt loam (fine-silty, mixed, superactive, mesic Udollic Epiaqualfs) in SF (Soil Survey Staff, USDA-NRCS, 2018; Runkle et al., 2019). During the 2015-2017 growing seasons, the irrigation treatments for NF for were DF, AWD, DF, and the irrigation treatments for SF were AWD, AWD, DF (Table 1).

2.2 Instrumentation

Each field is equipped with similar micrometeorological instruments, including an open-path eddy covariance (EC) system used to measure CO_2, H_2O, and CH_4. Further information regarding the suite of sensors and available measurements can be found in previous publications (Runkle et al., 2019; Suvočarev et al., 2019; Reavis et al., 2021). In addition to the EC system, each station had an identical set of meteorological instruments. The four components of net radiation (RN) were measured (CNR4, Kipp & Zonen, Inc., Delft, NL) at a height of 2.0 m. Air temperature (T_a) and relative humidity (RH) were measured using a shielded probe (HMP155A, Vaisala, Helsinki, FI) at approximately 2.1 m. Wind speed and direction were measured using a 2-D anemometer mounted at 3.2 m (05103−5 propeller wind monitor, R.M. Young, Traverse City, MI, USA). A local weather station located in Stuttgart, AR, which is approximately 20 miles from the field site, provided daily microclimatic measurements of T, RH, and wind speed over a reference surface for use in the FAO Dual crop coefficient partitioning method, described further below. These measurements over the reference surface were used in conjunction with a simple radiation model to estimate ET and T without using any measurements at the field site.

The stations also hosted a suite of soil measurements. Volumetric water content measurements were collected using soil moisture Time Domain Transmissometer probes (SDI–12, Acclima, Meridian, ID) buried approximately 2 m from the tower base at 8 cm and 15 cm for

all growing seasons across both fields. Measurements of water depth (WD) were collected using

a piezometric sensor (Series 46x, Keller USA Inc., Fort Mill, SC, USA), vented for automatic

compensation for barometric pressure changes. The WD sensors were installed 30 cm from the

tower in a perforated tube reaching approximately 30 cm below the soil surface. Soil heat flux

(G) measurements were collected using two soil heat flux plates (HFP01, Hukseflux, Delft, NL)

placed at different depths in each year: 8 cm, 5 cm, and 4 cm below the soil surface for the 2015,

2016, and 2017 growing seasons, respectively. Bulk density and soil temperature above the soil

heat flux plate were used in conjunction with WD measurements to correct for changes in heat

storage in the water and saturated soil matrix above the plate during flooded and dry conditions

(Fuchs and Tanner, 1968; Runkle et al., 2019). Thermistors (CS–107 (BetaTherm 100K6A1IA),

Campbell Scientific, Inc., Logan, UT, USA) were placed near the soil surface at approximately 2

cm above each soil heat flux plate. Estimates of soil bulk density were collected manually at

different times during the growing season to support the energy storage calculation across both

fields (Runkle et al., 2019).

Each station was also equipped with a field camera used to observe canopy development

throughout the growing season (PhenoCam; Milliman et al., 2019). Aside from instrumentation

deployed at the towers, phenological measurements were taken throughout the growing season,

including canopy height and LAI estimated using an inceptometer (LI-2200C, LI-COR, Lincoln,

NE). Across both fields, canopy height was measured 7 ,13, and 11 times during the 2015-2017

growing seasons. Likewise, LAI was measured 4, 2, and 10 times during the 2015-2017 growing

seasons, respectively. During the 2016 growing season, when only two LAI measurements were

taken during the peak LAI period, we calculated and applied a simple numerical scaling factor

for the MODIS LAI dataset to generate estimates of LAI throughout the growing season (Reavis

et al., 2021). Using the collected and scaled data for both LAI and canopy height, we employed simple growing degree day models to generate a daily time series for each variable during the 2015-2017 growing seasons, as described in Reavis et al. (2021).

Measurements of biometeorological variables were resolved at the half-hourly time step. Measurements were gap filled across fields when appropriate for variables including temperature, relative humidity, incoming longwave radiation (LW_{in}), and incoming shortwave radiation (SW_{in}) where differences between fields were minimal. Fluxes were calculated from the EC station using the EddyPro software (v. 6.2.2, LI-COR Inc., Lincoln, NE). Additionally, the latent heat flux (LE), sensible heat flux (H), and CO_2 time series were gap filled using artificial neural networks (Knox et al., 2016, 2015). In the case of CO_2 flux, the contributing portions of gross primary production (GPP) and ecosystem respiration (Reco) were estimated throughout the growing season as well (Reichstein et al., 2012, 2005).

2.3 Water use efficiency evaluation

Water use efficiency (WUE) is differentiated in this study as ecosystem WUE (eWUE), underlying water use efficiency (uWUE), and transpirative WUE (tWUE), which are defined in the introduction. In this study, we will refer to ET and transpiration in units of mm day^{-1}, translated from the molar basis using the estimated latent heat of vaporization. Vapor pressure deficit was calculated directly for each field using estimates of temperature and relative humidity at approximately 2.2 m above the soil surface. For all WUE terms (eWUE, uWUE, tWUE), observations and measurements of GPP, ET, and T used during calculation were limited to the daytime period ($SW_{in} > 30$ Wm^{-2}). Additionally, half hourly periods containing or within 6 hours of a precipitation event were removed. Additionally, only daytime values were used in the calculation of daily means for each WUE term as well as modeled T using the uWUE method.

Outliers in the WUE terms resulted from periods of the day where GPP, ET, and T were each low and the resulting WUE was unrealistically high or low while representing only a small portion of the daily flux. We thus removed half hourly data points exceeding three mean absolute deviations (MADs) for the eWUE, uWUE, T, and tWUE time series.

When determining the impacts of drying events on GPP, ET, and T, we provided analysis in two ways. First, we observed the impacts of drying when one field was undergoing AWD treatment while the other field was under DF treatment, which was only possible during the 2015 growing season. In this analysis, we compared differences in GPP, ET, and T across fields during periods where the AWD field was undergoing a drying event as a part of AWD management. For our analysis, a drying event was defined as a period where the water table declined below the soil surface for a period of at least 1 day. During the early growing season, short flushing events can be used to establish the crop across both AWD and DF systems, and the differences in the irrigation treatments is only apparent after the initial flood is established at tillering. We thus focused on drying events following the onset of the first flood as those events were implemented as a part of the AWD system by the producers. Second, we compared individual responses of GPP, ET, and T within the same field during AWD drying events. For the 2015 and 2016 growing seasons when AWD was applied in one or both fields (Table 1), we analyzed the response of each term during separate drying events to test whether a decline in soil moisture coincided with decreased GPP, ET, and/or T as a result of stress induced by drying. We normalized GPP, ET, and T by SW_{in} when comparing across fields or identifying responses during individual drying events. Additionally, we classified each event based on relevant microclimate conditions in each field, including minimum VWC during drying, maximum daily temperature, and the length of the drying event recorded in days (Table 2). By comparing AWD

and DF directly as well as highlighting individual responses of the key WUE terms, the resulting

analysis provided understanding on how drying affects individual fields while also giving insight

to how AWD and DF compare when practiced concurrently.

2.4 Evapotranspiration partitioning

Evapotranspiration (ET) was directly measured at each field site using the EC system. Its

partitioning is based on the direct proportionality of the ratio of apparent to potential underlying

WUE (uWUE) to the ratio T:ET during the growing season (Zhou et al., 2016). In the work

presented in Zhou et al. (2016) uWUE is the ratio of GPP to ET and scaled by VPD where the

traditional formulation is:

$$\text{uWUE} = \frac{\text{GPP}*\text{VPD}^{0.5}}{\text{ET}} \quad \text{Eqn 1}$$

Where GPP is in units of mmol C m^{-2} s^{-1}, ET is in units of mmol H_2O m^{-2} s^{-1}, and VPD is

in units of hPa. Underlying WUE ($uWUE_i$) was estimated with Eqn 1 across the growing season

using the half-hourly microclimate dataset. The potential uWUE ($uWUE_p$) was calculated using

quantile regression across the full growing season as the slope (m) of the relationship between

ET and GPP*$VPD^{0.5}$ at the 95th percentile. To compare our results across different growing

seasons and methods, we estimated transpiration using this approach at both the half-hourly and

daily time step. For the half hourly time step, the fraction of $uWUE_i$ to $uWUE_p$ was considered to

be equal to T:ET at that half hour. For the daily time step, we used a linear regression between

half hourly ET and GPP*$VPD^{0.5}$ for a given day to calculate the apparent uWUE ($uWUE_a$). The

mean relationship between ET and GPP*$VPD^{0.5}$ at the daily time scale, represented as $uWUE_a$,

was only estimated using daytime data, meaning the resulting T and ET estimates are only daily

daytime rate estimates rather than true daily estimates. Restricting data to the daytime period

provides a plausible physiological constraint for T and GPP as these fluxes are most significant

during the daytime and are inconsequential during the nighttime period. The fraction of $uWUE_a$

to $uWUE_p$ was then considered to be equal to the ratio of T to ET. Both regressions were forced

through zero to be consistent with work presented in Zhou et al. (2016). In both cases, when the

estimated ratio of T to ET at either the half hourly or daily time step exceeded 1 (i.e., $uWUE_i$ or

$uWUE_a$ were greater than $uWUE_p$), we fixed the ratio of T to ET to 1. The method was applied

across each individual site-year, with NF and SF having unique $uWUE_p$ values for each growing

season. We included the calculation of the uWUE terms and resulting T using both gap filled and

observed data. Gap filled data were used to deliver seasonal estimates of relevant parameters and

to generate daily estimates of T using the uWUE method. Estimates of WUE and T derived using

non gap filled data were used primarily in comparisons during individual portions of the growing

season when exploring response to drying events and comparing T across fields. Additionally,

derived transpiration estimates were reported in mm for seasonal sums and mm day^{-1} when

comparing rates across methods.

2.5 Evapotranspiration partitioning methods

We further compared the estimates of transpiration from the uWUE method with two

other methods for estimating growing season T. The dual crop coefficient variant of the FAO56

Penman Monteith (PM56Dual) estimates transpiration as the product of calculated reference ET

(ET_0) and a basal crop coefficient ($K_{c,b}$), where the crop coefficient contains a majority of the

phenology and subsequent seasonality of transpiration (Eqn 2):

$$ET_c = ET_0 * K_{c,b} = \frac{0.408\Delta(R_n - G) + \gamma\left(\frac{C_n}{T_a + 273}\right)(VPD)u_{2m}}{\Delta + \gamma(1 + C_d u_{2m})} * K_{c,b} \quad \text{Eqn 2}$$

Where ET_c is considered the transpiration component of ET across the given crop or surface, ET_0

is reference ET, $K_{c,b}$ is a basal crop coefficient, Δ is the slope of the vapor pressure deficit curve,

R_n is net radiation, G is soil heat flux, γ is the psychrometric constant, VPD is vapor pressure

deficit, u_{2m} is wind speed measured 2 m above the reference surface, and C_n and C_d are unique

coefficients of the reference surface at 900 and 0.34, respectively. The basal crop coefficient was

adjusted for local use using estimates of wind speed and relative humidity as recommended by

FAO56. The initial crop coefficient for rice from the FAO56 documentation is recommended for

transplanted systems where fields are inundated at planting and the recommended crop

coefficient is thus equivalent to the open water coefficient. Conversely, fields in this study are

drill seeded into non-inundated soil and the initial flood is delayed for up to 5 to 6 weeks.

Because both NF and SF were drill seeded rather than transplanted, the first 30 days of the

growing season where the initial crop coefficient would normally be applied were removed to

remove the effect of different planting practices on the estimation of ET and resulting T.

The Jet Propulsion Laboratory variant of the Priestley-Taylor equation (PT-JPL) provides

a partitioned estimate of ET, which includes contributing canopy transpiration (Eqn 3-6):

$$AET = ET_s + ET_c + ET_i \qquad\qquad \text{Eqn 3}$$

$$ET_c = (1 - f_{wet})f_g f_T f_m \alpha \frac{\Delta}{\Delta+\gamma} RN_{nc} \qquad\qquad \text{Eqn 4}$$

$$ET_s = \left(f_{wet} + f_{SM}(1 - f_{wet})\right)\alpha \frac{\Delta}{\Delta+\gamma} RN_{ns} \qquad \text{Eqn 5}$$

$$ET_i = f_{wet}\, \alpha \frac{\Delta}{\Delta+\gamma} RN_{nc} \qquad\qquad \text{Eqn 6}$$

Where actual ET (AET) is the sum of scaled actual ET from the canopy (ET_c), soil

surface (ET_s), and intercepted water (ET_i). The scaling terms are further defined in Appendix A,

where f_{wet} is the relative surface wetness, f_g is the green canopy fraction, f_T is a plant

temperature constraint, f_M is a plant moisture constraint, f_{SM} is a soil moisture constraint, RN_{nc} is

net radiation utilized by the canopy, RN_s is net radiation at the soil surface, and α is the

Priestley-Taylor coefficient with an assumed value of 1.26. The PT-JPL framework does not require site specific parameterization, but we did incorporate several field specific estimates of phenology rather than deriving them solely from remotely sensed vegetation indices. Specifically, we incorporated field measurements of upwelling and downwelling photosynthetically active radiation (PAR) to calculate the green canopy fraction and plant moisture constraint. We also provided direct field measurements of RN, G, T_a (including daily maxima and minima), and RH as inputs into the modeling framework.

The intercomparison between the three methods was done at the daily time step as dictated by the PM56Dual and PT-JPL approaches. Daily T was calculated for the uWUE method for direct comparison using gap filled daytime data. The methods were evaluated based on multiple metrics at both the daily and seasonal scales, including how well the models estimated the ratio of T to ET (hereafter, T:ET) and demonstrated reasonable seasonal dynamics. While we report T and ET from each method, the performance for each method was primarily focused on how well they predicted T:ET throughout the growing season, meaning the methods could differ in estimated T and ET and still provide a mechanistically sound method of partitioning ET. In our analysis, we considered the uWUE transpiration to be the most accurate field-based measurement of transpiration while the PT-JPL and PM56Dual methods were considered to be more widely applicable as each method could be applied without site specific data or parameterization.

3. Results

3.1 Impacts of drying on field observed ET and GPP

During the 2015-2017 growing seasons, both AWD and DF irrigation were practiced across both NF and SF in different combinations year-to-year (Table 1). The first flood applied

during the growing season occurred in the first 37 to 54 days after planting (DAP). The 2017

growing season experienced greater precipitation compared to the 2015 and 2016 growing

seasons.

Table 1. Summary of growing season irrigation treatments, ET, and GPP during the 2015-2017 growing seasons for NF and SF. First flood date is given as a calendar date and in days after planting (DAP).

Site	Year	Irrigation Treatment	Growing Season Length [days]	Growing Season ET [mm]	Growing Season Precip. [mm]	Growing Season GPP [gC m^{-2}]	First Flood Date (DAP)	Harvest Date
	2015	DF	133	551 ± 7.1	500	1087	14-May (40)	19-Aug
NF	2016	AWD	143	601 ± 10.5	556	1318	14-Jun (52)	19-Aug
	2017	DF	138	628 ± 6.9	795	1257	17-May (37)	13-Sep
	2015	AWD	134	598 ± 14.0	500	1225	15-May (41)	13-Sep
SF	2016	AWD	143	604 ± 9.7	556	1192	16-Jun (54)	26-Aug
	2017	DF	140	579 ± 13.4	795	1416	18-May (38)	27-Aug

The AWD treatments of SF in 2015 and both fields in 2016 allow us to examine a variety

of drying events for their impact on water use dynamics. The impacts of drying were directly

compared across fields in 2015 when SF was undergoing drying while NF was flooded. To

complement the treatment effects analysis in 2015, we also tested the impact of declining soil

moisture on GPP, ET, and uWUE-derived T across NF and SF during drying events within the

2015 and 2016 growing seasons. During the 2015 and 2016 drying events, soil moisture reached

minimums ranging from 20.5 to 35.0 %, and drying event length ranged from 1 to 10 days (Table

2). For reference, the soil moisture under inundation ranged between 52 to 58% across 2015 and

2016 in both NF and SF. The minimum water depth during drying ranged between 2.6 and 33.7

cm below the soil surface. During the AWD treatments in 2015 and 2016, the most severe events

in terms of soil moisture decline and WD occurred between 42 and 69 DAP in both NF and SF.

During the 2015 and 2016 growing seasons, the earliest drying event occurred 42 days after

planting (DAP) in 2015 and the latest was approximately 123 days after planting in 2015. During

drying events, daily maximum VPD ranged between 0.9 and 2.5 kPa, and the mean daily

maximum temperature ranged between 28.2 and 34.4 °C. Mean maximum SW_{in} ranged between

812 and $951Wm^2$ during the drying. The ranges in maximum VPD, T, and SW_{in} were consistent

across both fields.

Table 2. Characterization of AWD drying events occurring across NF and SF during the 2015
and 2016 growing seasons. Mean maximum temperature and SW_{in} were taken across all drying
event days. Minimum VWC values of "~" denote periods where soil moisture data was not
available.

Site	Date	DAP, days	Event Duration, days	Min VWC at 8 cm, %	Min Water Depth, cm	Max VPD range, kPa	Mean Daily Max Temp, °C	Mean Daily Max SW_{in}, Wm^{-2}
SF	23-May-15	46	4	~	-13.9	1.2 - 1.5	28.2	812.6
	13-Jun-15	67	5	30.80	-3.1	1.2 - 1.7	30.7	908.2
	20-Jun-15	74	2	31.00	-2.6	1.2 - 1.6	30.8	951.0
	21-Jul-15	105	2	30.29	-14.4	1.7 - 2.0	33.1	837.3
	30-Jul-15	114	1	35.03	-14.0	2.1	30.7	911.0
	5-Aug-15	120	1	~	-9.8	2.5	34.4	879.0
	4-Jun-16	42	10	24.3	-21.2	0.9 - 2.3	31.3	913.1
	25-Jun-16	62	4	21.7	-33.7	1.7 - 2.0	32.4	911.8
	1-Jul-16	69	1	33.6	-17.0	1.8	32.2	911.0
	23-Jul-16	91	3	29.1	-31.5	1.6 - 2.1	33.8	884.3
NF	26-Jun-16	64	3	20.5	-17.3	1.9 - 2.1	32.8	935.0

We examined the 2015 drying periods to determine the impacts of drying through a

comparison of AWD and DF treated fields where one field was dry and the other was wet during

one of the drying periods defined in Table 2. Of the listed drying events for SF in 2015, only two

events (13-Jun and 20-Jun) had adequate data coverage between observed (i.e., not gap–filled)

GPP, ET, T and VWC across both fields. We selected these two events to assess whether drying

in an AWD field was able to explain the differences in GPP, ET, and T across fields during

AWD drying events. During the 20-Jun drying event in SF, where soil moisture was most depleted in comparison to other events in 2015, there were no observable signs of stress in a drying SF compared to a flooded NF across GPP, ET, and T (Figure 1).
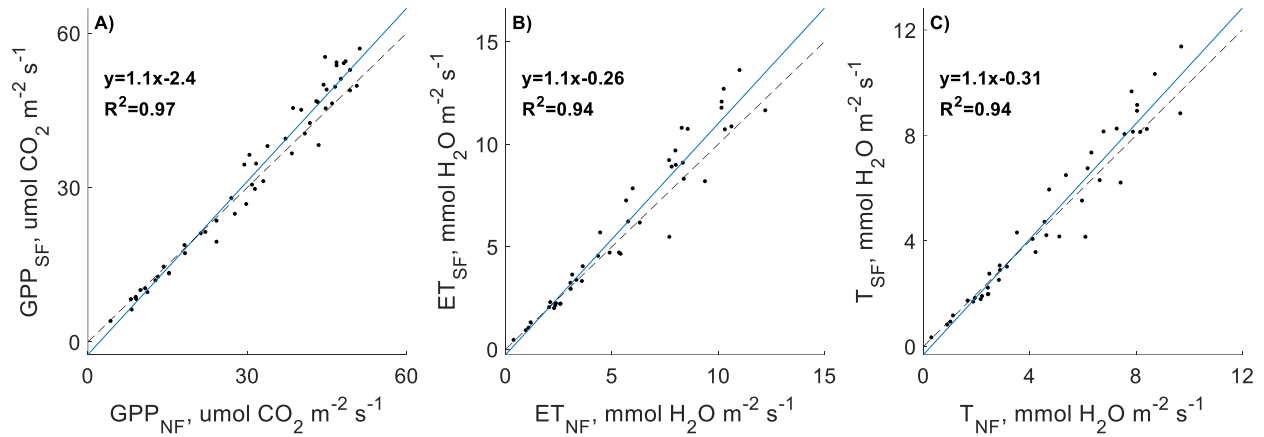

Figure 1. Comparison of half-hourly GPP, ET, and T (n= 41) during the June 20, 2015 drying event across NF and SF where SF is drying for approximately 2 days (to volumetric water content of 31%). The dashed line is 1:1 and the blue line is the line of best fit.

 The observations indicate that GPP, ET, and T across NF and SF are very similar during the drying event with SF exhibiting slightly higher GPP, ET, and T despite drying (slope of 1.1 relative to the NF for all three terms). We further compared the differences in each term across NF and SF to test if declining soil moisture or water depth could significantly explain variation across both fields during the drying event. Because the landscape fluxes are heavily energy driven, we normalized each term (GPP, ET, T) by SW_{in} measured across each field during the drying event. Differences in SW_{in}-normalized GPP and ET across NF and SF were not significantly explained by declining soil moisture in the drying field across 20-Jun drying event in 2015 (Figure 2).
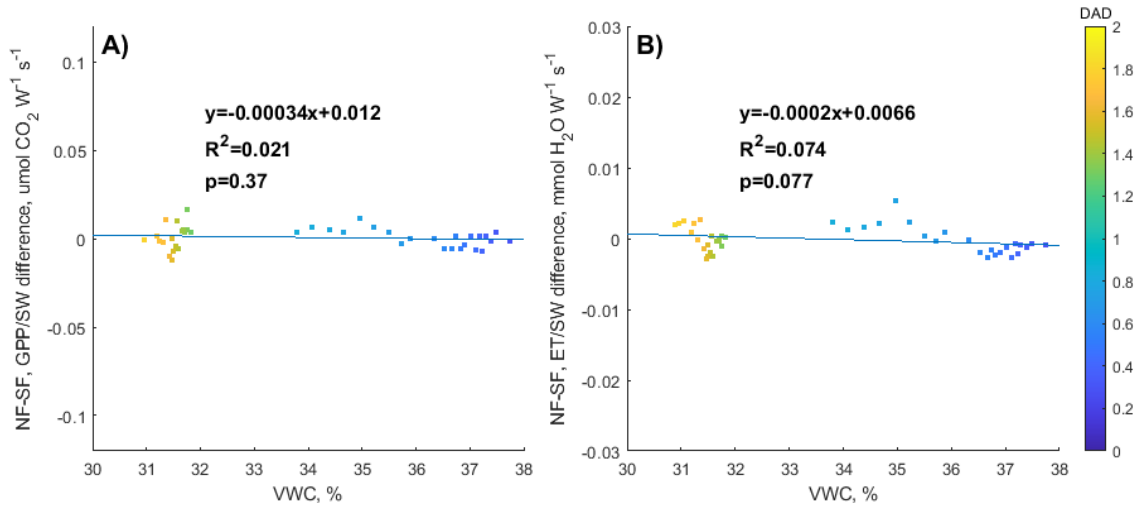
Figure 2. Analysis of the field-to-field difference in SW_{in}-normalized half-hourly A) GPP and B) ET (n=41) during the 20-Jun drying event in 2015 where SF is drying for approximately 2 days. Points are colored by days after drying (DAD). The blue line is the line of best fit between VWC and the differences in SW-normalized GPP or ET.

During the 13-Jun drying event, the declining soil moisture was able to significantly explain field-to-field differences in GPP, but not ET (Figure 3). However, the relationship between differences in GPP and declining soil moisture indicate that as SF dried, GPP was increasingly greater in SF compared to NF. Contrastingly, we would expect SF to exhibit decreasing GPP and ET when experiencing drought stress. The result of this comparison would indicate that neither the 20-Jun nor the 13-Jun drying event was severe enough to generate a noticeable amount of plant stress in SF when compared directly to NF.
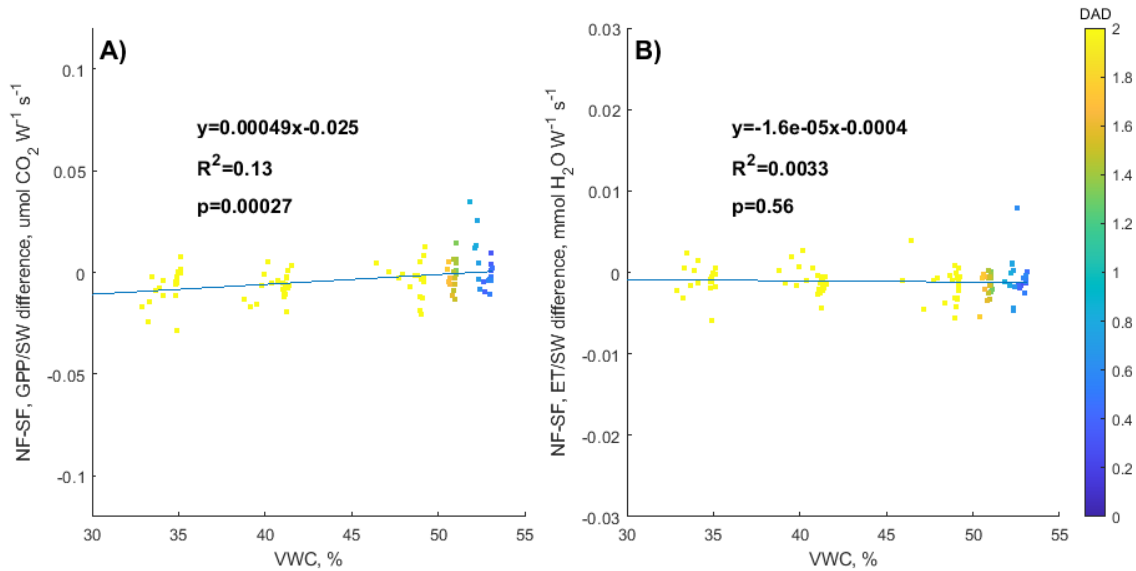
Figure 3. Analysis of the field-to-field difference in SWin-normalized half-hourly A) GPP and B) ET (n=101) during the 13-Jun 2015 drying event where SF is drying for approximately 2 days. Points are colored by days after drying (DAD). The blue line is the line of best fit between VWC and the differences in SW-normalized GPP or ET.

To further support our observations when comparing AWD directly to DF irrigation during drying events, we also compared the impacts of declining soil moisture with respect to GPP, ET and T within each field. Here, we observe the response of SW-normalized GPP, ET, and T across NF and SF to drying during AWD drying events to assess if drying has a significant impact on the terms individually. While we did observe significant responses of GPP and T during drying events, the responses both terms were not consistent across fields or during other drying events (Figure 4).
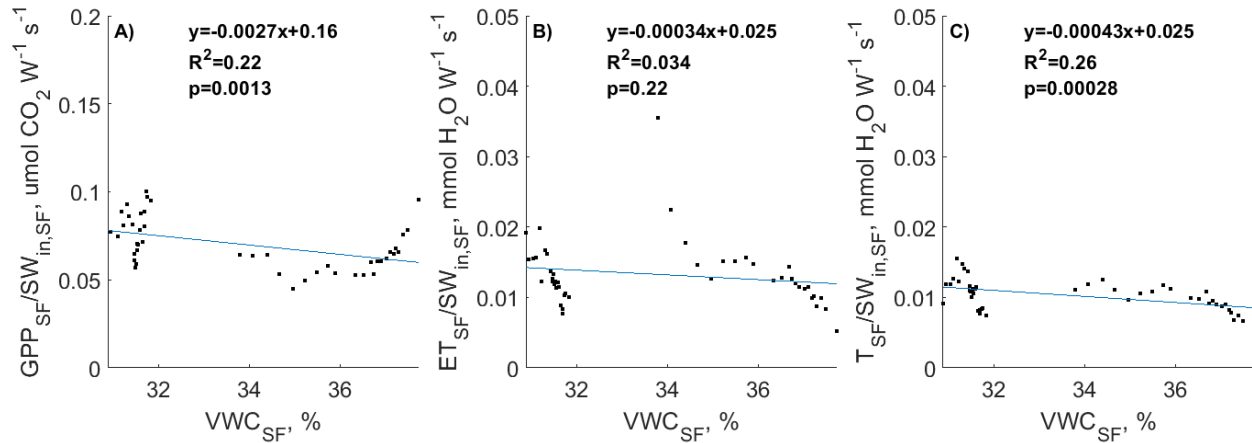
Figure 4. Comparison of SW_{in}-normalized, half-hourly GPP, ET, and T (n=41) response to declining soil moisture during the June 20, 2015 drying event in SF. The blue line is the line of best fit between VWC and SW-normalized GPP, ET, or T.

In the case of canopy stress due to drying, we would expect to see a decline in all three terms as a sign of significant drought stress. However, a majority of the drying events displayed opposing trends, as is the case in Figure 4, where both GPP and T were significantly correlated to declining VWC in SF during drying while ET was not.

We extended this comparison across all drying events where data coverage was available and found similar conflicting results wherein the responses of GPP, ET, and T were inconsistent across events and did not seem to explain any declines in activity due to drying. Across both NF and SF, the most severe drying event occurred from June 26 to June 29 during the 2016 growing season. During this event, NF and SF experienced the lowest VWC at 20.5% and 21.7%, respectively, and the overall shift in VWC from saturation to minimum dryness was approximately 35 percentage points. Comparing individual responses of GPP, ET, and T across both NF and SF during the most "severe" drying event, we still observed no significant drying response in ET and T (Figure 5,B-C, E-F) while the responses across fields in GPP were inconsistent (Figure 5, A,D). In this period, NF demonstrated a significant decline in radiation

79

SW$_{in}$-normalized GPP with respect to declining soil moisture (Figure 4A) while SF showed no such decline (Figure 5D).
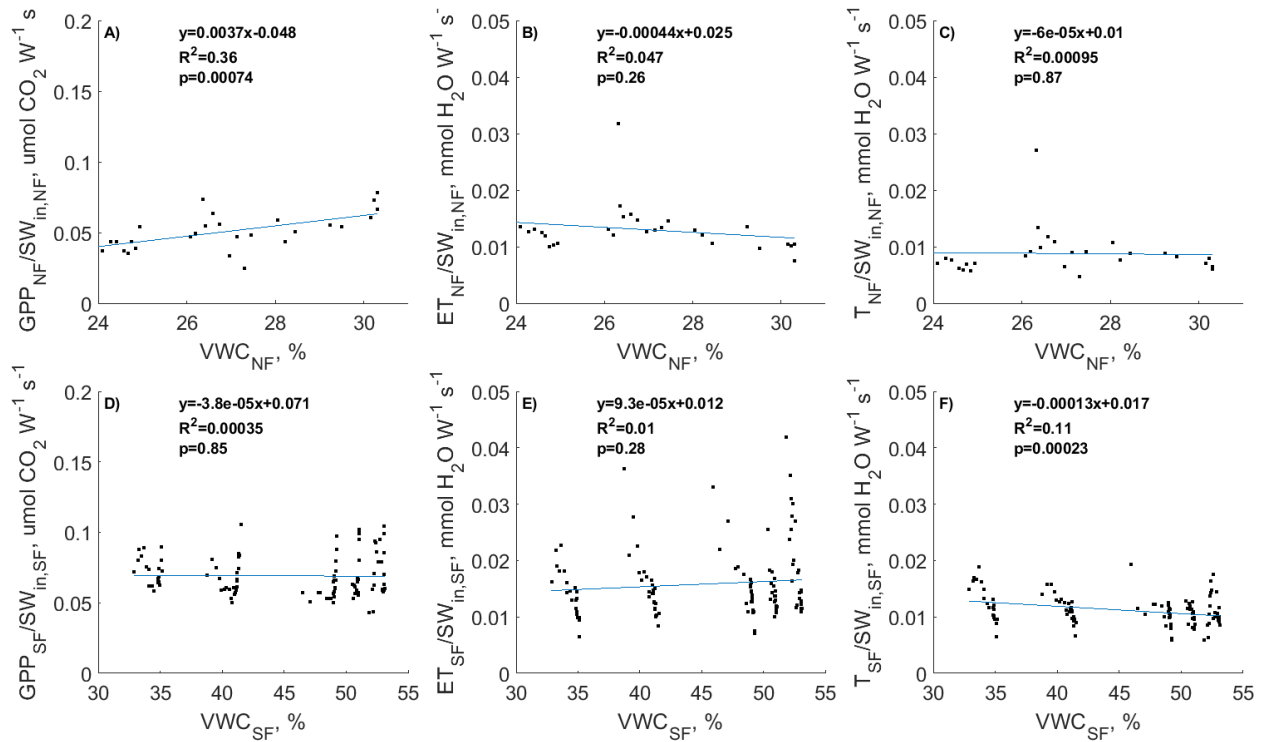

Figure 5. Comparison of drying responses in SW$_{in}$-normalized GPP, ET, and T between NF (A-C) and SF (D-F) during concurrent drying events beginning on 26-Jun in NF and 25-Jun in SF. The blue line is the line of best fit between VWC and SW-normalized GPP, ET, or T.

As a result of both analyses, we determined that soil moisture decline was unable to explain simultaneous differences in GPP, ET, and T between AWD and DF fields. Additionally, when looking at the impact of drying on GPP, ET, and T, there was no consistent response or decline in any of the terms that would indicate drought stress during drying events. Given the direct comparison of AWD to DF as well as the individual response analyses, we concluded that drying events were not likely to generate stress regardless of the minimum VWC during drying or the length of drying achieved in this experiment.

3.2 Dynamics and controls of WUE throughout the growing season

As demonstrated in Zhou et al. (2014), we examined the relationship between ET, VPD, and GPP to determine if the same water use efficiency relationships could be applied at our field sites. Between the relationships presented in Figure 6A, C, and D, the relationship between GPP and ET was best defined when accounting for VPD. Moreover, implementing the exponent of 0.5 on the VPD term improved the relationship slightly based on the greater R^2 values in Figure 6D compared to Figure 6C without it. Supported by these findings, we applied the relationship shown in Figure 6D in the uWUE approach, which is also consistent with Zhou et al. (2014). The relationship between ET and $GPP*VPD^{0.5}$ was consistent across both NF and SF as both GPP, ET, and VPD were always similar across both fields. Given the strong correlation ($R^2=0.8$) between ET and $GPPxVPD^{0.5}$ and the lack of response in GPP and ET to drying, we felt confident that the uWUE method could be used to estimate transpiration across both AWD and DF fields during all three growing seasons without the need for separate parameterization by irrigation management.
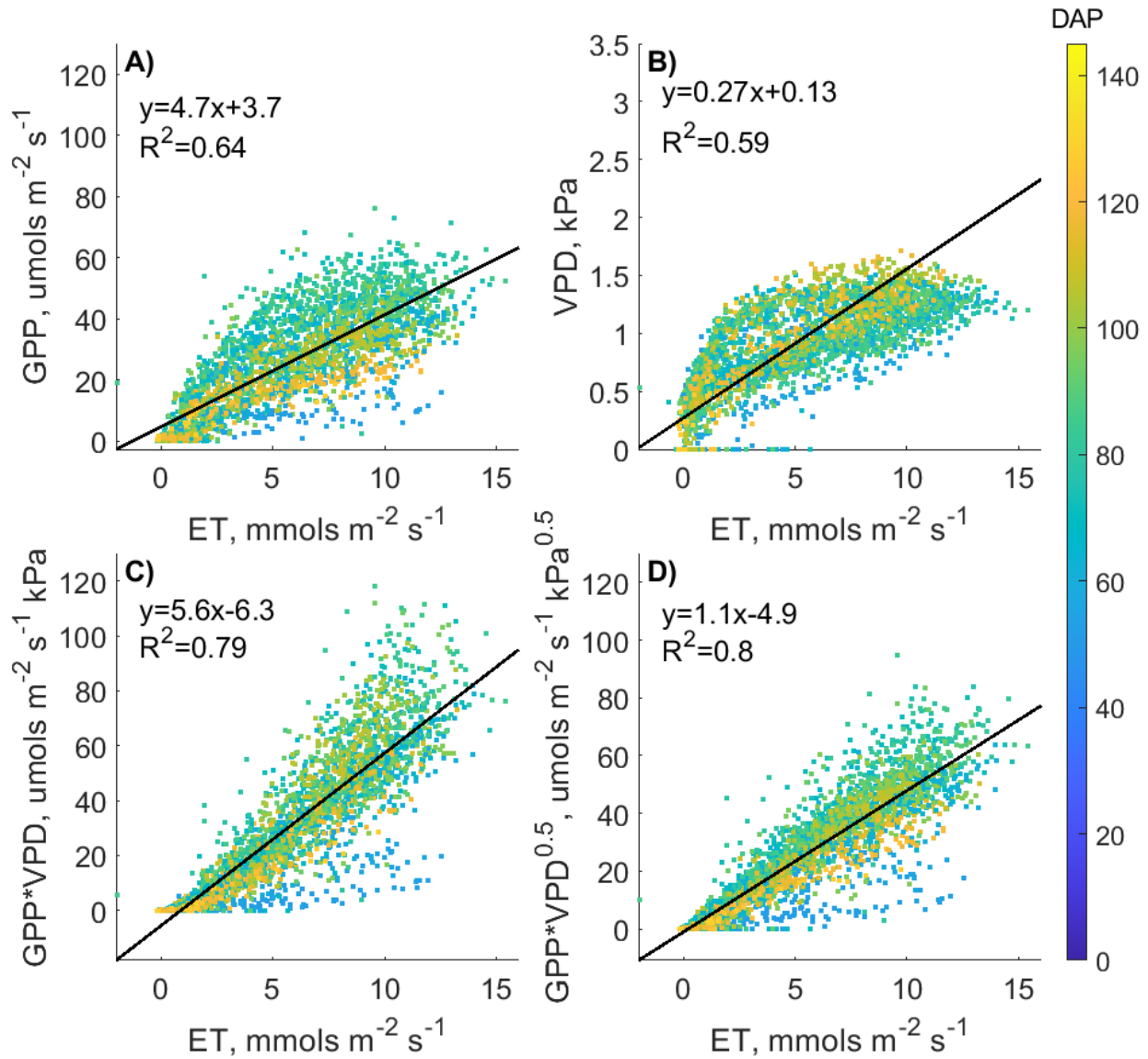
Figure 6. Comparison of half-hourly ET to GPP (A), VPD (B), GPPxVPD (C), and GPPxVPD$^{0.5}$ (D) across the 2015-2017 growing seasons at NF. The black line represents the linear regression taken in each plot between ET and the different variables represented on the y-axis.

Estimated daytime transpiration and associated WUE terms at the half-hourly time step were used to generate seasonal estimates for each term with respect to individual site-years (Table 3). The $uWUE_p$ ranged between 12.38 and 15.99 g CO_2 kg^{-1} H_2O hPa$^{0.5}$ across all site-years. Across the DF and AWD treatments, $uWUE_p$ was 14.26 ± 0.015 and 12.97 ± 0.012 g CO_2 kg^{-1} H_2O hPa$^{0.5}$, respectively, during the 2015-2017 growing seasons. Differences in mean

$uWUE_p$ between fields were minimal at 13.69 ± 0.19 g CO_2 kg^{-1} H_2O $hPa^{0.5}$ and 13.79 ± 0.12 g CO_2 kg^{-1} H_2O $hPa^{0.5}$ for SF and NF, respectively.

Table 3. Estimated $uWUE_p$, seasonal eWUE, tWUE, and estimated seasonal T:ET across NF and SF for the 2015-2017 growing seasons using half hourly gap filled daytime (SW_{in} >30 Wm^{-2}) data.

Field	Year	Irrigation Treatment	Cumulative T, mm	$uWUE_p$, g CO_2 kg^{-1} H_2O $hPa^{0.5}$	eWUE, g CO_2 kg^{-1} H_2O	tWUE, g CO_2 kg^{-1} H_2O	T:ET, mean
NF	2015	DF	287	12.22 ± 0.07	2.18 ± 0.03	4.17 ± 0.04	0.54 ± 0.006
	2016	AWD	259	15.94 ± 0.13	2.28 ± 0.03	5.05 ± 0.04	0.43 ± 0.006
	2017	DF	282	13.47 ± 0.09	2.34 ± 0.03	4.43 ± 0.04	0.46 ± 0.006
SF	2015	AWD	317	12.28 ± 0.07	2.35 ± 0.03	4.24 ± 0.04	0.56 ± 0.006
	2016	AWD	267	13.36 ± 0.19	2.34 ± 0.03	4.50 ± 0.04	0.49 ± 0.006
	2017	DF	270	15.29 ± 0.09	2.55 ± 0.03	5.06 ± 0.04	0.43 ± 0.013

Within each field, there was an inverse relationship between tWUE and $uWUE_p$ with mean seasonal T:ET, where increased tWUE and a higher $uWUE_p$ coincided with lower mean seasonal T:ET. Greater eWUE did not correlate well with tWUE or T:ET when looking at fields individually or collectively. The AWD and DF treatments did not have an identifiable effect on any of the observed WUE terms. Despite the small sample size for each irrigation treatment, values were comparable year to year for each term presented in Table 3. Across DF fields, mean eWUE, tWUE, and T:ET were 2.34 g CO_2 kg^{-1} H_2O, 4.58 g CO_2 kg^{-1} H_2O, and 0.47, respectively, for the 2015-2017 growing seasons. Comparatively, for AWD fields, mean eWUE, tWUE, and T:ET were 2.33 g CO_2 kg^{-1} H_2O, 4.64 g CO_2 kg^{-1} H_2O, and 0.50, respectively.

The patterns of eWUE and T:ET were consistent with each term increasing with canopy establishment and then slightly decreasing at harvest. Timing of peaks in eWUE varied year to year, ranging between 69 and 86 DAP for NF and 63 and 121 DAP for SF. The latest peaks in eWUE were during the 2016 growing season, where planting and harvest across both fields

occurred later in the year compared to 2015 and 2017. Peaks in T:ET occurred earlier on average compared to peaks in eWUE, ranging between 50 and 64 DAP for NF and 48 and 62 DAP for SF. For both NF and SF, tWUE was consistent throughout the growing season as both GPP and T scaled similarly, and there were no significant ($p>0.05$) differences between fields or irrigation treatments when comparing across all site-years.

At the daily time step, we compared the relationship of WUE to phenological development using daily LAI modeled for each site-year based on field measurements and growing degree days (GDD). Peak T:ET always preceded peak LAI by a period of 2 to 27 days across all growing seasons and fields. Patterns in peak eWUE and peak uWUE were less consistent in relation to peak LAI. Likewise, peaks in uWUE ranged between 51 and 73 DAP for NF and 72 and 118 for SF. In five of the six site-years, peak uWUE preceded peak LAI by a period ranging between 1 and 22 days (Figure 7). In SF during the 2015 growing season, peak uWUE lagged peak LAI by 17 days. Conversely, in all other site-years, uWUE preceded peak LAI by a period ranging between 14 and 48 days in NF and between 11 and 21 days in SF. From our observations of uWUE and eWUE with respect to LAI, the canopy was consistently more efficient in water use prior to the peak canopy area. We associate this observation with the differences in plant lifecycle and development, where peak eWUE and uWUE more closely align with the reproductive phase (60 to 90 DAP) of the plant lifecycle, where efficient water use is critical. For the timing of peak LAI, the timing was closer to the weeks following anthesis (90 to 100 DAP) at the end of reproduction, when grain filling begins.
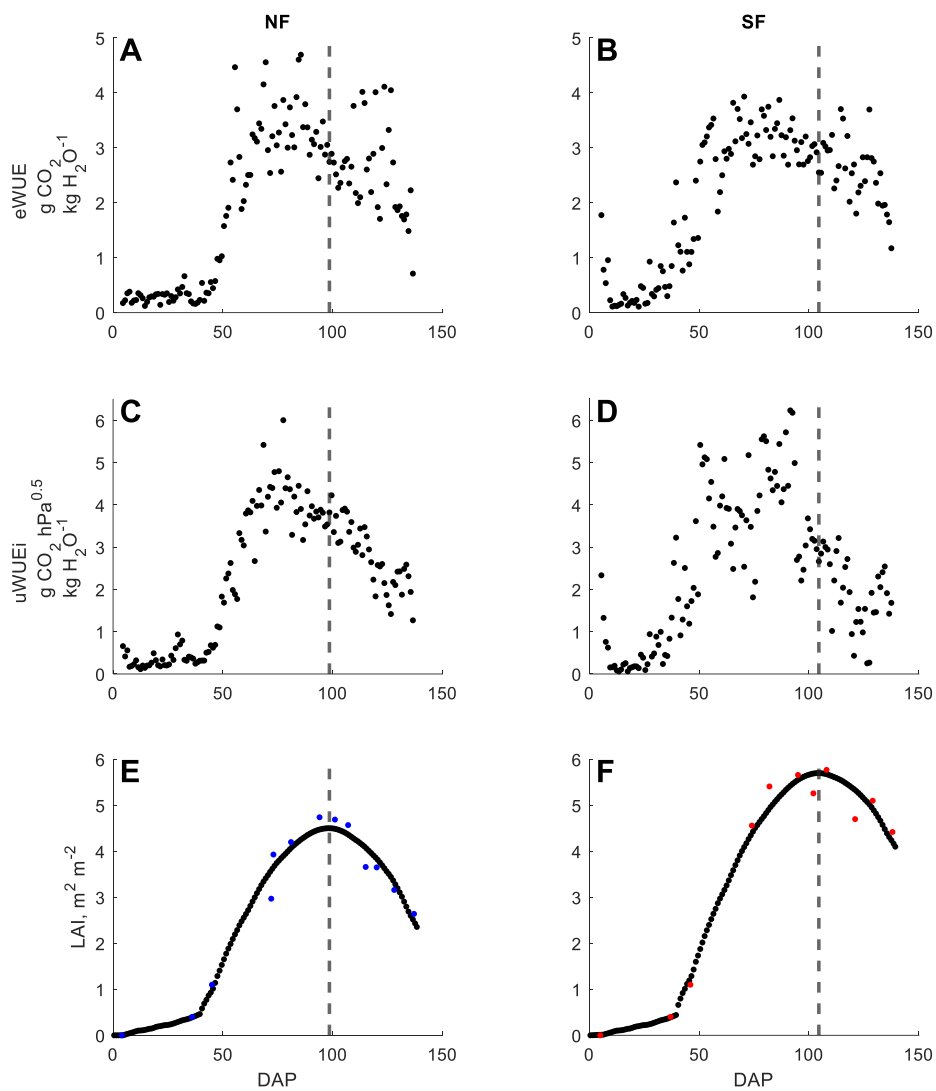
Figure 7. Daily eWUE (A&B), uWUE (C&D), and LAI (E&F) across NF and SF during the 2017 growing season. Dashed vertical line denotes day on which peak LAI occurred within each field.

To further highlight the role of phenological control on WUE, we examined the relationship between uWUE, eWUE, tWUE, and T:ET and LAI across each field using the full 2015-2017 dataset (Figure 8). Across both fields, eWUE, uWUE, and T:ET were positively correlated to growing season LAI and showed varying degrees of correlation.
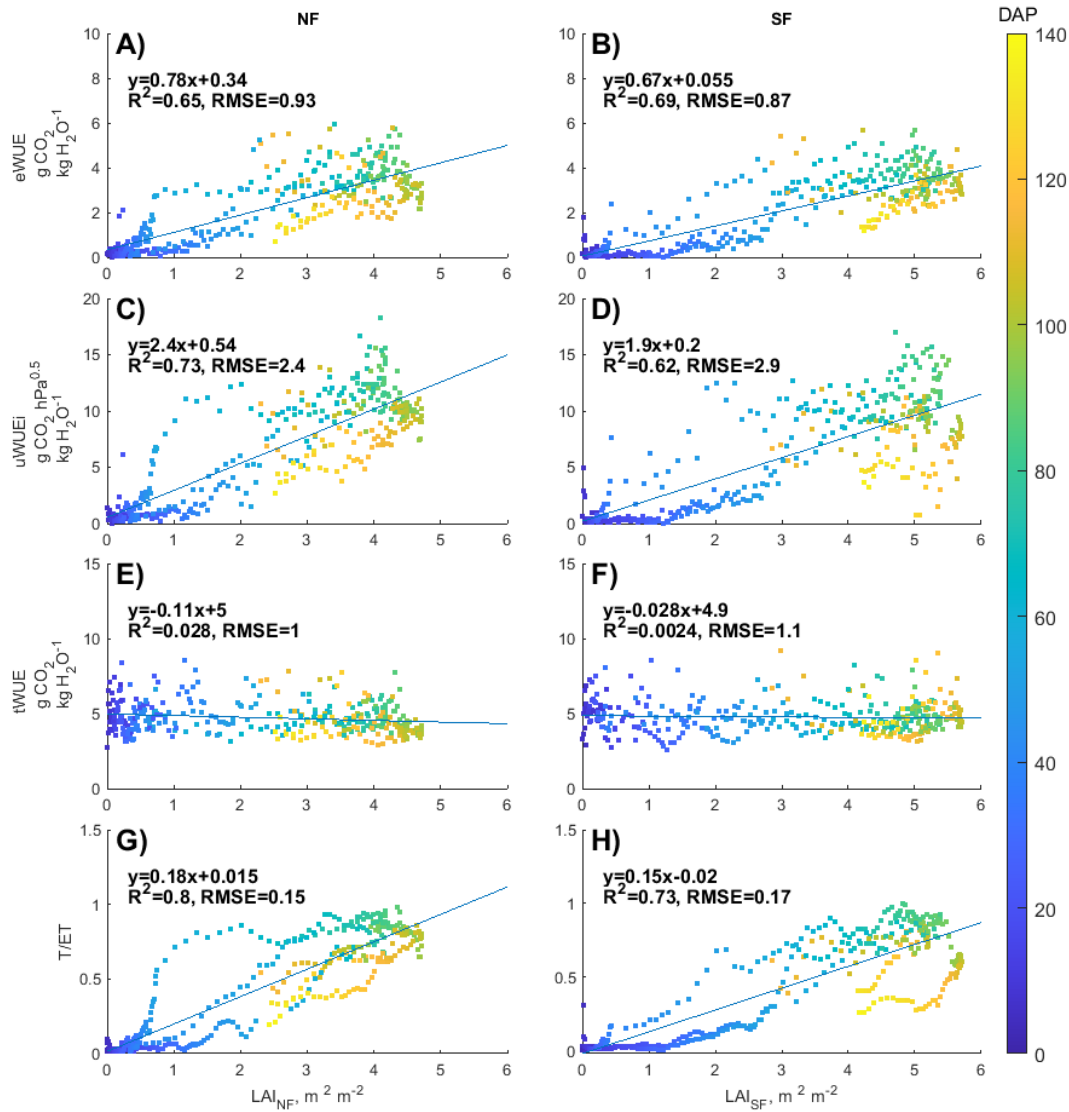
Figure 8. Daily eWUE, uWUE, tWUE, and weekly T/ET compared to LAI across NF and SF for the 2015-2017 growing seasons. Points are colored by DAP.

The relationship between tWUE and LAI was less dynamic as GPP, T, and LAI increase concurrently throughout the growing season. Our results indicated that increased leaf area did not explain a considerable portion of the seasonal variance in tWUE. In Figure 8E and 8F, we see that tWUE remains relatively stable, which suggests that the rate of exchange between GPP and T is independent of leaf area. Accordingly, increasing leaf area does not appear to influence the canopy's water use across the growing season. The strongest relationship defined in Figure 8,

86

was between LAI and T:ET, where LAI was able to explain 80% and 73% of the variance in T:ET at the daily time step across NF and SF, respectively. The relationship between eWUE and uWUE was also strong across both fields with LAI explaining at least 65% of the variance in daily eWUE and at least 63% of the variance in daily uWUE.

Across eWUE, uWUE, and T:ET, we also observed a clear hysteretic relationship where the peak values for each term occurred prior to peak LAI, and the mean relationship pre- and post-peak LAI was distinctly different. This disconnect between canopy productivity and development is also clear in the lag of peak LAI with respect to peak GPP, where maximum GPP precedes peak LAI across every site-year. During the 2015-2017 growing seasons, we observed a peak GPP preceding peak LAI with the time between peaks ranging from 9 to 27 days. If we discard the 2016 LAI time series based on the limited number of growing season observations and reliance on scaling from MODIS LAI, the time between peak GPP and LAI narrows to 15 to 27 days for the 2015 and 2017 growing seasons. We suspect that elevated production is likely tied to the canopy's prioritization of grain creation during the reproductive phases (60 to 90 DAP). The highest rates of GPP closely aligned with the reproductive phases between panicle differentiation and booting, occurring approximately 73 to 83 DAP across NF and SF during the 2015-2017 growing seasons. Peak LAI values then align with the transition from reproductive phases to grain filling during maturation, beginning around 90 to 110 DAP. Specifically, this transition was marked by the beginning of anthesis in the field, which occurred consistently between 90 and 94 DAP across all site-years based on field observations and PhenoCam imagery.

3.3 Comparison and challenges of methods used to partition evapotranspiration

When comparing T and ET rates across the uWUE, PM56Dual, and PT-JPL methods for the 2015-2017 growing seasons, the period of observation was limited to days where data were available for all three methods. During the overlapping period, modeled T accounted for at least 79% of seasonal ET across all three methods with PM56Dual indicating the highest T:ET at 87% (Figure 9). While the methods were similar in their determined T:ET, the overall magnitudes still varied with T estimates ranging between 768 mm (PT-JPL) and 1104 mm (PM56Dual) during the overlapping period of 206 days spanning the 2015-2017 growing seasons. The range of transpiration across individual years was more varied when comparing across all methods (Table 4). The PM56Dual method provided the highest estimates of both T and ET across each growing season.
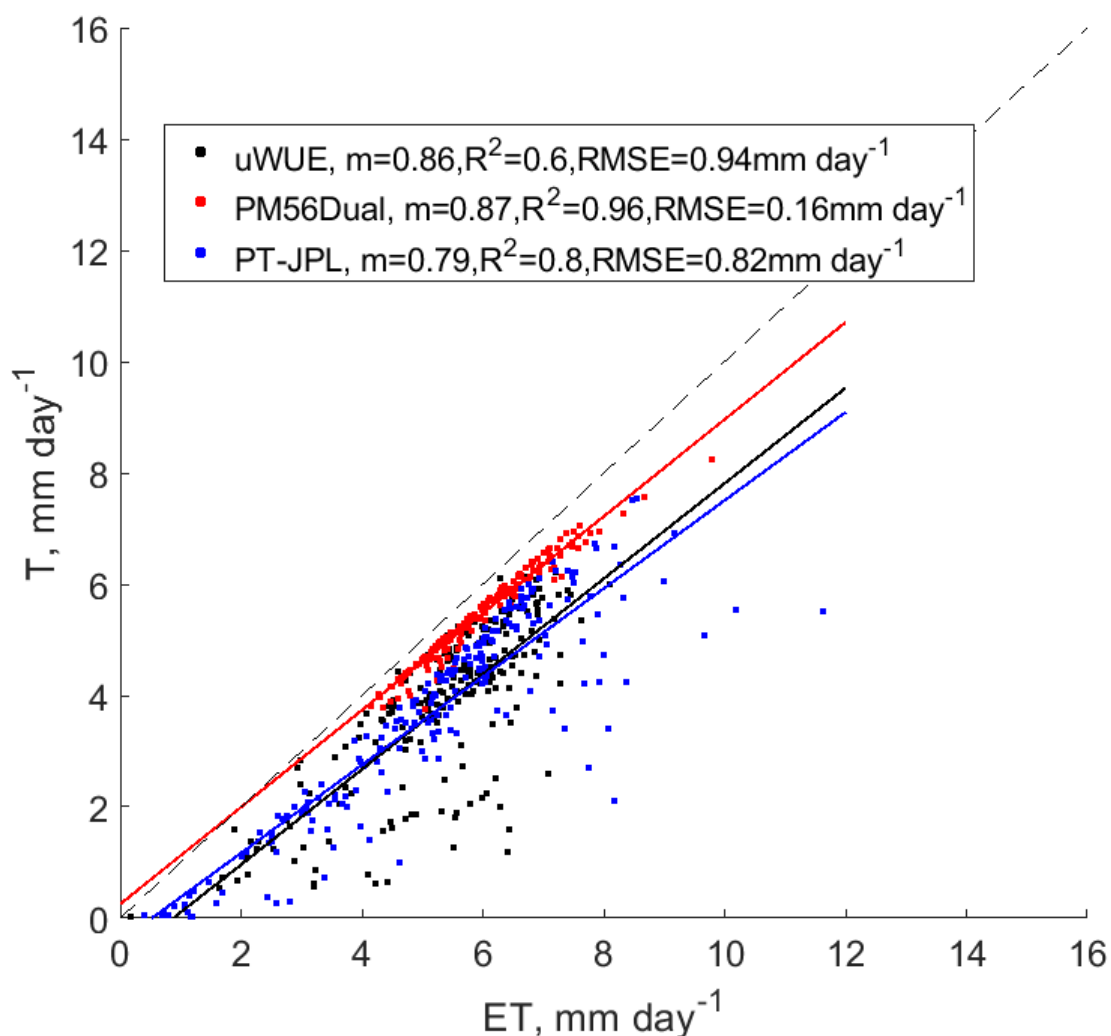
Figure 9. Comparison of daily T to ET for the uWUE, PM56Dual, and PT-JPL methods during the 2015-2017 growing seasons during periods where estimates from all methods were available. Estimates of PT-JPL and uWUE methods are aggregated across NF and SF while PM56Dual is scaled from reference site. Dashed line is 1:1.

The PT-JPL and uWUE methods were the most comparable of the methods in terms of both T and ET estimation during the periods of overlap across each growing season. While the mean relationship between the PM56Dual and uWUE methods was similar based on the slopes presented in Figure 9, the resulting ET and T sums from the overlap periods between the uWUE and PT-JPL methods were actually much closer to one another (Table 4). The PT-JPL and uWUE methods were able to estimate similar cumulative amounts of ET using data from the

field sites with only 7 to 9 mm during the 2015-2017 growing seasons. Using the local weather

station data, the PM56Dual estimated greater ET than the other methods in all three growing

seasons.

Table 4. T and ET estimates for each method during days of overlapping data collection within the 2015-2017 growing seasons.

Year	Method	Days of overlap	T, mm	ET, mm
2015	uWUE		287	358
	PM56Dual	63	380	417
	PT-JPL		266	362
2016	uWUE		245	362
	PM56Dual	70	379	413
	PT-JPL		252	373
2017	uWUE		257	382
	PM56Dual	73	345	376
	PT-JPL		250	344

Within each growing season, the PT-JPL and uWUE methods modeled transpiration with

phenological development, where transpiration increased similarly to LAI or GPP throughout the

growing season (Figure 10). Daily dynamics for the PM56Dual method were heavily dictated by

the basal crop coefficient, which did not reflect the magnitude of change present in LAI or GPP

throughout the growing season. Because the PM56Dual method did not exhibit strong seasonal

change with respect to canopy development, the maximum T:ET always occurred sooner

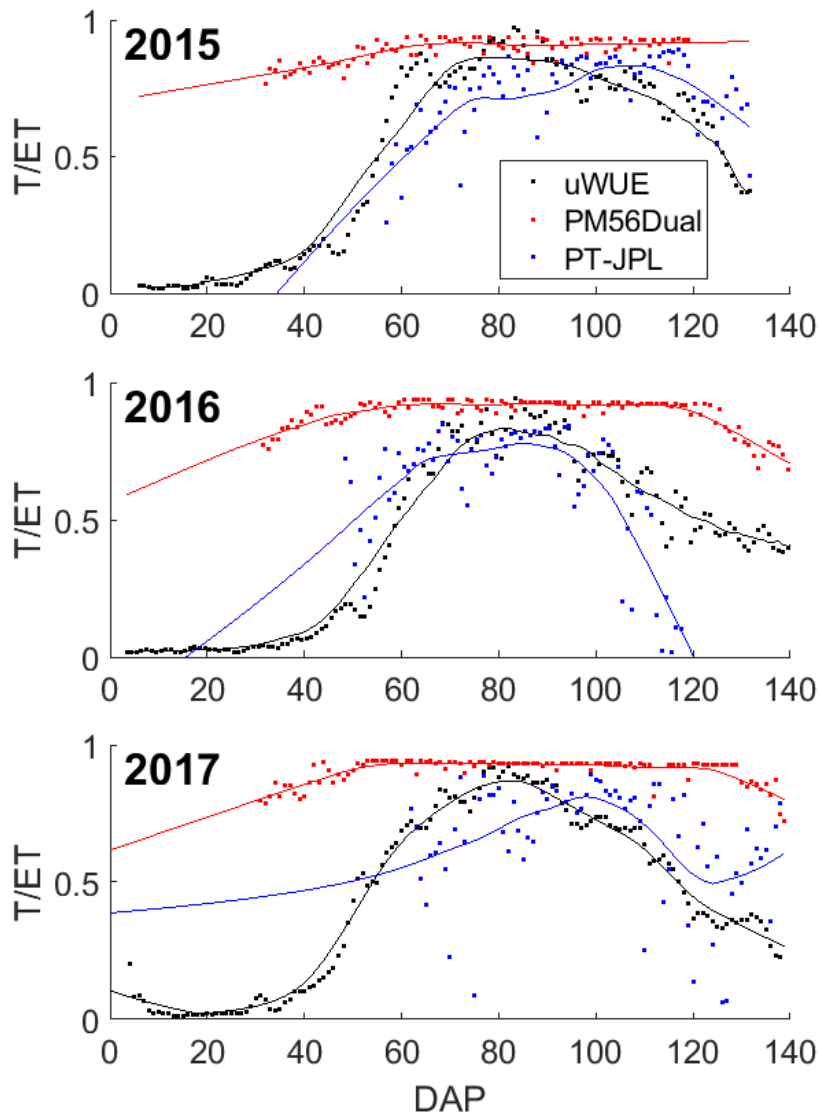compared to the PT-JPL and uWUE methods (Figure 10).

Figure 10. Time series of T:ET across the uWUE, PM56Dual, and PT-JPL methods during the 2015-2017 growing seasons averaged across NF and SF.

When comparing peak values of T:ET across the growing season when estimates were available for all three methods, the PM56Dual method preceded the other two methods consistently by at least 19 days across the 2015-2017 growing seasons. Peak T:ET for the PT-JPL method lagged the uWUE method between 17 to 34 days during the 2015 and 2017 growing seasons while preceding peak uWUE T:ET by 10 days. As mentioned earlier, the 2016 dataset is

somewhat limited as it reflects a scaled MODIS LAI rather than relying solely on field observations as in 2015 and 2016. If we remove the impact of the MODIS time series, the lag between the PT-JPL and uWUE is likely linked to the difference in peak timing between the LAI and GPP terms. The PT-JPL transpiration is largely energy driven with LAI being incorporated to partition total RN to available RN within the canopy. In contrast, the seasonality in uWUE transpiration is largely linked to GPP, which typically precedes LAI as shown earlier in our analysis of the control of LAI on GPP, eWUE, and uWUE. As a result, dynamics of transpiration can vary based on how either phenology and/or production are accounted for within different modeling frameworks.

4. Discussion

4.1 Impacts of drying on GPP in AWD irrigation treatments

During individual AWD drying events, we determined that there was no noticeable decline in GPP with respect to declining soil moisture after accounting for differences in incoming SW radiation as the primary driver. Given our previous work (Reavis et al. 2021), where drying also lacked a significant impact on ET, we felt confident that AWD and DF fields would exhibit similar patterns in WUE throughout the growing season. As a result, we were also confident in using the uWUE method to estimate transpiration across both DF and AWD fields given the lack of impact drying had on GPP and ET. In other studies, aggregated net ecosystem exchange of CO_2 , GPP, and yield showed no significant changes across fields under traditional irrigation practices and intermittent flooding practices across a variety of global rice production systems (Alberto et al., 2009; Oliver et al., 2019). However, given the differences in application of AWD and soil characteristics between fields, the degree of drying that occurs between fields is often difficult to compare. While we did not observe significant differences in the responses of

92

ET and GPP to drying, those responses will likely differ with respect to the degree of drying, including drying event length, field soil properties, and rice variety (Lin et al., 2014; Kar et al., 2018; Carrijo et al., 2018).

4.2 Growing season rice WUE dynamics

The WUE dynamics indicated a close relationship between eWUE, uWUE, and T:ET with canopy development using LAI as a proxy. However, we also observed a noticeable lag in peak LAI with respect to when the canopy was most efficient in terms of water use. Furthermore, differences in peak LAI and WUE were primarily a reflection of the differences in LAI and GPP throughout the growing season. The primary driver for differences in peak production and canopy infrastructure was the transition from reproductive growth to maturation. We determined that after the reproductive phases, the canopy largely prioritized grain filling during maturation over water use, which is consistent with other studies analyzing rice canopy development during the growing season (Xue et al., 2016, 2017). The shift in WUE during the maturation phases has been linked to decreases in canopy light use efficiency as additional plant material results in greater amounts of shading. In the context of our study, the rice canopy likely experienced a decline in GPP with respect to increasing LAI during anthesis around 90 DAP, resulting in lower WUE. The decline in light use efficiency post-anthesis has been observed in rice, where radiation use is decreased at similar levels of LAI pre- and post-anthesis (Campbell et al., 2001; Saito et al., 2005).

We observed an eWUE ranging from 2.18 to 2.55 g CO_2 kg^{-1} H_2O across the 2015-2017 growing seasons in NF and SF, which is higher than other studies reporting growing season eWUE in paddy rice globally (Wang et al., 2018, 2017; Jiang et al., 2020). Values of eWUE reported in Jiang et al. (2020) ranged were 1.38 g CO_2 kg^{-1} H_2O and 1.56 g CO_2 kg^{-1} H_2O for rice

grown in California, USA (US-Twt) and Ibaraki, Japan (JAN-MSE), respectively. The potential uWUE ($uWUE_p$) during the 2015-2017 growing seasons ranged between 12.20 and 15.99 g CO_2 kg^{-1} H_2O $hPa^{0.5}$ across NF and SF. The same sites from Jiang et al. (2020) were 8.94 (US-Twt; California) and 7.06 (JAN-MSE; Japan) g CO_2 kg^{-1} H_2O $hPa^{0.5}$. In NF and SF, tWUE ranged from 4.17 to 5.06 g CO_2 kg^{-1} H_2O across the 2015-2017 growing seasons. Compared to our study sites, rice tWUE reported in Jiang et al. (2020) was lower at both the US-Twt (2.57 g CO_2 kg^{-1} H_2O) and the JAN-MSE (2.23 g CO_2 kg^{-1} H_2O) sites. The effective growing season ET rates for the Jiang et al. (2020) sites were 4.61 ± 0.24 mm day^{-1} and 3.94 ± 0.17 mm day^{-1} for the US-Twt and JAN-MSE sites, respectively. Comparatively, the effective growing season ET rate for NF and SF ranged between 4.27 ± 0.10 mm day^{-1} and 4.30 ± 0.13 mm day^{-1}, which are within the range presented for US-Twt and JAN-MSE sites. Conversely, the mean effective daily GPP rates for NF and SF were 8.83 ± 0.51 gC m^{-2} day^{-1} and 9.20 ± 0.33 gC m^{-2} day^{-1}, respectively, which were greater than the reported mean value of 6.38 ± 0.45 g C m^{-2} d^{-1} across the US-Twt and JAN-MSE sites. Comparing yields, NF and SF averaged 10.03 and 10.4 t ha^{-1} normalized to 13% moisture content, and the US-Twt site produced yields ranging between 4.5 and 7.4 t ha^{-1} normalized to 14% moisture content (Knox et al., 2016). Given the higher GPP, WUE, and resulting yields, it seems likely that local meteorology or agronomic practices could explain the differences in water use between NF and SF and other paddy rice sites. Moreover, as $uWUE_p$ is likely related to photosynthetic capacity, varietal differences in rice could also play a large role in determining both tWUE and eWUE.

Differences in management and historical use present challenges for directly comparing between this study and the results from US-Twt. The US-Twt site is defined by a primarily Mediterranean climate with much lower annual precipitation, lower humidity, and cooler

nighttime temperatures compared to our sites in the humid Mid-South (Baldocchi et al., 2016; Hatala et al., 2012). The US-Twt site is also unique as a drained peatland in the Sacramento-San Joaquin Delta repurposed for agricultural production, including rice, and the soils are characterized by high soil organic matter (Chamberlain et al., 2018; Miller and Fujii, 2010). While our study sites are primarily used for commercial rice production, the US-Twt site is part of an ongoing assessment of rice production as a means to reduce soil subsidence while preventing oxidation of underlying peat and further mineralization (Kasak et al., 2021; Ye et al., 2016; Kirk et al., 2015). Given the differences in management styles and local climate, the added data and perspective on canopy water use in Arkansas rice production is valuable as Arkansas produces a majority of the rice in the US and has major economic and environmental impact (Hardke et al., 2021; Reba et al., 2017).

4.3 Comparison and evaluation of transpiration estimation methods

In our comparison of the uWUE, PM56Dual, and PT-JPL methods, we found that the uWUE and PT-JPL methods were superior in their ability to accurately reflect changes in growing season transpiration with respect to canopy development. One study indicated that local calibration of the PM56Dual method is necessary to yield accurate values of T in dry seeded rice systems similar to Mid-South practices as opposed to the practice of transplanting seedlings into flooded paddies (Alberto et al., 2014). Over the same period, the methods estimated a collective T:ET ranging between 0.79 to 0.87. The period of evaluation contained good coverage across the mid-to-late growing season from 50 DAP to harvest. The period is especially relevant as irrigation timing and decisions for producers typically do not occur until after the first 6 weeks. In comparing methods across each growing season, the PT-JPL and uWUE method produced

results that were close in proximity and the models generated a similar seasonal pattern of T:ET across the growing season.

The uWUE method yielded a growing season T:ET ranging between 0.43 and 0.56 across six site-years, which is consistent with several other studies utilizing a variety of methods to partition growing season ET in rice paddies (Table 5). Across the presented methods and this study, the PM56Dual method consistently estimated the highest T:ET ratio during the growing season.

Table 5. Summary of T, ET, and T:ET across multiple ET partitioning methods in rice paddy sites.

T, mm	ET, mm	T:ET	Partitioning Approach	Growing Season Length, days	Location	Transplanted Rice?	Study
		0.74	Isotope (Non steady-state)		Japan	No	(Wei et al., 2018)
		0.5	Shuttleworth Dual-Source				
360	480	0.75	Priestley-Taylor with scaling functions	138	China	No	(Qiu et al., 2019)
432	561	0.77		136			
358	527	0.68		161			
313	524	0.6	Empirical method	120	Philippines	No	(Alberto et al., 2014)
253	475	0.53		115			
285	348	0.82	FAO56 Dual Kc	116	India	Yes	(Anupoju and Kambhammettu, 2020)
322	384	0.84		109			
416	595	0.7	Leaf-level CO_2 Concentration Gradient w/ EC	147	Brazil	No	(Diaz et al., 2019)
418	762	0.55		164			
373	677	0.55		164			
434	733	0.59		162			
477	716	0.67		154			
338	693	0.49		168			

Methods incorporating direct observations of H_2O and CO_2 fluxes, similar to the uWUE method, indicated lower mean T:ET ratio across their respective studies, and the range of values presented in our study was still consistently lower. Given the differences in canopy GPP compared to canopy LAI, methods utilizing either variable as a major partitioning component will likely inherit the same differences in seasonal dynamics between LAI and GPP. We observed peak T:ET in the PT-JPL lagging the uWUE method across each growing season,

which was almost certainly due to the difference in peak LAI and GPP utilized in each method, respectively.

5. Conclusions

In this work, AWD had no appreciable impact on water use during the growing season when compared directly to DF irrigation. Furthermore, we observed the individual responses of GPP, ET, and T to declining soil moisture across multiple drying events and found no indicators of stress consistent across fields or irrigation treatment. Using the uWUE method, we determined that growing season T for Mid-South rice ranged between 259 and 317 mm with mean growing season T:ET ranging between 0.43 and 0.56 across six site-years. The fields were most water efficient prior to peak LAI across all growing seasons, which was consistent with GPP peaking during the end of the reproductive phases prior to maturation and grain filling. The uWUE, PM56Dual, and PT-JPL methods indicated a mean seasonal T:ET ranging between 0.79 and 0.86 during of the mid-to-late growing season across all three study years. While the ratios of T:ET were comparable across methods, the differences in ET and resulting transpiration across methods were as much as 50 and 100 mm, respectively. Like the differences between GPP and LAI with respect to WUE, methods relying on LAI as a partitioning variable resulted in different T and T:ET dynamics compared to GPP-based methods. The uWUE and PT-JPL methods utilized different indicators of phenology and associated canopy activity in GPP and LAI, respectively. Consequently, the methods exhibited similar seasonal dynamics in T and T:ET with the lag between GPP and LAI, where the uWUE method yielded a maximum T:ET prior to the PT-JPL method across each growing season. Our study provided estimates of T, eWUE, tWUE, and $uWUE_p$ which were greater than other applications of the uWUE at paddy rice sites reported in the literature The elevated WUE and GPP also translated to greater yields when comparing NF

and SF to other rice paddy sites. The increased water use efficiency could be reflective of the decreased VPD and sunlight due to cloud cover in the humid Mid-South as compared to other rice production areas like California. Additionally, our estimates of T and T:ET were well within the range provided by other methods across different rice sites. Given our findings, we considered the uWUE method a valuable approach for partitioning fluxes and providing better insight to canopy WUE dynamics during the growing season. Moreover, our findings support the adoption of AWD as a water saving technique where drying events did not impact GPP, ET, or T, which indicates that canopy water use was undeterred.

6. Acknowledgements

Chapter 2 References:

Alberto, Ma.C.R., Quilty, J.R., Buresh, R.J., Wassmann, R., Haidar, S., Correa, T.Q., Sandro, J.M., 2014. Actual evapotranspiration and dual crop coefficients for dry-seeded rice and hybrid maize grown with overhead sprinkler irrigation. Agricultural Water Management 136, 1–12. https://doi.org/10.1016/j.agwat.2014.01.005

Alberto, Ma.C.R., Wassmann, R., Hirano, T., Miyata, A., Kumar, A., Padre, A., Amante, M., 2009. CO2/heat fluxes in rice fields: Comparative assessment of flooded and non-flooded fields in the Philippines. Agricultural and Forest Meteorology 149, 1737–1750. https://doi.org/10.1016/j.agrformet.2009.06.003

Allen, R.G., 2000. Using the FAO-56 dual crop coefficient method over an irrigated region as part of an evapotranspiration intercomparison study. Journal of Hydrology 229, 27–41. https://doi.org/10.1016/S0022-1694(99)00194-8

Allen, R.G., Pereira, L.S., Raes, D., Smith, M., 1998. Crop evapotranspiration - Guidelines for computing crop water requirements - FAO Irrigation and drainage paper 56. FAO, Rome 300, D05109.

Allen, R.G., Pereira, L.S., Smith, M., Raes, D., Wright, J.L., 2005. FAO-56 dual crop coefficient method for estimating evaporation from soil and application extensions. Journal of irrigation and drainage engineering 131, 2–13.

Anupoju, V., Kambhammettu, B.V.N.P., 2020. Role of deficit irrigation strategies on ET partition and crop water productivity of rice in semi-arid tropics of south India. Irrig Sci 38, 415–430. https://doi.org/10.1007/s00271-020-00684-1

Baldocchi, D., Knox, S., Dronova, I., Verfaillie, J., Oikawa, P., Sturtevant, C., Matthes, J.H., Detto, M., 2016. The impact of expanding flooded land area on the annual evaporation of rice. Agricultural and Forest Meteorology 223, 181–193. https://doi.org/10.1016/j.agrformet.2016.04.001

Béziat, P., Rivalland, V., Tallec, T., Jarosz, N., Boulet, G., Gentine, P., Ceschia, E., 2013. Evaluation of a simple approach for crop evapotranspiration partitioning and analysis of the water budget distribution for several crop species. Agricultural and Forest Meteorology 177, 46–56. https://doi.org/10.1016/j.agrformet.2013.03.013

Bouman, B.A.M., Peng, S., Castañeda, A.R., Visperas, R.M., 2005. Yield and water use of irrigated tropical aerobic rice systems. Agricultural Water Management 74, 87–105. https://doi.org/10.1016/j.agwat.2004.11.007

Cahoon, J., Ferguson, J., Edwards, D., Tacker, P., 1990. A microcomputer-based irrigation scheduler for the humid mid-south region. Applied Engineering in Agriculture 6, 289–295.

Campbell, C.S., Heilman, J.L., McInnes, K.J., Wilson, L.T., Medley, J.C., Wu, G., Cobos, D.R., 2001. Seasonal variation in radiation use efficiency of irrigated rice. Agricultural and Forest Meteorology 110, 45–54. https://doi.org/10.1016/S0168-1923(01)00277-5

Carrijo, D.R., Akbar, N., Reis, A.F.B., Li, C., Gaudin, A.C.M., Parikh, S.J., Green, P.G., Linquist, B.A., 2018. Impacts of variable soil drying in alternate wetting and drying rice systems on yields, grain arsenic concentration and soil moisture dynamics. Field Crops Research 222, 101–110. https://doi.org/10.1016/j.fcr.2018.02.026

Carrijo, D.R., Lundy, M.E., Linquist, B.A., 2017. Rice yields and water use under alternate wetting and drying irrigation: A meta-analysis. Field Crops Research 203, 173–180. https://doi.org/10.1016/j.fcr.2016.12.002

Chamberlain, S.D., Anthony, T.L., Silver, W.L., Eichelmann, E., Hemes, K.S., Oikawa, P.Y., Sturtevant, C., Szutu, D.J., Verfaillie, J.G., Baldocchi, D.D., 2018. Soil properties and sediment accretion modulate methane fluxes from restored wetlands. Global Change Biology 24, 4107–4121. https://doi.org/10.1111/gcb.14124

Cheng, W., Sakai, H., Yagi, K., Hasegawa, T., 2009. Interactions of elevated $[CO_2]$ and night temperature on rice growth and yield. Agricultural and Forest Meteorology 149, 51–58. https://doi.org/10.1016/j.agrformet.2008.07.006

Collatz, G.J., Ball, J.T., Grivet, C., Berry, J.A., 1991. Physiological and environmental regulation of stomatal conductance, photosynthesis and transpiration: a model that includes a laminar boundary layer. Agricultural and Forest Meteorology 54, 107–136. https://doi.org/10.1016/0168-1923(91)90002-8

Diaz, M.B., Roberti, D.R., Carneiro, J.V., Souza, V. de A., de Moraes, O.L.L., 2019. Dynamics of the superficial fluxes over a flooded rice paddy in southern Brazil. Agricultural and Forest Meteorology 276–277, 107650. https://doi.org/10.1016/j.agrformet.2019.107650

Fisher, J.B., Lee, B., Purdy, A.J., Halverson, G.H., Dohlen, M.B., Cawse-Nicholson, K., Wang, A., Anderson, R.G., Aragon, B., Arain, M.A., Baldocchi, D.D., Baker, J.M., Barral, H., Bernacchi, C.J., Bernhofer, C., Biraud, S.C., Bohrer, G., Brunsell, N., Cappelaere, B., Castro-Contreras, S., Chun, J., Conrad, B.J., Cremonese, E., Demarty, J., Desai, A.R., Ligne, A.D., Foltýnová, L., Goulden, M.L., Griffis, T.J., Grünwald, T., Johnson, M.S., Kang, M., Kelbe, D., Kowalska, N., Lim, J.-H., Maïnassara, I., McCabe, M.F., Missik, J.E.C., Mohanty, B.P., Moore, C.E., Morillas, L., Morrison, R., Munger, J.W., Posse, G., Richardson, A.D., Russell, E.S., Ryu, Y., Sanchez-Azofeifa, A., Schmidt, M., Schwartz, E., Sharp, I., Šigut, L., Tang, Y., Hulley, G., Anderson, M., Hain, C., French, A., Wood, E., Hook, S., 2020. ECOSTRESS: NASA's Next Generation Mission to Measure Evapotranspiration From the International Space Station. Water Resources Research 56, e2019WR026058. https://doi.org/10.1029/2019WR026058

Fisher, J.B., Tu, K.P., Baldocchi, D.D., 2008. Global estimates of the land–atmosphere water flux based on monthly AVHRR and ISLSCP-II data, validated at 16 FLUXNET sites. Remote Sensing of Environment 112, 901–919. https://doi.org/10.1016/j.rse.2007.06.025

Gong, X., Qiu, R., Ge, J., Bo, G., Ping, Y., Xin, Q., Wang, S., 2021. Evapotranspiration partitioning of greenhouse grown tomato using a modified Priestley–Taylor model. Agricultural Water Management 247, 106709. https://doi.org/10.1016/j.agwat.2020.106709

Haefele, S.M., Siopongco, J.D.L.C., Boling, A.A., Bouman, B.A.M., Tuong, T.P., 2009. Transpiration efficiency of rice (Oryza sativa L.). Field Crops Research 111, 1–10. https://doi.org/10.1016/j.fcr.2008.09.008

Hardke, J., Sha, X., Bateman, N., 2021. BR Wells Arkansas Rice Research Studies 2020.

Hatala, J.A., Detto, M., Sonnentag, O., Deverel, S.J., Verfaillie, J., Baldocchi, D.D., 2012. Greenhouse gas (CO_2, CH_4, H_2O) fluxes from drained and flooded agricultural peatlands in the Sacramento-San Joaquin Delta. Agriculture, Ecosystems & Environment 150, 1–18. https://doi.org/10.1016/j.agee.2012.01.009

Henry, A., Gowda, V.R.P., Torres, R.O., McNally, K.L., Serraj, R., 2011. Variation in root system architecture and drought response in rice (Oryza sativa): Phenotyping of the OryzaSNP panel in rainfed lowland fields. Field Crops Research 120, 205–214. https://doi.org/10.1016/j.fcr.2010.10.003

Henry, C.G., Daniels, M., Hamilton, M., Hardke, J.T., 2013. Water Management, in: Arkansas Rice Production Handbook. University of Arkansas Extension Service, pp. 103–128.

Howell, T.A., 2001. Enhancing water use efficiency in irrigated agriculture. Agronomy journal 93, 281–289.

Hsiao, T.C., Steduto, P., Fereres, E., 2007. A systematic and quantitative approach to improve water use efficiency in agriculture. Irrig Sci 25, 209–231. https://doi.org/10.1007/s00271-007-0063-2

Jiang, S., Liang, C., Cui, N., Zhao, L., Liu, C., Feng, Y., Hu, X., Gong, D., Zou, Q., 2020. Water use efficiency and its drivers in four typical agroecosystems based on flux tower measurements. Agricultural and Forest Meteorology 295, 108200. https://doi.org/10.1016/j.agrformet.2020.108200

Kar, I., Sudhir-Yadav, Mishra, A., Behera, B., Khanda, C., Kumar, V., Kumar, A., 2018. Productivity trade-off with different water regimes and genotypes of rice under non-puddled conditions in Eastern India. Field Crops Research 222, 218–229. https://doi.org/10.1016/j.fcr.2017.10.007

Kasak, K., Espenberg, M., Anthony, T.L., Tringe, S.G., Valach, A.C., Hemes, K.S., Silver, W.L., Mander, Ü., Kill, K., McNicol, G., Szutu, D., Verfaillie, J., Baldocchi, D.D., 2021. Restoring wetlands on intensive agricultural lands modifies nitrogen cycling microbial communities and reduces N_2O production potential. Journal of Environmental Management 299, 113562. https://doi.org/10.1016/j.jenvman.2021.113562

Kato, Y., Okami, M., Katsura, K., 2009. Yield potential and water use efficiency of aerobic rice (Oryza sativa L.) in Japan. Field Crops Research 113, 328–334. https://doi.org/10.1016/j.fcr.2009.06.010

Kim, H.-Y., Lieffering, M., Kobayashi, K., Okada, M., Miura, S., 2003. Seasonal changes in the effects of elevated CO_2 on rice at three levels of nitrogen supply: a free air CO_2 enrichment (FACE) experiment. Global Change Biology 9, 826–837. https://doi.org/10.1046/j.1365-2486.2003.00641.x

Kima, A.S., Chung, W.G., Wang, Y.-M., Traoré, S., 2015. Evaluating water depths for high water productivity in irrigated lowland rice field by employing alternate wetting and drying technique under tropical climate conditions, Southern Taiwan. Paddy Water Environ 13, 379–389. https://doi.org/10.1007/s10333-014-0458-7

Kirk, E.R., van Kessel, C., Horwath, W.R., Linquist, B.A., 2015. Estimating annual soil carbon loss in agricultural peatland soils using a nitrogen budget approach. PloS one 10, e0121432.

Knox, S.H., Matthes, J.H., Sturtevant, C., Oikawa, P.Y., Verfaillie, J., Baldocchi, D., 2016. Biophysical controls on interannual variability in ecosystem-scale CO2 and CH4 exchange in a California rice paddy. Journal of Geophysical Research: Biogeosciences 121, 978–1001. https://doi.org/10.1002/2015JG003247

Knox, S.H., Sturtevant, C., Matthes, J.H., Koteen, L., Verfaillie, J., Baldocchi, D., 2015. Agricultural peatland restoration: effects of land-use change on greenhouse gas (CO2 and CH4) fluxes in the Sacramento-San Joaquin Delta. Global Change Biology 21, 750–765. https://doi.org/10.1111/gcb.12745

Kobayasi, K., Matsui, T., Yoshimoto, M., Hasegawa, T., 2010. Effects of Temperature, Solar Radiation, and Vapor-Pressure Deficit on Flower Opening Time in Rice. Plant Production Science 13, 21–28. https://doi.org/10.1626/pps.13.21

Kool, D., Agam, N., Lazarovitch, N., Heitman, J.L., Sauer, T.J., Ben-Gal, A., 2014. A review of approaches for evapotranspiration partitioning. Agricultural and Forest Meteorology 184, 56–70. https://doi.org/10.1016/j.agrformet.2013.09.003

Lampayan, R.M., Rejesus, R.M., Singleton, G.R., Bouman, B.A.M., 2015a. Adoption and economics of alternate wetting and drying water management for irrigated lowland rice. Field Crops Research 170, 95–108. https://doi.org/10.1016/j.fcr.2014.10.013

Lampayan, R.M., Samoy-Pascual, K.C., Sibayan, E.B., Ella, V.B., Jayag, O.P., Cabangon, R.J., Bouman, B.A.M., 2015b. Effects of alternate wetting and drying (AWD) threshold level and plant seedling age on crop performance, water input, and water productivity of transplanted rice in Central Luzon, Philippines. Paddy Water Environ 13, 215–227. https://doi.org/10.1007/s10333-014-0423-5

Law, B.E., Falge, E., Gu, L., Baldocchi, D.D., Bakwin, P., Berbigier, P., Davis, K., Dolman, A.J., Falk, M., Fuentes, J.D., Goldstein, A., Granier, A., Grelle, A., Hollinger, D., Janssens, I.A., Jarvis, P., Jensen, N.O., Katul, G., Mahli, Y., Matteucci, G., Meyers, T., Monson, R., Munger, W., Oechel, W., Olson, R., Pilegaard, K., Paw U, K.T., Thorgeirsson, H., Valentini, R., Verma, S., Vesala, T., Wilson, K., Wofsy, S., 2002. Environmental controls over carbon dioxide and water vapor exchange of terrestrial vegetation. Agricultural and Forest Meteorology, FLUXNET 2000 Synthesis 113, 97–120. https://doi.org/10.1016/S0168-1923(02)00104-1

Lin, L., Zhang, Z., Janssen, M., Lennartz, B., 2014. Infiltration properties of paddy fields under intermittent irrigation. Paddy Water Environ 12, 17–24. https://doi.org/10.1007/s10333-013-0354-6

Martin, D.L., Stegman, E.C., Fereres, E., 1990. Irrigation scheduling principles. IN: Management of Farm Irrigation Systems. American Society of Agricultural Engineers, St. Joseph, MI. 1990. p 155-203, 19 fig, 9 tab, 81 ref.

Massey, J.H., Walker, T.W., Anders, M.M., Smith, M.C., Avila, L.A., 2014. Farmer adaptation of intermittent flooding using multiple-inlet rice irrigation in Mississippi. Agricultural Water Management 146, 297–304. https://doi.org/10.1016/j.agwat.2014.08.023

Massmann, A., Gentine, P., Lin, C., 2019. When Does Vapor Pressure Deficit Drive or Reduce Evapotranspiration? Journal of Advances in Modeling Earth Systems 11, 3305–3320. https://doi.org/10.1029/2019MS001790

Miller, R.L., Fujii, R., 2010. Plant community, primary productivity, and environmental conditions following wetland re-establishment in the Sacramento-San Joaquin Delta, California. Wetlands Ecol Manage 18, 1–16. https://doi.org/10.1007/s11273-009-9143-9

Milliman, T., Seyednasrollah, B., Young, A.M., Hufkens, K., Friedl, M.A., Frolking, S., Richardson, A.D., Abraha, M., Allen, D.W., Apple, M., Arain, M.A., Baker, J., Baker, J.M., Bernacchi, C.J., Bhattacharjee, J., Blanken, P., Bosch, D.D., Boughton, R., Boughton, E.H., Brown, R.F., Browning, D.M., Brunsell, N., Burns, S.P., Cavagna, M., Chu, H., Clark, P.E., Conrad, B.J., Cremonese, E., Debinski, D., Desai, A.R., Diaz-Delgado, R., Duchesne, L., Dunn, A.L., Eissenstat, D.M., El-Madany, T., Ellum, D.S.S., Ernest, S.M., Esposito, A., Fenstermaker, L., Flanagan, L.B., Forsythe, B., Gallagher, J., Gianelle, D., Griffis, T., Groffman, P., Gu, L., Guillemot, J., Halpin, M., Hanson, P.J., Hemming, D., Hove, A.A., Humphreys, E.R., Jaimes-Hernandez, A., Jaradat, A.A., Johnson, J., Keel, E., Kelly, V.R., Kirchner, J.W., Kirchner, P.B., Knapp, M., Krassovski, M., Langvall, O., Lanthier, G., Maire, G. l., Magliulo, E., Martin, T.A., McNeil, B., Meyer, G.A., Migliavacca, M., Mohanty, B.P., Moore, C.E., Mudd, R., Munger, J.W., Murrell, Z.E., Nesic, Z., Neufeld, H.S., Oechel, W., Oishi, A.C., Oswald, W.W., Perkins, T.D., Reba, M.L., Rundquist, B., Runkle, B.R., Russell, E.S., Sadler, E.J., Saha, A., Saliendra, N.Z., Schmalbeck, L., Schwartz, M.D., Scott, R.L., Smith, E.M., Sonnentag, O., Stoy, P., Strachan, S., Suvocarev, K., Thom, J.E., Thomas, R.Q., Van den berg, A.K., Vargas, R., Vogel, C.S., Walker, J.J., Webb, N., Wetzel, P., Weyers, S., Whipple, A.V., Whitham, T.G., Wohlfahrt, G., Wood, J.D., Yang, J., Yang, X., Yenni, G., Zhang, Y., Zhang, Q., Zona, D., Baldocchi, D., Verfaillie, J., 2019. PhenoCam Dataset v2.0: Digital Camera Imagery from the PhenoCam Network, 2000-2018. https://doi.org/10.3334/ORNLDAAC/1689

Moldenhauer, K., Counce, P., Hardke, J., 2013. Rice Growth and Development, in: Arkansas Rice Production Handbook. University of Arkansas Extension Service, pp. 9–20.

Moreno-García, B., Coronel, E., Reavis, C.W., Suvočarev, K., Runkle, B.R.K., 2021. Environmental sustainability assessment of rice management practices using decision support tools. Journal of Cleaner Production 315, 128135. https://doi.org/10.1016/j.jclepro.2021.128135

Nelson, J.A., Pérez-Priego, O., Zhou, S., Poyatos, R., Zhang, Y., Blanken, P.D., Gimeno, T.E., Wohlfahrt, G., Desai, A.R., Gioli, B., Limousin, J.-M., Bonal, D., Paul-Limoges, E., Scott, R.L., Varlagin, A., Fuchs, K., Montagnani, L., Wolf, S., Delpierre, N., Berveiller, D., Gharun, M., Belelli Marchesini, L., Gianelle, D., Šigut, L., Mammarella, I., Siebicke, L., Andrew Black, T., Knohl, A., Hörtnagl, L., Magliulo, V., Besnard, S., Weber, U., Carvalhais, N., Migliavacca, M., Reichstein, M., Jung, M., 2020. Ecosystem transpiration and evaporation: Insights from three water flux partitioning methods across FLUXNET sites. Global Change Biology 26, 6916–6930. https://doi.org/10.1111/gcb.15314

Norton, G.J., Shafaei, M., Travis, A.J., Deacon, C.M., Danku, J., Pond, D., Cochrane, N., Lockhart, K., Salt, D., Zhang, H., Dodd, I.C., Hossain, M., Islam, M.R., Price, A.H., 2017. Impact of alternate wetting and drying on rice physiology, grain production, and grain quality. Field Crops Research 205, 1–13. https://doi.org/10.1016/j.fcr.2017.01.016

Oliver, V., Cochrane, N., Magnusson, J., Brachi, E., Monaco, S., Volante, A., Courtois, B., Vale, G., Price, A., Teh, Y.A., 2019. Effects of water management and cultivar on carbon dynamics, plant productivity and biomass allocation in European rice systems. Science of The Total Environment 685, 1139–1151. https://doi.org/10.1016/j.scitotenv.2019.06.110

O'Toole, J.C., Baldia, E.P., 1982. Water Deficits and Mineral Uptake in Rice. Crop Science 22, cropsci1982.0011183X002200060014x. https://doi.org/10.2135/cropsci1982.0011183X002200060014x

Pan, J., Liu, Y., Zhong, X., Lampayan, R.M., Singleton, G.R., Huang, N., Liang, K., Peng, B., Tian, K., 2017. Grain yield, water productivity and nitrogen use efficiency of rice under different water management and fertilizer-N inputs in South China. Agricultural Water Management 184, 191–200. https://doi.org/10.1016/j.agwat.2017.01.013

Paredes, P., Rodrigues, G.C., Alves, I., Pereira, L.S., 2014. Partitioning evapotranspiration, yield prediction and economic returns of maize under various irrigation management strategies. Agricultural Water Management 135, 27–39. https://doi.org/10.1016/j.agwat.2013.12.010

Qiu, R., Liu, C., Cui, N., Wu, Y., Wang, Z., Li, G., 2019. Evapotranspiration estimation using a modified Priestley-Taylor model in a rice-wheat rotation system. Agricultural Water Management 224, 105755. https://doi.org/10.1016/j.agwat.2019.105755

Reavis, C.W., Suvočarev, K., Reba, M.L., Runkle, B.R.K., 2021. Impacts of alternate wetting and drying and delayed flood rice irrigation on growing season evapotranspiration. Journal of Hydrology 596, 126080. https://doi.org/10.1016/j.jhydrol.2021.126080

Reba, M.L., Massey, J.H., Adviento-Borbe, M.A., Leslie, D., Yaeger, M.A., Anders, M., Farris, J., 2017. Aquifer Depletion in the Lower Mississippi River Basin: Challenges and Solutions. Journal of Contemporary Water Research & Education 162, 128–139. https://doi.org/10.1111/j.1936-704X.2017.03264.x

Reichstein, M., Falge, E., Baldocchi, D., Papale, D., Aubinet, M., Berbigier, P., Bernhofer, C., Buchmann, N., Gilmanov, T., Granier, A., Grünwald, T., Havránková, K., Ilvesniemi, H., Janous, D., Knohl, A., Laurila, T., Lohila, A., Loustau, D., Matteucci, G., Meyers, T., Miglietta, F., Ourcival, J.-M., Pumpanen, J., Rambal, S., Rotenberg, E., Sanz, M., Tenhunen, J., Seufert, G., Vaccari, F., Vesala, T., Yakir, D., Valentini, R., 2005. On the separation of net ecosystem exchange into assimilation and ecosystem respiration: review and improved algorithm. Global Change Biology 11, 1424–1439. https://doi.org/10.1111/j.1365-2486.2005.001002.x

Reichstein, M., Stoy, P.C., Desai, A.R., Lasslop, G., Richardson, A.D., 2012. Partitioning of Net Fluxes, in: Aubinet, M., Vesala, T., Papale, D. (Eds.), Eddy Covariance: A Practical Guide to Measurement and Data Analysis, Springer Atmospheric Sciences. Springer Netherlands, Dordrecht, pp. 263–289. https://doi.org/10.1007/978-94-007-2351-1_9

Runkle, B.R.K., Suvočarev, K., Reba, M.L., Reavis, C.W., Smith, S.F., Chiu, Y.-L., Fong, B., 2019. Methane Emission Reductions from the Alternate Wetting and Drying of Rice Fields Detected Using the Eddy Covariance Method. Environ. Sci. Technol. 53, 671–681. https://doi.org/10.1021/acs.est.8b05535

Saito, M., Miyata, A., Nagai, H., Yamada, T., 2005. Seasonal variation of carbon dioxide exchange in rice paddy field in Japan. Agricultural and Forest Meteorology 135, 93–109. https://doi.org/10.1016/j.agrformet.2005.10.007

Schlesinger, W.H., Jasechko, S., 2014. Transpiration in the global water cycle. Agricultural and Forest Meteorology 189–190, 115–117. https://doi.org/10.1016/j.agrformet.2014.01.011

Shuttleworth, W.J., 1991. Evaporation models in hydrology, in: Land Surface Evaporation. Springer, pp. 93–120.

Shuttleworth, W.J., Wallace, J.S., 1985. Evaporation from sparse crops-an energy combination theory. Quarterly Journal of the Royal Meteorological Society 111, 839–855. https://doi.org/10.1002/qj.49711146910

Soil Survey Staff, USDA-NRCS, 2018. Web Soil Survey [WWW Document]. URL https://websoilsurvey.sc.egov.usda.gov (accessed 12.3.18).

Stannard, D.I., 1993. Comparison of Penman-Monteith, Shuttleworth-Wallace, and Modified Priestley-Taylor Evapotranspiration Models for wildland vegetation in semiarid rangeland. Water Resources Research 29, 1379–1392. https://doi.org/10.1029/93WR00333

Stoy, P.C., El-Madany, T.S., Fisher, J.B., Gentine, P., Gerken, T., Good, S.P., Klosterhalfen, A., Liu, S., Miralles, D.G., Perez-Priego, O., Rigden, A.J., Skaggs, T.H., Wohlfahrt, G., Anderson, R.G., Coenders-Gerrits, A.M.J., Jung, M., Maes, W.H., Mammarella, I., Mauder, M., Migliavacca, M., Nelson, J.A., Poyatos, R., Reichstein, M., Scott, R.L., Wolf, S., 2019. Reviews and syntheses: Turning the challenges of partitioning ecosystem evaporation and transpiration into opportunities. Biogeosciences 16, 3747–3775. https://doi.org/10.5194/bg-16-3747-2019

Sudhir-Yadav, Humphreys, E., Li, T., Gill, G., Kukal, S.S., 2012. Evaluation of tradeoffs in land and water productivity of dry seeded rice as affected by irrigation schedule. Field Crops Research 128, 180–190. https://doi.org/10.1016/j.fcr.2012.01.005

Suvočarev, K., Castellví, F., Reba, M.L., Runkle, B.R.K., 2019. Surface renewal measurements of H, λE and CO2 fluxes over two different agricultural systems. Agricultural and Forest Meteorology 279, 107763. https://doi.org/10.1016/j.agrformet.2019.107763

Tanner, C.B., Jury, W.A., 1976. Estimating Evaporation and Transpiration from a Row Crop during Incomplete Cover1. Agronomy Journal 68, 239–243. https://doi.org/10.2134/agronj1976.00021962006800020007x

Tian, H., Chen, G., Liu, M., Zhang, C., Sun, G., Lu, C., Xu, X., Ren, W., Pan, S., Chappelka, A., 2010. Model estimates of net primary productivity, evapotranspiration, and water use efficiency in the terrestrial ecosystems of the southern United States during 1895–2007. Forest Ecology and Management, Managing landscapes at multiple scales for sustainability of ecosystem functions 259, 1311–1327. https://doi.org/10.1016/j.foreco.2009.10.009

Tomar, V.S., O'Toole, J.C., 1980. Water use in lowland rice cultivation in Asia: A review of evapotranspiration. Agricultural Water Management 3, 83–106. https://doi.org/10.1016/0378-3774(80)90017-7

Tuong, T.P., Bhuiyan, S.I., 1999. Increasing water-use efficiency in rice production: farm-level perspectives. Agricultural Water Management 40, 117–122. https://doi.org/10.1016/S0378-3774(98)00091-2

Wallace, J.S., 2000. Increasing agricultural water use efficiency to meet future food production. Agriculture, Ecosystems & Environment 82, 105–119. https://doi.org/10.1016/S0167-8809(00)00220-6

Wang, L., Good, S.P., Caylor, K.K., 2014. Global synthesis of vegetation control on evapotranspiration partitioning. Geophysical Research Letters 41, 6753–6757. https://doi.org/10.1002/2014GL061439

Wang, T., Tang, X., Zheng, C., Gu, Q., Wei, J., Ma, M., 2018. Differences in ecosystem water-use efficiency among the typical croplands. Agricultural Water Management 209, 142–150. https://doi.org/10.1016/j.agwat.2018.07.030

Wang, Y., Zhou, L., Jia, Q., Yu, W., 2017. Water use efficiency of a rice paddy field in Liaohe Delta, Northeast China. Agricultural Water Management 187, 222–231. https://doi.org/10.1016/j.agwat.2017.03.029

Wei, Z., Lee, X., Wen, X., Xiao, W., 2018. Evapotranspiration partitioning for three agro-ecosystems with contrasting moisture conditions: a comparison of an isotope method and a two-source model calculation. Agricultural and Forest Meteorology 252, 296–310. https://doi.org/10.1016/j.agrformet.2018.01.019

Wopereis, M.C.S., Kropff, M.J., Maligaya, A.R., Tuong, T.P., 1996. Drought-stress responses of two lowland rice cultivars to soil water status. Field Crops Research 46, 21–39. https://doi.org/10.1016/0378-4290(95)00084-4

Xu, Y., Ge, J., Tian, S., Li, S., Nguy-Robertson, A.L., Zhan, M., Cao, C., 2015. Effects of water-saving irrigation practices and drought resistant rice variety on greenhouse gas emissions from a no-till paddy in the central lowlands of China. Science of The Total Environment 505, 1043–1052. https://doi.org/10.1016/j.scitotenv.2014.10.073

Xue, W., Lindner, S., Dubbert, M., Otieno, D., Ko, J., Muraoka, H., Werner, C., Tenhunen, J., 2017. Supplement understanding of the relative importance of biophysical factors in determination of photosynthetic capacity and photosynthetic productivity in rice ecosystems. Agricultural and Forest Meteorology 232, 550–565. https://doi.org/10.1016/j.agrformet.2016.10.009

Xue, W., Lindner, S., Nay-Htoon, B., Dubbert, M., Otieno, D., Ko, J., Muraoka, H., Werner, C., Tenhunen, J., Harley, P., 2016. Nutritional and developmental influences on components of rice crop light use efficiency. Agricultural and Forest Meteorology 223, 1–16. https://doi.org/10.1016/j.agrformet.2016.03.018

Yang, J., Liu, K., Wang, Z., Du, Y., Zhang, J., 2007. Water-Saving and High-Yielding Irrigation for Lowland Rice by Controlling Limiting Values of Soil Water Potential. Journal of Integrative Plant Biology 49, 1445–1454. https://doi.org/10.1111/j.1672-9072.2007.00555.x

Yang, J., Zhou, Q., Zhang, J., 2017. Moderate wetting and drying increases rice yield and reduces water use, grain arsenic level, and methane emission. The Crop Journal, Advances in Crop Science: Innovation and Sustainability 5, 151–158. https://doi.org/10.1016/j.cj.2016.06.002

Yang, X., Wang, B., Chen, L., Li, P., Cao, C., 2019. The different influences of drought stress at the flowering stage on rice physiological traits, grain yield, and quality. Sci Rep 9, 3742. https://doi.org/10.1038/s41598-019-40161-0

Yao, F., Huang, J., Cui, K., Nie, L., Xiang, J., Liu, X., Wu, W., Chen, M., Peng, S., 2012. Agronomic performance of high-yielding rice variety grown under alternate wetting and drying irrigation. Field Crops Research 126, 16–22. https://doi.org/10.1016/j.fcr.2011.09.018

Ye, R., Espe, M.B., Linquist, B., Parikh, S.J., Doane, T.A., Horwath, W.R., 2016. A soil carbon proxy to predict CH4 and N2O emissions from rewetted agricultural peatlands. Agriculture, Ecosystems & Environment 220, 64–75. https://doi.org/10.1016/j.agee.2016.01.008

Zhang, B., Kang, S., Li, F., Zhang, L., 2008. Comparison of three evapotranspiration models to Bowen ratio-energy balance method for a vineyard in an arid desert region of northwest China. Agricultural and Forest Meteorology 148, 1629–1640. https://doi.org/10.1016/j.agrformet.2008.05.016

Zhao, P., Li, S., Li, F., Du, T., Tong, L., Kang, S., 2015. Comparison of dual crop coefficient method and Shuttleworth–Wallace model in evapotranspiration partitioning in a vineyard of northwest China. Agricultural Water Management 160, 41–56.

Zhou, S., Yu, B., Huang, Y., Wang, G., 2014. The effect of vapor pressure deficit on water use efficiency at the subdaily time scale. Geophysical Research Letters 41, 5005–5013. https://doi.org/10.1002/2014GL060741

Zhou, S., Yu, B., Zhang, Y., Huang, Y., Wang, G., 2018. Water use efficiency and evapotranspiration partitioning for three typical ecosystems in the Heihe River Basin, northwestern China. Agricultural and Forest Meteorology 253–254, 261–273. https://doi.org/10.1016/j.agrformet.2018.02.002

Zhou, S., Yu, B., Zhang, Y., Huang, Y., Wang, G., 2016. Partitioning evapotranspiration based on the concept of underlying water use efficiency. Water Resources Research 52, 1160–1175. https://doi.org/10.1002/2015WR017766

Zwart, S.J., Bastiaanssen, W.G.M., 2004. Review of measured crop water productivity values for irrigated wheat, rice, cotton and maize. Agricultural Water Management 69, 115–133. https://doi.org/10.1016/j.agwat.2004.04.007

Chapter 2: Appendix A

PT-JPL Functions

The following equations are used to estimate the scalars within the PT-JPL framework (Fisher et al., 2020). Any adjustments to the original formulations are referenced in the methods and we include those adjustments here:

$$f_{wet} = RH^4 \qquad \text{Eqn 7}$$

$$f_g = \frac{f_{APAR}}{f_{IPAR}} \qquad \text{Eqn 8}$$

$$f_{APAR} = \frac{PAR_{in} - PAR_{out}}{PAR_{in}} \quad \text{Eqn 9}$$

$$f_{IPAR} = \frac{PAR_{out}}{PAR_{in}} \qquad \text{Eqn 10}$$

$$f_T = e^{-\left(\frac{T_{max} - T_{opt}}{T_{opt}}\right)^2} \qquad \text{Eqn 11}$$

$$f_M = \frac{f_{APAR}}{f_{APAR,max}} \quad \text{Eqn 12}$$

$$f_{SM} = RH^{VPD} \qquad \text{Eqn 13}$$

Where RH is relative humidity, f_{APAR} is the fraction of absorbed PAR at the canopy, f_{IPAR} is the fraction of intercepted PAR by the canopy, PAR_{in} is incoming PAR with respect to the canopy surface, PAR_{out} is outgoing PAR with respect to the canopy surface, T_{max} is maximum air temperature, and T_{opt} is an optimum air temperature assumed to be 28 °C.

Chapter 3: Assessing the potential for ECOSTRESS and the PT-JPL model to estimate evapotranspiration in Mid-South rice

Authors: Colby W. Reavis[1], Beatriz Moreno-García[1], Kosana Suvočarev[3], Michele L. Reba[2], Benjamin R.K. Runkle[1]

[1] Department of Biological and Agricultural Engineering, University of Arkansas, Fayetteville, AR, USA

[2] USDA ARS Delta Water Management Research Unit, Jonesboro, AR, USA

[3] Department of Land, Air, and Water Resources, University of California–Davis, CA, USA

Author's Note: This work is currently in preparation for journal submission. Additional data will be added for the 2021 growing seasons for our EC datasets. My plan is to submit the document to my respective co-authors for review. Our target journals are either Journal of Hydrology or Water Resources Research.

1. Introduction

Evapotranspiration (ET) is critical component of the irrigation management process in agricultural systems (Anapalli et al., 2019; Farahani et al., 2007). In areas where ET is used to inform management decisions, timely estimates of ET for individual fields are needed (Howell, 2001; Liu et al., 2009; McAneney and Itier, 1996). Additionally, heavily irrigated areas face challenges associated with declining water resources. In the US, Arkansas is the largest producer of rice and faces notable challenges in declining groundwater levels in the eastern portion of the state where rice production is intensive (Reba et al., 2017). To reduce the amount of water consumed by irrigation, multiple strategies provide opportunities to reduce overall water use and improve irrigation efficiency (Massey et al., 2014). Alternate wetting and drying (AWD) is an irrigation strategy that makes use of drying events to capture precipitation, which in turn offsets

required water by as much as 20% along with associated pumping costs (Massey et al., 2017). However, there are also concerns that drying can lead to declines in yield and grain quality due to drought-induced stressed during certain developmental stages (Norton et al., 2017; Graham-Acquaah et al., 2019). In rice production, ET is a valuable term that can inform growers in the irrigation management process while also providing some indication of canopy health via water use (i.e., reduced ratio of T to ET due to stress) during the growing season (Pan et al., 2017). Given the value of ET in the rice production system, there is a need for a method which provides an accessible, well-constrained estimate of ET during the growing season (Shih, 1982). Estimating ET at relevant temporal and spatial scales (i.e., at the field scale near daily or sub-daily timescale) is challenging with the cost of equipment and maintenance to model or directly measure ET across multiple fields (Fisher et al., 2018).

Applications of remote sensing have advantages in their ability to estimate fluxes consistently at a variety of spatial scales over longer periods of time. In applying remote sensing in agricultural settings, an additional challenge is downscaling to the field scale as satellite pixels are typically greater in area than most individual agricultural fields (Wang et al., 2017). Additionally, remote sensing products such as MODIS often rely on statistical and machine learning approaches, which are semi-empirical in nature and lack mechanistic details present in many land-surface processes that incorporate known canopy scale dynamics such as plant response or stomatal regulation (Huang et al., 2018; Mu et al., 2011; Zhao et al., 2005). To overcome this gap, researchers have started to integrate known mechanistic relationships and remote sensing data into advanced process-based models that are able to generate continuous estimates of ET across fine (~1 km^2) spatial resolutions (Baldocchi et al., 2019; Jiang et al., 2020). These models can also be validated using direct measurements of different flux,

112

phenological, and meteorological variables at the surface (Fisher et al., 2008; Velpuri et al., 2013). In addition to validation, ground observations can be used to determine which measurements are key when attempting to derive an estimate of ET from some combination of land surface features (LAI or conductance) and local meteorology.

Methods such as the Priestley-Taylor (PT) can provide accurate estimates of ET with relatively fewer inputs compared to more complex iterations of the Penman-Monteith equation (Monteith, 1981, 1965; Penman, 1948; Priestley, 1959). The Priestley-Taylor provides an estimate of potential ET under assumed conditions (Priestley and Taylor, 1972). The assumptions include a well-wetted surface, where water vapor resistance is assumed to be negligible between the surface and atmosphere, and some amount of dry air mixing where the amount of actual ET can exceed potential evapotranspiration (PET). The required inputs for using the Priestley-Taylor approach include an estimate of available energy, air temperature, and pressure at the scale of observation. In addition to meteorological inputs, the PT method also requires a parameter α_{PT} to account for violations in the assumed PT framework, such as inconsistent wetting of the surface. In the Priestley-Taylor equation, α_{PT} is applied to available energy modified by the slope of the vapor pressure deficit curve to scale from potential to actual ET. The parameter α_{PT} typically assumes a value of 1.26, but studies have also sought to alter the parameter to scale directly from PET to actual ET using different modeling strategies (Flint and Childs, 1991; Sumner and Jacobs, 2005). The parameter α_{PT} is also sensitive to changes in temperature, relative humidity, and soil moisture availability across different landscapes (Ershadi et al., 2014; Stannard, 1993). Remote sensing products like ECOSTRESS apply the PT method to estimate ET at high resolution (70 m x 70 m) spatial scales during the daytime period during

113

the growing season in agricultural settings (Chen et al., 2014; Fisher et al., 2009, 2008; Vinukollu et al., 2011).

In this study, we estimated ET across different periods of crop growth and management during the growing season. The classification of water use utilized staging data collected throughout two growing seasons (2018 & 2020) as well as 10 site-years of data. The selected periods were meant to reflect canopy development as well as floodwater management during the growing season. To validate remote sensing as a viable solution for estimating growing season ET, we first aim to test the ECOSTRESS product in two commercial sized rice fields across five site-years. We compare eddy covariance (EC) observations to ECOSTRESS ET as LE during the growing season. Second, we validate the application of the PT model for estimating growing season LE using field-specific microclimate data. Modeling using local data tested the performance of the framework used in the PT model, which is the same set of equations used in the ECOSTRESS product. We hypothesize that given the consistent inundation periods in the rice growing system, the PT method will perform exceptionally well as actual ET will approach PET. Because ECOSTRESS uses the same PT method for estimating ET, we expect the model to provide accurate estimates of LE throughout the growing season.

2. Methods

2.1 Site Information

The study site was composed of two adjacent commercial fields (~24 ha each) in eastern Arkansas, USA (34° 35' 8.6" N, 91° 45' 05" W). Rice has been grown in continuous rotation since 2004 and are zero–graded. For this study, the fields are identified as North Field (NF) and South Field (SF). The soil within the fields is primarily characterized as poorly drained Perry silty clay (USDA classification: very-fine, smectitic, thermic Chromic Epiaquerts), which

represents 100% of NF and 93.2% of SF (Runkle et al., 2019). The remaining portion of SF soil (~2 ha) is a Herbert silt loam (fine-silty, mixed, superactive, mesic Udollic Epiaqualfs). The irrigation treatments for each field were altered year to year in an experimental setup designed to assess the impacts of alternate wetting and drying (AWD) irrigation on methane emissions and ET during the growing season when compared to the traditional delayed flood (DF) irrigation.

Since 2015, instrumentation has been deployed during the growing season at both NF and SF. During the growing season, the instruments are typically deployed the following day after planting and removed no earlier than three days prior to harvest. When the stations are deployed, instrumentation in each field was located on the northern edge of each field at approximately half the distance of the field edge and approximately 20 m into the field interior. Each field was outfitted with an EC system, including a 3D sonic anemometer (CSAT3, Campbell Scientific, Inc., Logan, UT, USA) and an open–path infrared CO_2/H_2O analyzer (LI–7500A, LI–COR, Inc., Lincoln, NE, USA) measuring dominant southern winds during the growing season at 20 Hz. Fluxes from the sites were gap filled using artificial neural networks as used in similar other applications of EC (Knox et al., 2016, 2015).

For this study, we used different portions of our EC dataset to match product availability. When comparing to models and remote sensing products, we discarded data from the 2019 growing seasons in NF and SF and the 2021 growing season in NF due to equipment issues that resulted in poor estimates of ET that could not be gap-filled. Additionally, because the ECOSTRESS product was only recently launched in June 2018, we further limited our model comparisons to only include the 2018-2021 growing seasons. For determining seasonal dynamics of ET during the growing season using development and irrigation management, we used data from the 2015-2020 growing seasons minus the data that was discarded due to equipment issues.

The 2021 growing season data was used in the seasonal analysis as cumulative ET could not be quantified across both NF and SF.

We delineated the growth stage information across each site year based on staging data collected during the 2018 and 2020 growing seasons. The staging data was collected and recorded using staging guides developed for rice in AR (Counce et al., 2000; Moldenhauer et al., 2013). We define the following ranges of time for the individual growth phases: Vegetative (10 to 60 DAP), Reproductive-Panicle Initiation (70 to 80 DAP), Reproductive (80 to 100 DAP), Grain filling and Maturation (110 to 145 DAP). In the context of water management, we highlight the start of both the reproductive and grain filling periods as key stages of development where the crop is most vulnerable to stress (Henry et al., 2013; Moldenhauer et al., 2013). We discarded the first 10 days after planting to ensure the canopy had transitioned from emergence to vegetative growth. Staging data was collected approximately 2 to 4 times a month during weekly visits to the field site during the 2018-2020 growing seasons.

The timeline of development was then extrapolated to across other site-years. Segmenting water use during the growing season identified target periods to validate model performance. Additionally, two of the periods being examined represented developmental periods where inundation is commonly recommended to reduce canopy stress. Combined irrigation information collected at the site, we used the following stages to characterize periods of DAP during the growing season: 1) Vegetative, Pre-First flood (VPre), 2) Vegetative, Post- First Flood (VPost), 3) Reproductive-Panicle Initiation (RPI), 4) Reproductive (RPD), 5) Grain filling and Maturation, Pre-drain (GMPre), and 6) Grain filling and Maturation, Post-drainage (GMPost). Of these six periods, we identified the RPI and GMPre period as periods where inundation should be

prioritized to ensure the canopy develops properly without lowering yield or grain quality (Henry et al., 2013; Moldenhauer et al., 2013).

Measured energy terms included 4-component net radiation at 2 m (CNR4, Kipp & Zonen, Inc., Delft, NL), photosynthetically active radiation at 1.85 m (LI–190SB, LI–COR, Inc., Lincoln, NE, USA), and ground heat flux using plates (HFP01, Hukseflux, Delft, NL) placed at different 5 cm below the soil surface. Additional meteorological and phenological measurements included leaf area index (LAI), canopy height, air temperature (T), relative humidity (RH), barometric pressure, water depth (WD), volumetric water content (VWC), wind speed (u_z), and wind direction as described in Reavis et al., 2021 and Runkle et al., 2019.

2.2 Priestly-Taylor Model overview

The Priestley Taylor (PT) equation estimates PET that is primarily driven by available energy with a single modeling parameter α_{PT} (Equations 1-3):

$$PET_{PT} = \alpha_{PT} \frac{\Delta}{\Delta+\gamma}(RN - G) \qquad \text{(Equation 1)}$$

$$\Delta = \frac{4096*0.6108 \; exp \left(\frac{17.27*T}{T+237.3}\right)}{(T+237.3)^2} \qquad \text{(Equation 2)}$$

$$\gamma = \frac{c_p*P}{\epsilon*\lambda} \qquad \text{(Equation 3)}$$

Where G is soil heat flux (W m^{-2}), RN is net radiation (W m^{-2}), Δ is the slope of the vapor pressure deficit curve (kPa °C^{-1}), γ is the psychrometric constant (kPa °C^{-1}), P is atmospheric pressure (kPa), T is air temperature (°C), c_p is the specific heat (MJ kg^{-1} °C^{-1}), ϵ is the molecular weight ratio of water vapor to dry air (0.622), λ is the latent heat of vaporization (2.45 MJ kg^{-1}) and α_{PT} is the Priestley-Taylor coefficient (commonly given as 1.26). The generalized form of the PT equation present in the ECOSTRESS application (PT-JPL) estimates actual ET from PET

using scalar functions acting on individual contributing terms of ET. In this approach, actual ET

is estimated as the sum of canopy ET (ET_c), soil ET (ET_s), and intercepted moisture ET (ET_i)

such that:

$$ET_{PT-JPL} = ET_c + ET_s + ET_i \qquad \text{(Equation 4)}$$

$$ET_c = (1 - f_{wet})f_g f_T f_M \alpha_{PT} \frac{\Delta}{\Delta+\gamma} RN_c \qquad \text{(Equation 5)}$$

$$ET_s = (f_{wet} + f_{SM}(1 - f_{wet}))\alpha_{PT} \frac{\Delta}{\Delta+\gamma} (RN_s - G) \qquad \text{(Equation 6)}$$

$$ET_i = f_{wet}\alpha_{PT} \frac{\Delta}{\Delta+\gamma} RN_c \qquad \text{(Equation 7)}$$

$$LAI_{JPL} = (-\ln(1 - fIPAR) / 0.5) \qquad \text{(Equation 8)}$$

$$RN_s = RN * e^{-0.6*LAI_{JPL}} \qquad \text{(Equation 9)}$$

$$RN_c = RN - RN_s \qquad \text{(Equation 10)}$$

Where f_{wet} is relative surface wetness, f_g is green canopy fraction, f_T is a limiter based on plant

temperature, f_M is a limiter based on plant moisture, f_{IPAR} is fraction of intercepted PAR, and

f_{SM} is a limiter based on soil moisture. All individual scalars are unitless and range in value

between 0 and 1. The terms RN_c and RN_s represent net radiation present at the canopy and soil,

respectively, in Wm^{-2}. The individual scaling functions are derived from multiple studies and are

based on common meteorological measurements supported by most weather stations and Earth

observation datasets (Fisher et al., 2008):

$$f_{wet} = RH^4 \qquad \text{(Equation 11)}$$

$$f_g = \frac{f_{APAR}}{f_{IPAR}} \qquad \text{(Equation 12)}$$

$$f_T = \exp\left(-\left(\frac{T_{max} - T_{opt}}{T_{opt}}\right)^2\right) \quad \text{(Equation 13)}$$

$$T_{opt} = T_{max}\left(\max\left(RN * T_{max} * \frac{SAVI}{VPD}\right)\right) \quad \text{(Equation 14)}$$

$$f_M = \frac{f_{APAR}}{f_{APAR,max}} \quad \text{(Equation 15)}$$

$$f_{SM} = RH^{VPD} \quad \text{(Equation 16)}$$

Where RH is relative humidity, f_{APAR} is absorbed photosynthetically active radiation (PAR), T_{max} is maximum air temperature in °C, T_{opt} is the optimum temperature for growth in °C, SAVI is the soil adjusted vegetation index, and VPD is vapor pressure deficit in kPa.

The current modeling framework does not rely on any parameterization as each of the given scaling functions can be calculated using data measured in the field or using remote sensing. While ECOSTRESS utilizes remotely sensed information to drive the PT-JPL model, field observations of microclimate conditions were leveraged to improve model performance. In the scope of this study, we used direct measurements of incoming and outgoing SW radiation, incoming and outgoing PAR, T, RH, G, and LAI with the scaling functions (Equations 8 – 16) to estimate partitioned ET for both NF and SF. Because the sites do not have ground-based estimate of NDVI to distinguish fIPAR from fAPAR, we only utilized periods where vegetation was dense (LAI>1) under the assumption that fIPAR would equal fAPAR under such conditions. Additionally, we assumed that mean G was effectively zero over a 24-hr period (Oliver et al., 1987). The field specific PT-JPL ET estimates were then compared to ECOSTRESS and EC ET across both fields.

2.4 ECOSTRESS data collection and organization

ECOSTRESS data were collected using the Application for Extracting and Exploring Analysis Ready Samples (AρρEEARS) API provided by the USGS (AppEEARS Team, 2021; Hook and Fisher, 2019). The pixel for observation was selected based on the dominant wind direction and estimated footprint of the tower during the growing season. The selected pixels were a subset of the 70 m ECOSTRESS datasets provided through AppEEARS. The product outputs were filtered for cloud cover and uncertainty in land surface temperature estimates prior to being delivered as a quality-controlled Level 3 product. Level 3 denotes the product application level where the output is estimated using a combination of ECOSTRESS land surface temperature at Level 2 and other remote sensing products (Fisher and ECOSTRESS algorithm development team, 2015). For our study, we sampled pixels in our fields beginning at the launch of ECOSTRESS in June 2018 to the end of the most recent growing season, August 2021.

The ECOSTRESS product delivers ET estimates as latent energy flux (LE). The ECOSTRESS product uses the same framework presented in equations 4 through 16, but the model is driven by remotely collected data. The product provides an estimated instantaneous LE taken at different hours of the day as well as a daily estimate of ET, which provided two points of comparison to the EC data collected at both NF and SF. For comparing instantaneous rates between ECOSTRESS and EC, we assume the instantaneous rate of LE to be representative of the entire half-hour in which the measurement was taken. For comparing daily measurements between ECOSTRESS and EC, we calculated the daily mean LE for each field using gap-filled EC datasets. When calculating the mean values of LE using EC data, we only took the mean of the daytime ($SW_{in} > 30$ Wm^{-2}) values to be consistent with the mean provided by ECOSTRESS.

2.5 Comparison framework for observations and models

To test the performance of the ECOSTRESS product, we compared instantaneous and daily LE provided by ECOSTRESS to daily mean LE estimated during the daytime period in NF and SF. We used regression slope (m), percent bias (PBIAS), coefficient of determination (R^2), root-mean-square error (RMSE), and Nash-Sutcliffe efficiency coefficient (NSE) to evaluate how well ECOSTRESS estimated LE at both the daily and instantaneous time steps compared to our EC observations. For evaluating model performance, we characterized "good" model performance with NSE and R^2 greater than 0.6, which is in line with other studies examining performance of remote sensing products estimating ET as LE (Parajuli et al., 2018; Herman et al., 2018). In addition to estimating LE, we also examined factors of change that resulted in better or worse model performance including seasonal development and ECOSTRESS time of measurement.

To test the performance of the PT-JPL model, we used the same statistics as the ECOSTESS performance evaluation (m, PBIAS, R^2, RMSE, and NSE). The performance of the PT-JPL model with respect to canopy development was also tested. The evaluation with respect to canopy development was done by comparing differences in modeled and measured LE over the course of the growing season to LAI. Additionally, we tested the potential of using field measured LAI instead of modeled LAI to see if model performance was improved.

3. Results

3.1 Growing season ET observations using EC

Seasonal estimates of ET were measured using EC for both NF and SF to be used in the analysis of water use with respect to canopy development and irrigation management (Table 1). Growing season ET ranged between 547 and 792 mm across NF and SF during the selected

121

growing seasons. For the collective of site-years, timing of the first flood ranged between 31 and

45 DAP, and final drainage began between 112 and 120 DAP. The time between the application

of the first flood and final drainage ranged between 69 and 85 days.

Table 1. Field management information for NF and SF during the 2015-2020 growing seasons.
First flooding is presented using dates and days after planting (DAP). Data presented for 2015-
2017 in NF and SF is adapted from Reavis et al., 2021.

Site	Year	Irrigation Treatment	Growing Season Length [days]	Growing Season ET [mm]	Planting Date	First Flood Date (DAP)	Drainage Date (DAP)	Harvest Date
NF	2015	DF	133	551 ± 7.1	8-Apr	14-May (36)	6-Aug (120)	19-Aug
	2016	AWD	143	601 ± 10.5	23-Apr	26-May (33)	17-Aug (116)	13-Sep
	2017	DF	138	628 ± 6.9	10-Apr	17-May (37)	3-Aug (115)	26-Aug
	2018	DF	123	547 ± 2.4	30-Apr	12-Jun (43)	20-Aug (112)	31-Aug
	2020	AWD	139	792 ± 7.1	2-Apr	17-May (45)	27-Jul (116)	17-Aug
SF	2015	AWD	134	598 ± 14.0	8-Apr	15-May (37)	3-Aug (117)	19-Aug
	2016	AWD	143	604 ± 9.7	23-Apr	24-May (31)	17-Aug (116)	13-Sep
	2017	DF	140	579 ± 13.4	9-Apr	18-May (38)	4-Aug (117)	27-Aug
	2018	AWD	122	572 ± 1.8	30-Apr	3-Jun (34)	23-Aug (115)	30-Aug
	2020	AWD	139	550 ± 4.1	2-Apr	17-May (45)	30-Jul (119)	19-Aug

For each growing season, ET was calculated for desired growth periods in both NF and

SF (Table 2). The general pattern of water use in the canopy was a steady increase during the

vegetative period marked by the first 21-35 DAP, peak water use during the vegetative and

reproductive period between 35 and 110 DAP, and a decrease in water use during the grain

filling and maturation periods until harvest. For the vegetative (VPre and VPost) and Grain-

filling and Maturation (GMPre and GMPost) stages, the length of time varied with the timing of

the first flood establishment and drainage, respectively. The Reproductive periods (RPI and

RPD) were fixed in duration as periods of 10 and 30 days, respectively. Across all site-years, the

greatest amount of ET occurred during the vegetative periods (VPre, VPost), which collectively

represent the period of 10 to 70 DAP. The vegetative periods accounted for between 40 % and

60% of the estimated cumulative ET across all periods for each site-year. While the mean ET experienced by the VPost period was greater than the VPre period on average, both the VPre and VPost periods had similar durations across all site years at 31 ± 3 and 27 ± 2 days, respectively. Mean ET across the VPost period was similar across NF and SF at 164.9 ± 6.2 and 171.9 ± 16.6 mm, respectively. Mean ET across the VPre period was more varied year to year across NF and SF at 120.9 ± 17.5 and 90 ± 4.7 mm, respectively.

Table 2. Cumulative ET estimates for unique periods of time defined by canopy development and irrigation management in NF and SF. SE is Standard Error.

Field	Year	Treatment	Estimated ET by period [mm]					
			VPre	VPost	RPI	RPD	GMPre	GMPost
NF	2015	DF	84.5	152.4	54.7	152.9	54.4	48.2
	2016	AWD	90.7	180.5	57.5	151.3	19.7	87.8
	2017	DF	102.1	152.2	58.9	158.4	32.3	66.9
	2018	DF	155.7	157.9	47.4	113.8	6.1	40.8
	2020	AWD	171.6	177.6	74.3	168.9	38.6	121.8
SF	2015	AWD	99.1	155.6	59.0	162.7	40.1	77.5
	2016	AWD	85.0	194.2	57.4	154.0	20.4	84.0
	2017	DF	74.5	156.2	52.1	171.1	34.7	81.8
	2018	AWD	99.4	222.7	50.7	129.0	17.9	27.0
	2020	AWD	89.3	128.3	56.7	138.4	41.8	80.5
		Mean=	105.2	167.8	56.9	150.0	30.6	71.6
		SE=	10.2	8.4	2.3	5.7	4.5	8.6

The reproductive periods accounted for 31 to 39% of cumulative growth period ET during across all site-years. The duration of RPI and RPD periods were 10 and 30 days across all site-years. RPI represented approximately 23 to 31% of the reproductive period ET. The RPI period exhibited similar ET across NF and SF with mean ET across all site-years at 58.5 ± 4.4 and 55.2 ± 1.6 mm, respectively. Differences between fields during the RPD period were also minimal at 149.1 ± 9.3 mm in NF and 151.8 ± 7.7 mm in SF. The grain filling and maturation periods (GMPre and GMPost) portion of ET was between 8 and 20% of the cumulative growth

period ET across all site years. The GMPre period was considerably shorter compared to all the other periods, lasting approximately 1 week across all site years. The timing of the GMPost period was consistent across all site years with a mean duration of 33 ± 1 days.

Across each growth period in site years, mean ET rates indicated that water use was greatest during the VPost and RPI periods, representing approximately 30 to 60 DAP across all site-years (Table 3). This pattern was consistent across both NF and SF.

Table 3. Mean ET rates for individual growth periods estimated from EC observations during the site-years between 2015 and 2020.

Field	Year	Estimated ET rates by period [mm day^{-1}]					
		VPre	VPost	RPI	RPD	GMPre	GMPost
NF	2015	4.4	4.9	5.5	5.1	7.8	1.5
	2016	2.2	10.0	5.7	5.0	3.3	2.6
	2017	3.5	4.9	5.9	5.3	4.6	2.0
	2018	4.7	5.8	4.7	3.8	3.0	1.1
	2020	4.9	7.1	7.4	5.6	6.4	3.6
SF	2015	3.7	4.7	5.9	5.4	5.7	2.3
	2016	1.9	12.1	5.7	5.1	3.4	2.5
	2017	3.9	5.0	5.2	5.7	5.0	2.5
	2018	4.1	6.2	5.1	4.3	3.6	0.8
	2020	2.6	5.1	5.7	4.6	4.6	2.6
Mean=		3.6	6.6	5.7	5.0	4.7	2.1
SE=		0.3	0.8	0.2	0.2	0.5	0.3

Previous work for the 2015-2017 growing seasons indicated that growing season ET rates between NF and SF were similar, including during seasons where the fields were not under the same irrigation regime. The same pattern was observed in the 2018 growing season, where NF was under DF irrigation and SF was under AWD irrigation. Seasonal ET in NF was greater in the 2020 growing season when compared to other site-years. Additionally, cumulative ET was greater in the AWD treatments compared to the single DF treatment in 2018. Maximum LAI for

NF and SF were 8.23 and 4.56 in 2018 and 7.84 and 4.56 in 2020, respectively. When comparing

observed ET rates (i.e., not gap filled), NF consistently exhibited greater ET during the 2020

growing season while ET was similar between fields in 2018 (Figure 1). Given the difference in

ET presented in Figure 1B, further investigation may be required to validate the flux estimates in
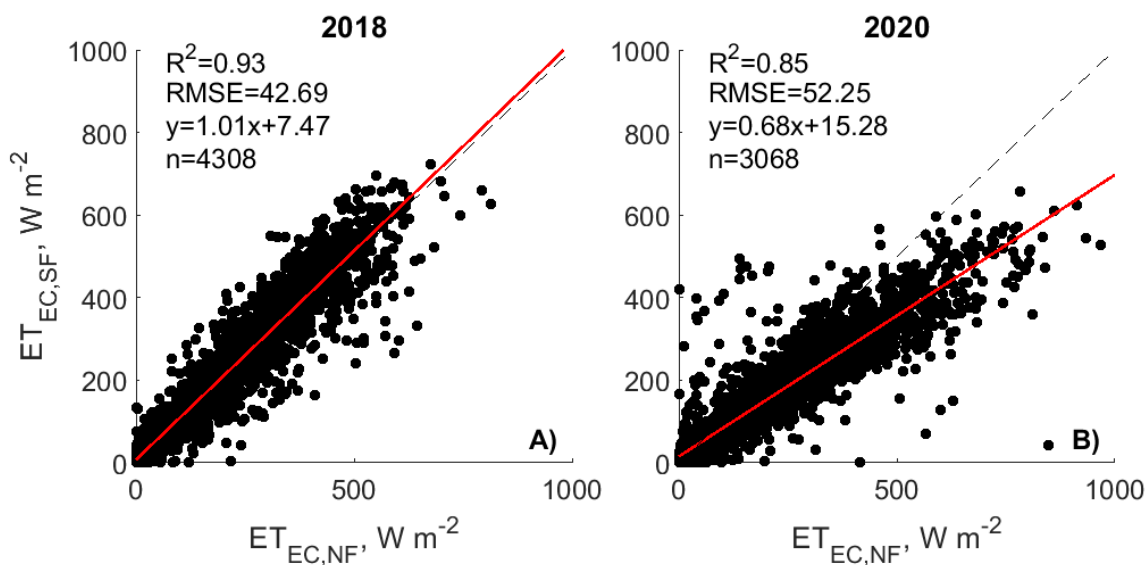
SF and NF during the 2020 growing season.

Figure 1. Comparison of half-hourly ET rates between NF and SF in 2018 (A) and 2020 (B) during the growing season. The line of best fit (red) is compared to the one-to-one line (dashed, gray).

3.2 Comparison of EC observations to ECOSTRESS

Instantaneous LE estimates were collected for both NF (n=13) and SF (n=17) using

ECOSTRESS across 5 site years during the 2018, 2020, and 2021 growing seasons (Figure 2).

For example, the 2020 growing season contained twelve observations of ECOSTRESS LE across

the growing season in both NF and SF. The distribution of points during the growing season was

slightly skewed towards the beginning of the growing season, where the months of May and June

contained 8 of the 12 data points collected for the season. During May and June in 2020, the

collective ECOSTRESS instantaneous measurements covered the diurnal pattern of LE well with

the times of measurement at hours 7.5, 8, 9, 10.5, 13.5, 18, 18.5, 19.5, and 20 on the 24-hr time scale, local time.
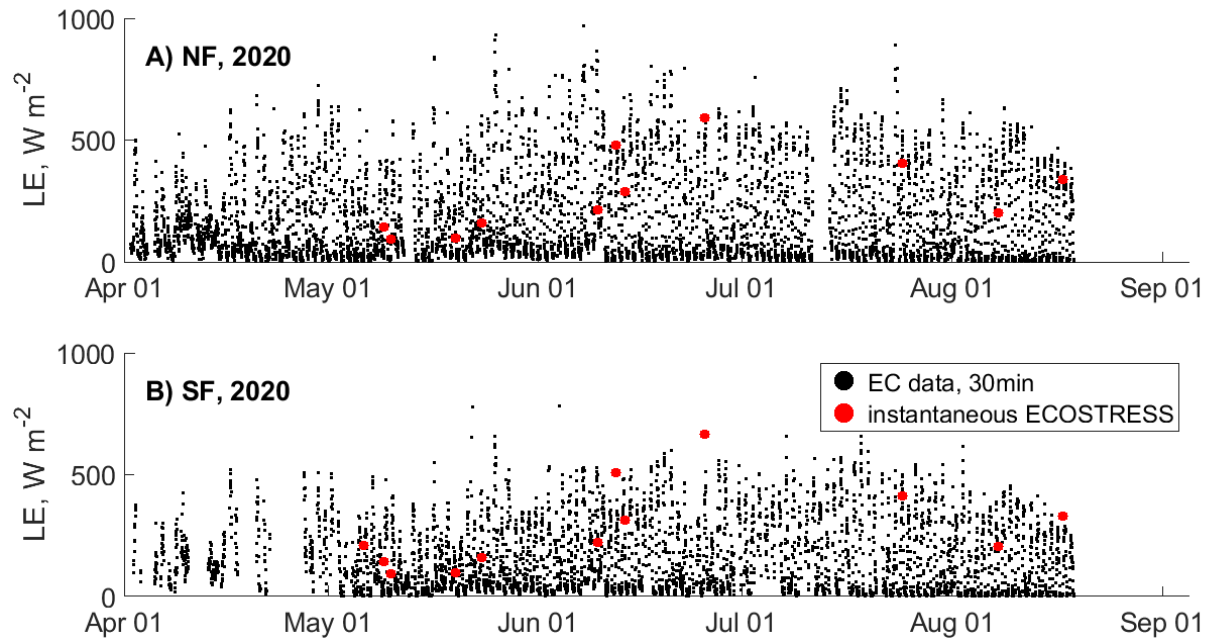
Figure 2. Time series of gap-filled half-hourly EC LE (black) during the 2020 growing season for (A) NF and (B) SF with instantaneous ECOSTRESS LE (red).

ECOSTRESS overestimated LE in both NF and SF during the collective growing seasons (Figure 3). Instantaneous LE measurements for ECOSTRESS were taken between hours 7.5 and 20 local time across both fields. Cumulative LE from ECOSTRESS exceeded EC LE by 34.8% and 48.9%, respectively.
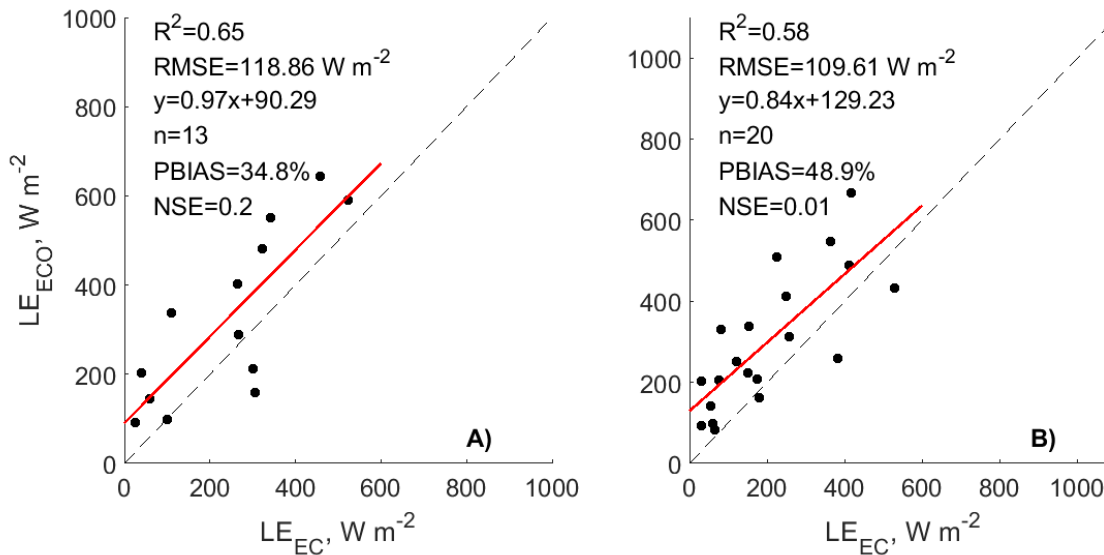
Figure 3. Comparison of instantaneous LE from ECOSTRESS (LE$_{ECO}$) to half-hourly LE from the EC technique (LE$_{EC}$) at (A) NF and (B) SF during the 2018, 2020, and 2021 (SF only) growing seasons. The line of best fit (red) is compared to the one-to-one line (dashed, gray).

Positive NSE values indicated that the modeled instantaneous LE from ECOSTRESS provided a better fit than the mean of LE measured using EC during the growing seasons. However, the NSF was close to 0, which indicated that modeled LE estimated using ECOSTRESS was only slightly better than the mean taken across the observed LE from EC. The bias between ECOSTRESS and EC was greater in SF compared to NF.

There was not a significant relationship with ECOSTRESS instantaneous measurement time and model performance (Figure 4). The difference in ECOSTRESS and EC ET was significantly ($p<0.05$) correlated to DAP, where the ECOSTRESS ET progressively overestimated ET as the growing season progressed.
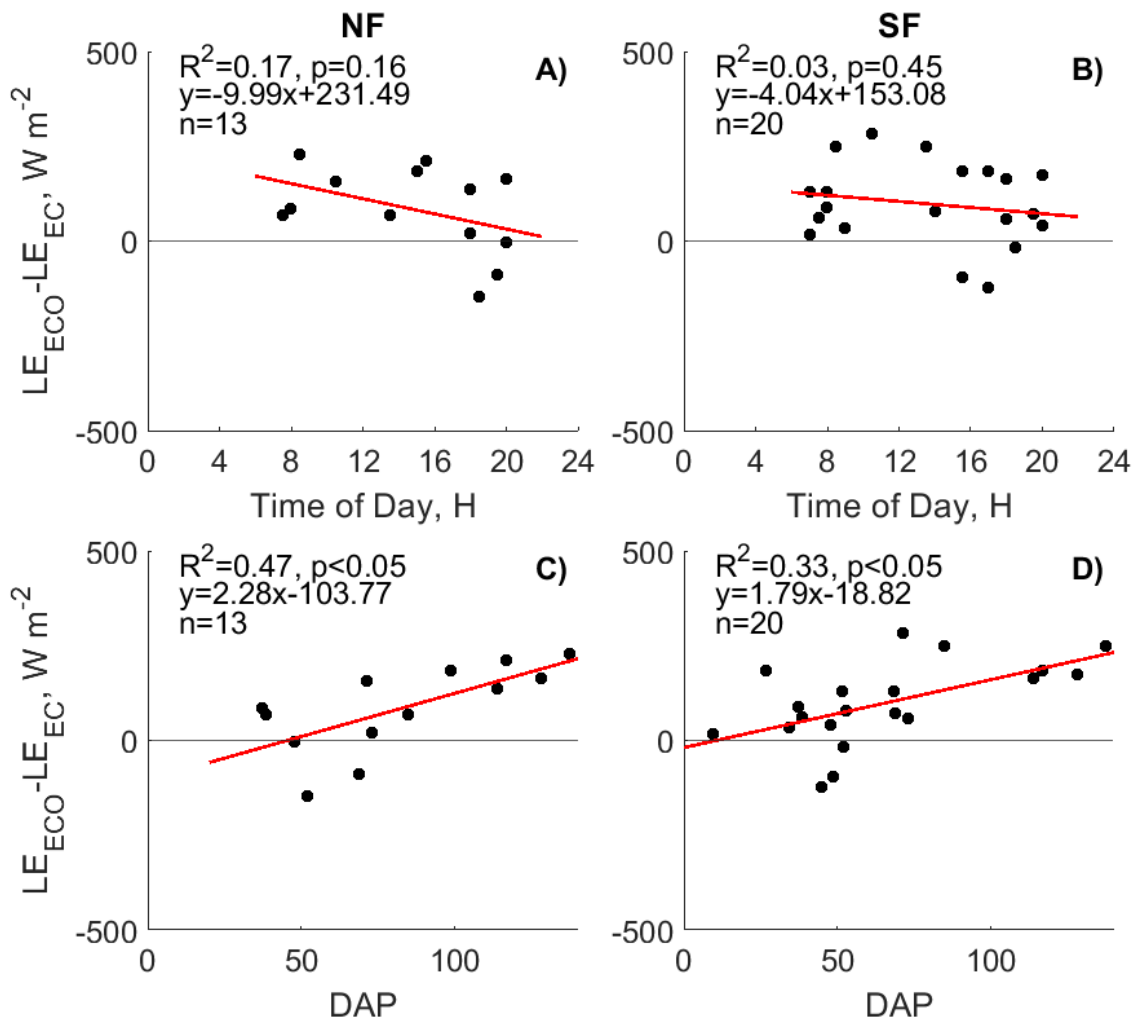
Figure 4. Comparison of ECOSTRESS measurement time of day (A & B) and DAP (C & D) to differences in LE between ECOSTRESS (LE_{ECO}) and EC(LE_{EC}) during the 2018, 2020, and 2021 (SF-only) growing seasons. The black horizontal line denotes y=0. The line of best fit is red.

To better explain the variation of differences in instantaneous LE between ECOSTRESS and EC with respect to growing season progression, we tested the impact of increasing LAI (Figure 5). We found that increasing LAI across both fields was able to explain between 39% and 48% of the variance, and the amount of variance explained was 1 to 6 percentage points greater compared to the comparison between DAP and differences in ECOSTRESS and EC LE (shown in Figure 4 C,D).

128
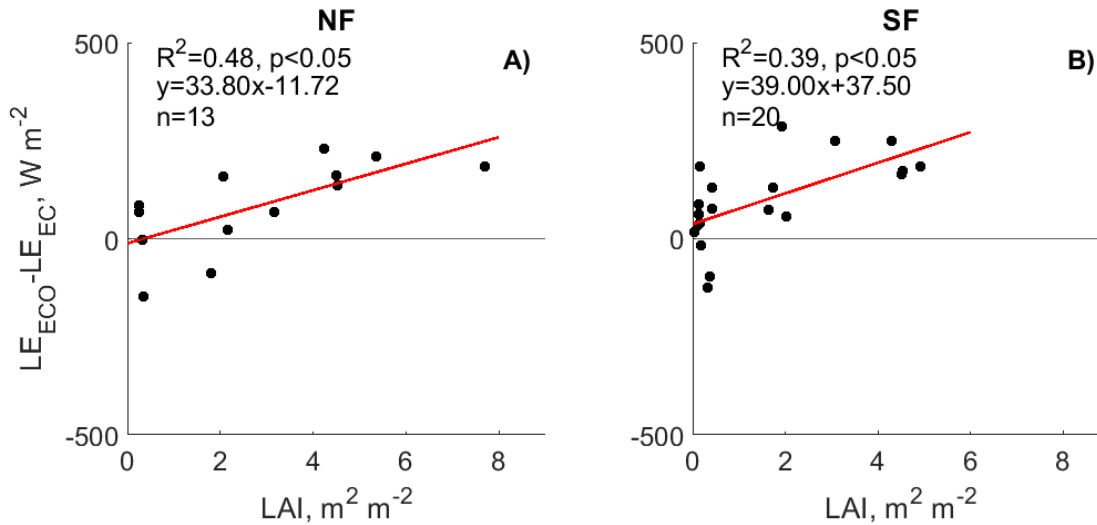
Figure 5. Comparison of the differences in ECOSTRESS (LE_{ECO}) and EC (LE_{EC}) LE to measured LAI in (A) NF and (B) SF during the 2018, 2020, and 2021 (SF-only) growing seasons. The black horizontal line denotes y=0. The line of best fit is red.

When comparing the derived daily daytime LE from ECOSTRESS to mean daily daytime LE from the EC systems, we observed similar levels of overestimation as in the analysis of instantaneous LE (Figure 6). In the comparison of daily LE, the performance in NF was considerably better than SF considering the lower PBIAS and RMSE. Regression slopes were similar across both NF and SF. The NSE in SF indicated that ECOSTRESS did not provide a better approximation of LE with respect to the observed mean of daily LE values measured using EC.
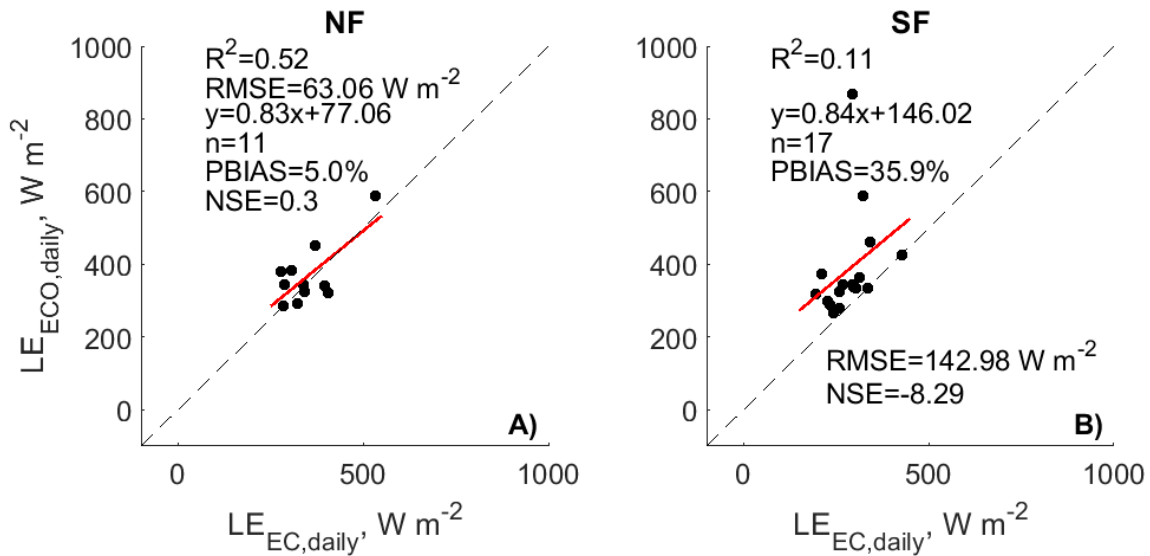
Figure 6. Comparisons of daily derived daytime ECOSTRESS LE ($LE_{ECO,daily}$) to mean daily daytime EC LE ($LE_{EC,daily}$) across (A) NF and (B) SF during the 2018, 2020, and 2021 (SF-only) growing seasons. The line of best fit (red) is compared to the one-to-one line (dashed, gray).

The differences in daily daytime ET were compared to both time of ECOSTRESS measurement and DAP similarly to the analysis of instantaneous rates. Neither DAP nor measurement time were able to provide consistent explanation of differences in ECOSTRESS and EC LE across both NF and SF. In NF, there was no significant ($p>0.05$) relationship between differences in ECOSTRESS ET and EC LE, but DAP was able to explain up to 43% of the variance in differences in ECOSTRESS ET and EC LE (Figure 7). In contrast, neither DAP or time of ECOSTRESS measurement had a significant ($p>0.05$) relationship to differences in ECOSTRESS LE and EC LE in SF.
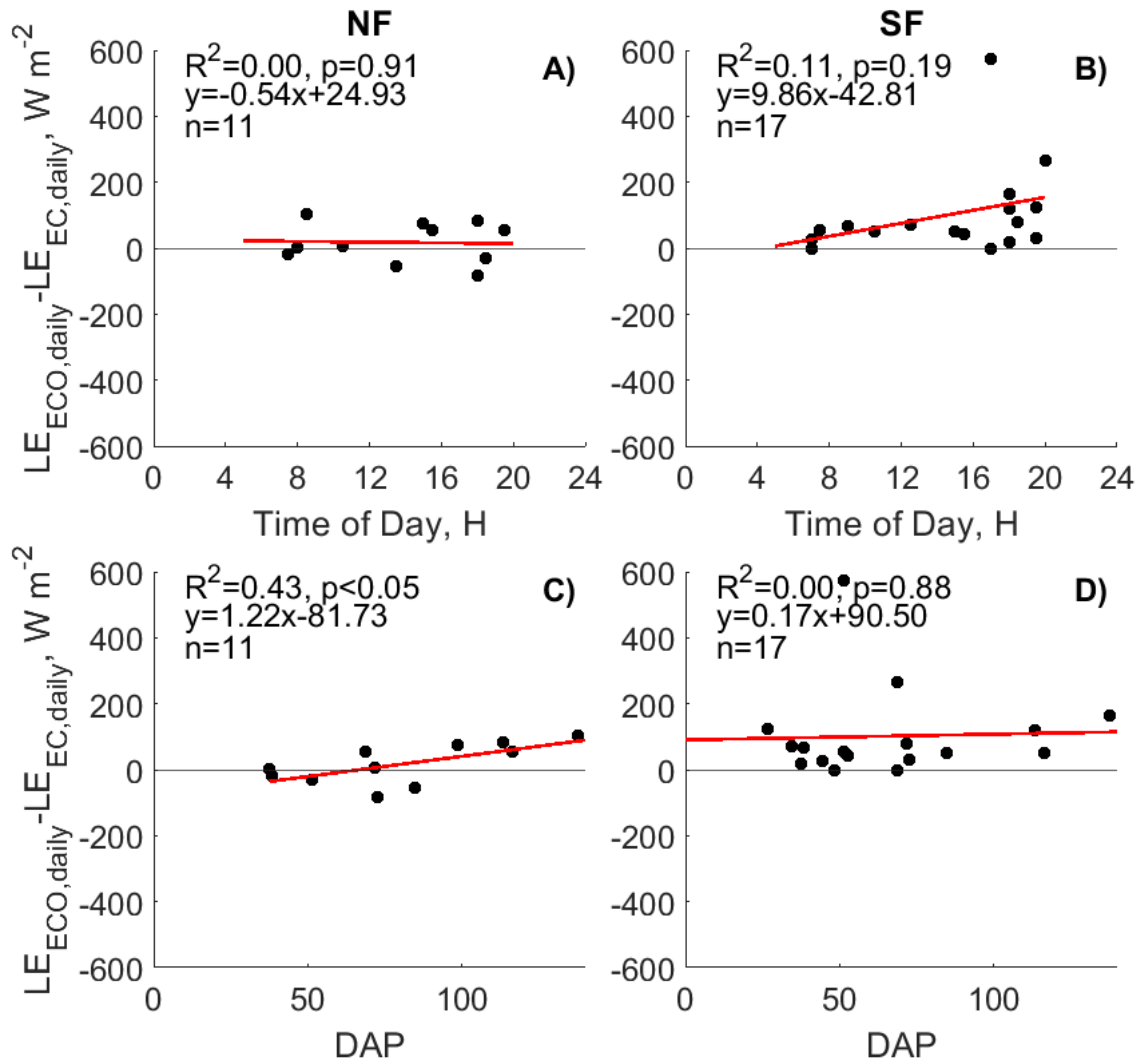
Figure 7. Comparison of the differences in daily LE from ECOSTRESS LE (LE$_{ECO,daily}$) and EC LE (LE$_{EC,daily}$) compared to ECOSTRESS measurement time of day (A & B) and DAP (C & D) during the 2018, 2020, and 2021 (SF-only) growing seasons. The black horizontal line denotes y=0. The line of best fit is red.

At the daily timescale, both DAP and time of measurement were not able to explain

between ECOSTRESS and EC ET to the degree observed in the instantaneous LE rates analysis.

To stay consistent across the instantaneous and daily analyses, we compared differences in

ECOSTRESS and EC LE at the daily timescale to LAI during the 2018 and 2020 growing

seasons (Figure 8). In NF, there was a near significant (p=0.05) relationship between the difference in daily ECOSTRESS and EC LE and increasing LAI. This pattern would corroborate the relationship between the methods' differences with respect to DAP, where ECOSTRESS overestimated LE as the growing season, and LAI, progressed. In NF and SF, ECOSTRESS performed well during the early growing season period (LAI<1), where differences between the methods were generally lower in magnitude. Distribution of ECOSTRESS points along SF was weighted towards periods of low LAI (LAI<1), which could explain the field-to-field differences in the relationship between model performance and canopy development.
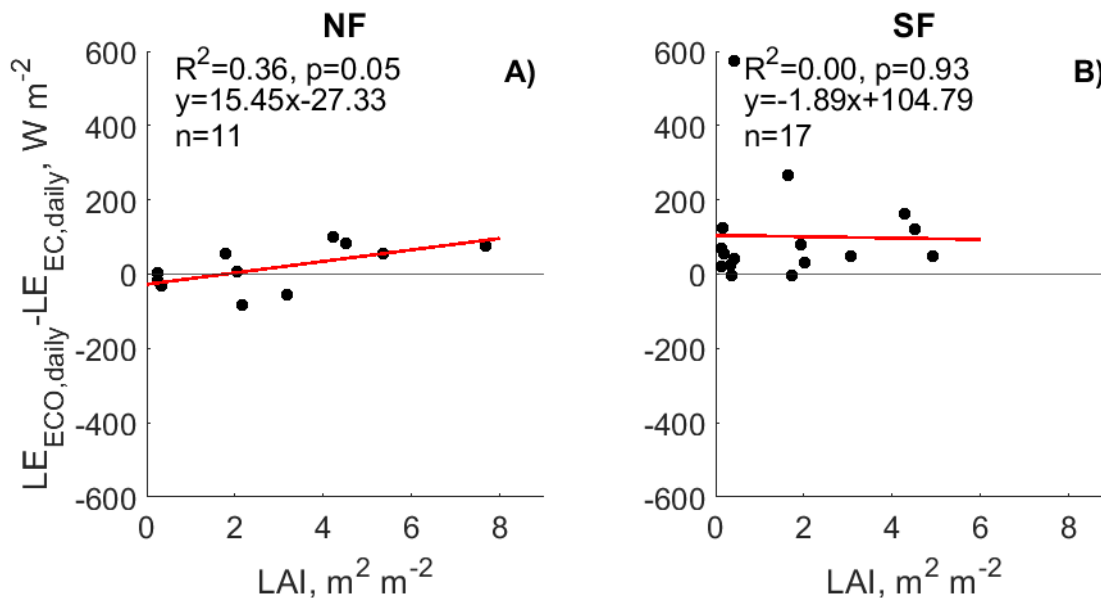
Figure 8. Comparison of the differences in daily daytime ET from ECOSTRESS and EC to LAI across (A) NF and (B) SF during the 2018 and 2020 growing seasons. The black horizontal line denotes y=0.

From our comparisons between ECOSTRESS and EC, we determined that the performance of the ECOSTRESS product was linked to canopy development the instantaneous time scale, where growing season progression resulted in overestimate LE. At the daily time scale, we saw good agreement between ECOSTESS and EC in NF, but the results in SF

indicated that ECOSTRESS was not able to provide a better estimate than the mean value of the EC LE datapoints. We were also unable to verify a performance linkage to canopy development when comparing differences in LE from ECOSTRESS and EC to measured LAI in NF and SF.

3.3 Comparison of PT-JPL to EC observations

The PT-JPL model was used to estimate during the 2018 and 2020 growing seasons under conditions where canopy coverage was considerable (LAI>1). Across both fields, the PT-JPL model underestimated LE across the collective growing seasons (Figure 9).
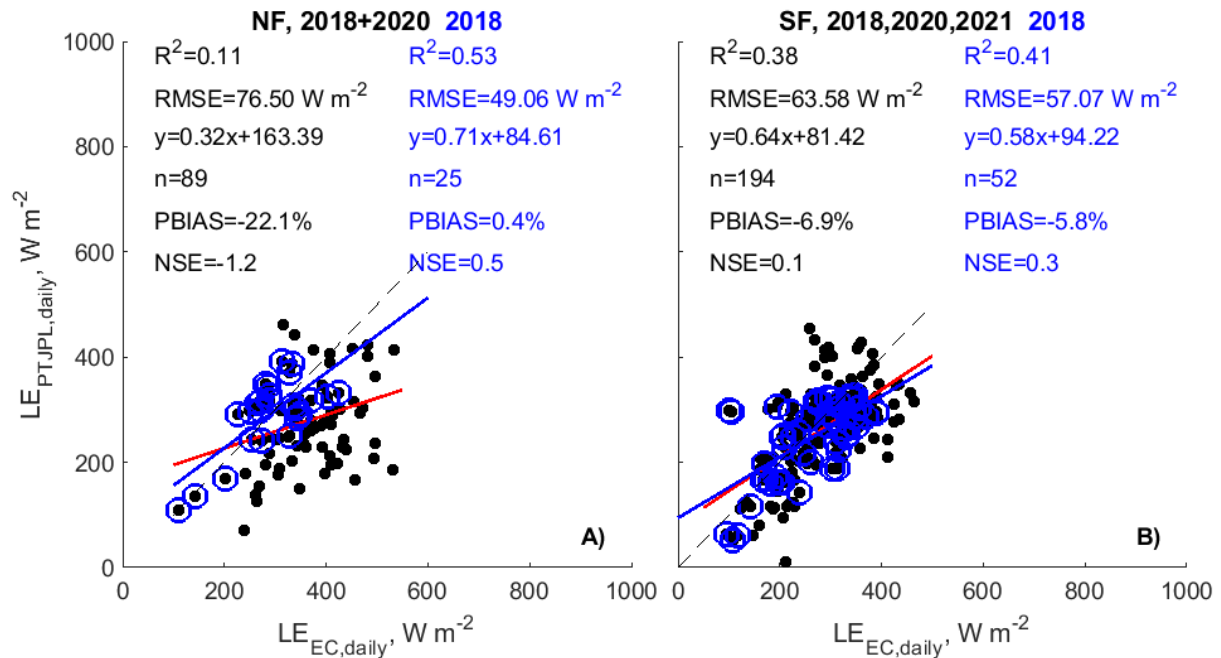
Figure 9. Comparison of mean daily daytime PT-JPL LE to EC LE across (A) NF and (B) SF during all growing seasons (black points) and only during the 2018 growing season (blue circles). For all growing seasons (black), the line of best fit (red) is compared to the one-to-one line (dashed, gray). For the 2018 growing season, datapoints are marked in blue circles and the line of best fit is also blue.

The PT-JPL model's performance was poor in NF, where the NSE indicated that the model was unable to predict LE better than the mean of the EC measurements. Given the

discrepancies observed in ET during the 2020 growing season where NF cumulative LE was

approximately 44% greater than SF, we narrowed the analysis to only include the 2018 growing

season to ensure both fields had similar observed LE during the growing season (shown in

Figure 9 A,B in blue). The comparison indicated that the PT-JPL still underestimated LE despite

both fields having similar EC ET during the 2018 growing season. However, the PBIAS in both

fields decreased, indicating that the model underestimated LE less when the fields had similar

LE. Additionally, the overall variance decreased in modeled estimates and the NSE improved

when using only 2018 measurement of LE. Neither LAI or DAP was able to explain a significant

(p>0.05) portion of the variance in differences between PT-JPL and EC LE across NF and SF

during the 2018 growing season. However, the PT-JPL model did perform similarly across both

fields with relatively small underestimation as compared to the overestimation present in the

ECOSTRESS daily product (Figure 6). When comparing the differences between observed and

modeled LE, we did not observe an impact of DAP or LAI on model performance that was

consistent across both fields. In NF, the relationship between differences in observed and

modeled LE and DAP was significant, but only 5% of the remaining variance. Neither field

indicated a significant relationship between modeled PT-JPL LAI and differences in observed

and modeled LE.

3.4 Incorporation of field measured LAI into PT-JPL

Because the PT-JPL model consistently underestimated LE during the 2018 and 2020

growing seasons, we compared LAI derived from the PT-JPL Equation 8 to direct measurements

of LAI taken during the growing season in both NF and SF. The relationship between both LAI

terms was not significant across both fields, meaning the modeled LAI did not accurately reflect

the changes in LAI present in field observations. Specifically, the minimum modeled LAI during

134

the early growing season (DAP<50) was around 2.8 m^2 m^{-2}, and the method underestimated LAI

by as much as 5.2 m^2 m^{-2} in the same timeframe. Additionally, the method used to model LAI

did not capture peak LAI during the latter portion of each growing season (DAP>80) and

consistently underestimated LAI by as much as 5.8 m^2 m^{-2}. We ran the PT-JPL model with the

field measured LAI during the 2018 growing season to identify potential for improvement.

Improvements to LE estimation using field LAI in the PT-JPL model were more apparent in NF
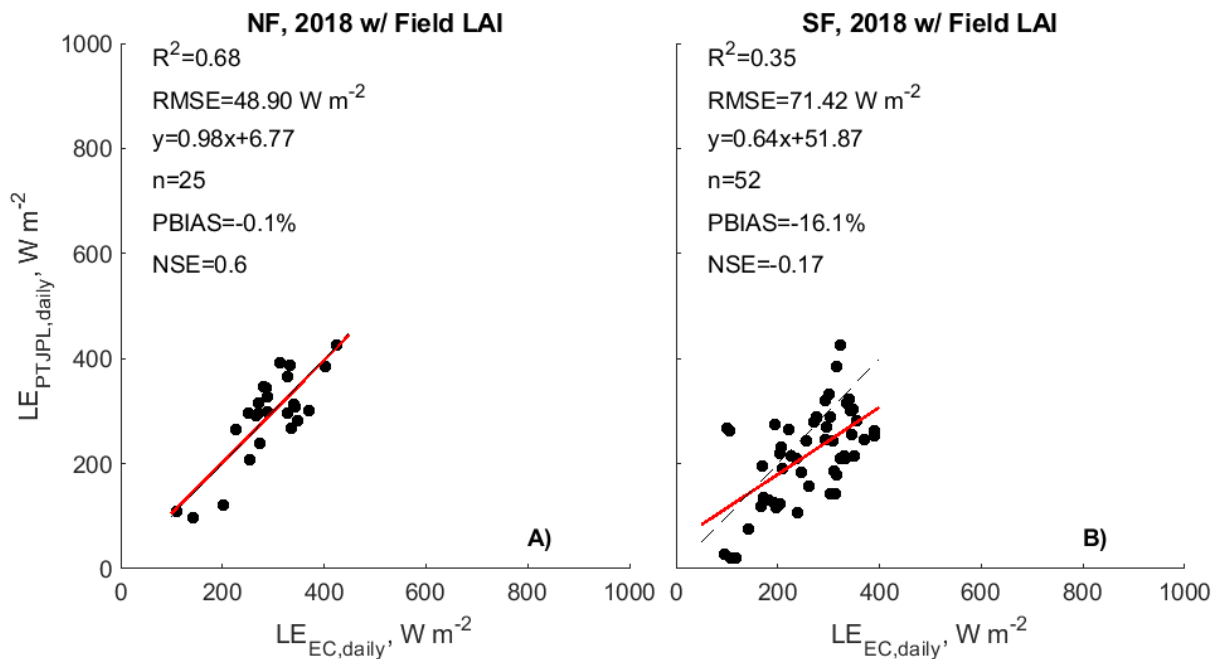
compared to SF (Figure 11).

Figure 11. Comparison of daily modeled PT-JPL LE using field LAI compared to daily EC ET in (A) NF and (B) SF during the 2018 growing season. The line of best fit (red) is compared to the one-to-one line (dashed, gray).

While regression slopes improved when using field LAI compared to modeled LAI, the

bias and error in predicted rates increased in SF. In contrast, NF showed noticeable improvement

as the PT-JPL predicted LE with a slope of 0.98 with low PBIAS and a relatively high NSE

compared to our analysis across both the PT-JPL and ECOSTRESS modeling approaches.

4. Discussion

4.1 Growing Season ET

In this study, ET estimated using EC was compared across ten site-years. Values ranged between 547 and 792 mm across all site-years. Estimated ET was comparable across both irrigation regimes and fields in all growing seasons except for the 2020 growing season, where ET in NF was 44% greater than SF. During the growing season, the VPost and RPI periods had the highest estimated ET rates across all site-years. The vegetative periods, VPre and VPost, occurring between 10 and 70 DAP accounted for between 40% and 60% of cumulative seasonal ET across all site-years. The comparison of mean ET rates across growth periods in all growing seasons indicated that peak ET rates occurred during the VPost and RPI periods, which represented approximately 41 to 78 DAP. Studies focused on crop water use modeling have identified the development and reproductive stages as the highest period of canopy water use during the growing season (Qiu et al., 2019; Zhai et al., 2019; Shah and Edling, 2000). A field study in China examining water use under different irrigation regimes identified a similar pattern to our dataset, where ET was greatest during the vegetative periods marked by middle- and late tillering (Liu et al., 2018). In that study, the calculated ET rates for middle and late tillering ranged from 4.87 to 5.34 mm day^{-1} using EC and 5.58 to 7.29 mm day^{-1} using micro-lysimeters over a 20 to 30 day period during the growing season. The same growth stages have also been identified and incorporated into irrigation schedulers recommended for a number of crops, including rice (Cao et al., 2019; Earl D. Vories and Phil L. Tacker, 2006; Martin et al., 1990). In practical applications of water management, ET used during periods of develop can also define the potential for soil water stress during periods of drying in AWD irrigation (Ishfaq et al., 2020; Xu et al., 2019; Chu et al., 2014). In the context of our study, the mean ET rates given during the

VPost, RPI, and GMPre are all relevant for producers or irrigation managers who may be planning to practice AWD and want to better understand how quickly water is used at different stages of development. Future research could also incorporate estimates of photosynthesis and canopy mediated water use as transpiration to further isolate and evaluate canopy water needs during the season (Riaz et al., 2020).

4.2 Using ECOSTRESS to model ET in rice

In our study, ECOSTRESS was able to estimate LE in NF well. In SF, we observed poor performance in the ECOSTRESS product. At both time scales, the NSE values were either close to zero or negative, indicating the model was not able to predict LE better than the mean value of LE taken across all the observations. In our work, we identified the challenge of ECOSTRESS to estimate instantaneous LE accurately with respect to canopy development, where the product consistently overestimated instantaneous LE with increasing LAI. While the ECOSTRESS product has potential, the studies comparing performance at the field scale are few (Anderson et al., 2021; Fisher et al., 2020). Fisher et al. (2020) provide the best evaluation of ECOSTRESS performance when compared to EC sites globally. The study highlights good agreement between the ECOSTRESS 70-m product with EC observations from a collection of agricultural sites (R^2=0.89) while also demonstrating how performance improves moving 1-km to 70-m resolution. Other studies have described the difficulty in measuring LE as ET in flooded rice, where ET contributions from the open water above the soil surface were not always captured well and especially so under increasing LAI (Teluguntla et al., 2020; Bastiaanssen et al., 2000). As seen in our study, the number of data points available for comparison during the growing season made comparison to different methods difficult. To address the issue of collection frequency, there have also been concentrated efforts to generate ensemble values of LE using a

variety of remote sensing products, including MODIS, Atmosphere-Land Exchange Inverse

model (ALEXI), and disaggregated Atmosphere-Land Exchange Inverse model (disALEXI)

(Stisen et al., 2021; Xue et al., 2021; Zhu et al., 2016). Recent efforts have also included the

development of platforms where estimates across methods are aggregated and readily available

for use by individuals, including growers, irrigation managers, or other interested parties (Melton

et al., 2021).

4.3 Using the PT-JPL model to estimate ET in rice

The PT-JPL model performed well when estimating LE during the 2018 growing season,

when observed LE was similar between both NF and SF. The inclusion of field measured LAI to

the PT-JPL model instead of using modeled LAI improved the PT-JPL model performance in

NF, but the amount of bias and variance increased in SF. With respect to studies modeling LE as

ET, others have applied the PT-JPL model using field measurements across a variety of

landscapes, including croplands, and found good agreement with direct estimates of ET (Ershadi

et al., 2014; García et al., 2013). The clear advantage of the PT-JPL over other complex models

is the relatively small amount of input information required as well as the lack of any site-

specific parameterization. Improvements to the PT-JPL, similar to our incorporation of LAI,

have focused on providing more information in the form of additional scaling variables or new

formulations of the scaling functions to accommodate for unique features of landscapes, such as

aridity or drought sensitivity (Marshall et al., 2020; Mobe et al., 2021). With respect to applying

the PT-JPL in rice, Marshall et al. (2020) found good agreement between the PT-JPL and EC ET

measured in rice grown in California with a different index describing soil moisture state. There

are no applications of the PT-JPL model driven by field observations of microclimate in the state

of Arkansas, where a majority of rice in the US is grown.

5. Conclusions

We observed ET dynamics across periods of the growing season defined by both canopy development and irrigation management. Across ten site-years, cumulative growing season ET ranged between 547 and 792 mm. We determined that ET was greatest during the vegetative periods in terms of both cumulative ET and in estimated daily ET rates. The rates were similar across fields as well as irrigation treatments across all growing seasons except one. Based on our findings, ET rates were greatest after the first flood was applied (VPost) and before grain filling and maturation (GMPre), which aligns with a major portion of biomass accumulation aboveground within the field. Comparisons to ECOSTRESS showed good agreement with EC observations at the instantaneous and daily time scale in NF, but ECOSTRESS performance in SF was worse based on the observed bias and the NSE values. When estimating instantaneous ET, model performance significantly ($p<0.05$) declined as the magnitude of overestimation from ECOSTRESS increased with time and LAI during the growing season. The relationship between model performance and canopy development in the instantaneous LE analysis was not consistent with the daily LE analysis, where no patterns in model performance related to canopy development were observed. While ECOSTRESS LE rates were higher on average compared EC across both fields, the practical implication would mean that irrigation decisions based on the amount of LE recommended by ECOSTRESS would likely not result in a deficit. The PT-JPL provided good estimates of daily LE in the 2018 growing season, where LE was comparable between NF and SF based on EC observations. During the 2018 growing season, cumulative LE was only underestimated by a maximum of 6% when comparing PT-JPL to EC. When incorporating field estimates of LAI, the level of improvement was not consistent across NF and SF during the 2018 growing season. Future work could improve the method in which LAI or

other variables are used in the PT-JPL model to generate accurate estimates of LE without the need for site-specific parameterization.

6. Acknowledgements

Chapter 3 References

Anapalli, S.S., Fisher, D.K., Reddy, K.N., Rajan, N., Pinnamaneni, S.R., 2019. Modeling evapotranspiration for irrigation water management in a humid climate. Agricultural Water Management 225, 105731. https://doi.org/10.1016/j.agwat.2019.105731

Anderson, M.C., Yang, Yang, Xue, J., Knipper, K.R., Yang, Yun, Gao, F., Hain, C.R., Kustas, W.P., Cawse-Nicholson, K., Hulley, G., Fisher, J.B., Alfieri, J.G., Meyers, T.P., Prueger, J., Baldocchi, D.D., Rey-Sanchez, C., 2021. Interoperability of ECOSTRESS and Landsat for mapping evapotranspiration time series at sub-field scales. Remote Sensing of Environment 252, 112189. https://doi.org/10.1016/j.rse.2020.112189

AppEEARS Team, 2021. Application for Extracting and Exploring Analysis Ready Samples (AppEEARS). NASA EOSDIS Land Processes Distributed Active Archive Center (LP DAAC), USGS/Earth Resources Observation and Science (EROS) Center, Sioux Falls, South Dakota, USA.

Baldocchi, D., Dralle, D., Jiang, C., Ryu, Y., 2019. How Much Water Is Evaporated Across California? A Multiyear Assessment Using a Biophysical Model Forced With Satellite Remote Sensing Data. Water Resources Research 55, 2722–2741. https://doi.org/10.1029/2018WR023884

Bastiaanssen, W.G., Molden, D.J., Makin, I.W., 2000. Remote sensing for irrigated agriculture: examples from research and possible applications. Agricultural water management 46, 137–155.

Cao, J., Tan, J., Cui, Y., Luo, Y., 2019. Irrigation scheduling of paddy rice using short-term weather forecast data. Agricultural Water Management 213, 714–723. https://doi.org/10.1016/j.agwat.2018.10.046

Chen, Y., Xia, J., Liang, S., Feng, J., Fisher, J.B., Li, Xin, Li, Xianglan, Liu, S., Ma, Z., Miyata, A., Mu, Q., Sun, L., Tang, J., Wang, K., Wen, J., Xue, Y., Yu, G., Zha, T., Zhang, L., Zhang, Q., Zhao, T., Zhao, L., Yuan, W., 2014. Comparison of satellite-based evapotranspiration models over terrestrial ecosystems in China. Remote Sensing of Environment 140, 279–293. https://doi.org/10.1016/j.rse.2013.08.045

Chu, G., Chen, T., Wang, Z., Yang, J., Zhang, J., 2014. Reprint of "Morphological and physiological traits of roots and their relationships with water productivity in water-saving and drought-resistant rice." Field Crops Research, Crop root system behaviour and yield 165, 36–48. https://doi.org/10.1016/j.fcr.2014.06.026

Counce, P.A., Keisling, T.C., Mitchell, A.J., 2000. A Uniform, Objective, and Adaptive System for Expressing Rice Development. Crop Science 40, 436–443. https://doi.org/10.2135/cropsci2000.402436x

Earl D. Vories, Phil L. Tacker, 2006. Effect of ET Calculation Method on Irrigation Scheduling in Midsouth, in: 2006 Portland, Oregon, July 9-12, 2006. Presented at the 2006 Portland, Oregon, July 9-12, 2006, American Society of Agricultural and Biological Engineers. https://doi.org/10.13031/2013.20753

Ershadi, A., McCabe, M.F., Evans, J.P., Chaney, N.W., Wood, E.F., 2014. Multi-site evaluation of terrestrial evaporation models using FLUXNET data. Agricultural and Forest Meteorology 187, 46–61. https://doi.org/10.1016/j.agrformet.2013.11.008

Fisher, J.B., ECOSTRESS algorithm development team, 2015. ECOsystem Spaceborne Thermal Radiometer Experiment on Space Station (ECOSTRESS): Level-3 evapotranspiration LE (ET_PT-JPL) Algorithm Theoretical Basis Document.

Fisher, J.B., Lee, B., Purdy, A.J., Halverson, G.H., Dohlen, M.B., Cawse-Nicholson, K., Wang, A., Anderson, R.G., Aragon, B., Arain, M.A., Baldocchi, D.D., Baker, J.M., Barral, H., Bernacchi, C.J., Bernhofer, C., Biraud, S.C., Bohrer, G., Brunsell, N., Cappelaere, B., Castro-Contreras, S., Chun, J., Conrad, B.J., Cremonese, E., Demarty, J., Desai, A.R., Ligne, A.D., Foltýnová, L., Goulden, M.L., Griffis, T.J., Grünwald, T., Johnson, M.S., Kang, M., Kelbe, D., Kowalska, N., Lim, J.-H., Maïnassara, I., McCabe, M.F., Missik, J.E.C., Mohanty, B.P., Moore, C.E., Morillas, L., Morrison, R., Munger, J.W., Posse, G., Richardson, A.D., Russell, E.S., Ryu, Y., Sanchez-Azofeifa, A., Schmidt, M., Schwartz, E., Sharp, I., Šigut, L., Tang, Y., Hulley, G., Anderson, M., Hain, C., French, A., Wood, E., Hook, S., 2020. ECOSTRESS: NASA's Next Generation Mission to Measure Evapotranspiration From the International Space Station. Water Resources Research 56, e2019WR026058. https://doi.org/10.1029/2019WR026058

Fisher, J.B., Malhi, Y., Bonal, D., Rocha, H.R.D., Araújo, A.C.D., Gamo, M., Goulden, M.L., Hirano, T., Huete, A.R., Kondo, H., Kumagai, T., Loescher, H.W., Miller, S., Nobre, A.D., Nouvellon, Y., Oberbauer, S.F., Panuthai, S., Roupsard, O., Saleska, S., Tanaka, K., Tanaka, N., Tu, K.P., Randow, C.V., 2009. The land–atmosphere water flux in the tropics. Global Change Biology 15, 2694–2714. https://doi.org/10.1111/j.1365-2486.2008.01813.x

Fisher, J.B., Melton, F., Middleton, E., Hain, C., Anderson, M., Allen, R., McCabe, M.F., Hook, S., Baldocchi, D., Townsend, P.A., Kilic, A., Tu, K., Miralles, D.D., Perret, J., Lagouarde, J.-P., Waliser, D., Purdy, A.J., French, A., Schimel, D., Famiglietti, J.S., Stephens, G., Wood, E.F., 2018. The future of evapotranspiration: Global requirements for ecosystem functioning, carbon and climate feedbacks, agricultural management, and water resources. Reviews of Geophysics 2618–2626. https://doi.org/10.1002/2016WR020175@10.1002/(ISSN)1944-9208.COMHES1

Fisher, J.B., Tu, K.P., Baldocchi, D.D., 2008. Global estimates of the land–atmosphere water flux based on monthly AVHRR and ISLSCP-II data, validated at 16 FLUXNET sites. Remote Sensing of Environment 112, 901–919. https://doi.org/10.1016/j.rse.2007.06.025

Flint, A.L., Childs, S.W., 1991. Use of the Priestley-Taylor evaporation equation for soil water limited conditions in a small forest clearcut. Agricultural and Forest Meteorology 56, 247–260. https://doi.org/10.1016/0168-1923(91)90094-7

García, M., Sandholt, I., Ceccato, P., Ridler, M., Mougin, E., Kergoat, L., Morillas, L., Timouk, F., Fensholt, R., Domingo, F., 2013. Actual evapotranspiration in drylands derived from in-situ and satellite data: Assessing biophysical constraints. Remote Sensing of Environment 131, 103–118. https://doi.org/10.1016/j.rse.2012.12.016

Graham-Acquaah, S., Siebenmorgen, T.J., Reba, M.L., Massey, J.H., Mauromoustakos, A., Adviento-Borbe, A., January, R., Burgos, R., Baltz-Gray, J., 2019. Impact of alternative irrigation practices on rice quality. Cereal Chemistry 96, 815–823. https://doi.org/10.1002/cche.10182

H. J., Farahani, T. A. Howell, W. J. Shuttleworth, W. C. Bausch, 2007. Evapotranspiration: Progress in Measurement and Modeling in Agriculture. Transactions of the ASABE 50, 1627–1638. https://doi.org/10.13031/2013.23965

Henry, C.G., Daniels, M., Hamilton, M., Hardke, J.T., 2013. Water Management, in: Arkansas Rice Production Handbook. University of Arkansas Extension Service, pp. 103–128.

Herman, M.R., Nejadhashemi, A.P., Abouali, M., Hernandez-Suarez, J.S., Daneshvar, F., Zhang, Z., Anderson, M.C., Sadeghi, A.M., Hain, C.R., Sharifi, A., 2018. Evaluating the role of evapotranspiration remote sensing data in improving hydrological modeling predictability. Journal of Hydrology 556, 39–49. https://doi.org/10.1016/j.jhydrol.2017.11.009

Hook, S., Fisher, J., 2019. ECOSTRESS Evapotranspiration PT-JPL Daily L3 Global 70 m V001 [Data set]. NASA EOSDIS Land Processes DAAC.

Howell, T.A., 2001. Enhancing water use efficiency in irrigated agriculture. Agronomy journal 93, 281–289.

Huang, Y., Ryu, Y., Jiang, C., Kimm, H., Kim, S., Kang, M., Shim, K., 2018. BESS-Rice: A remote sensing derived and biophysical process-based rice productivity simulation model. Agricultural and Forest Meteorology 256–257, 253–269. https://doi.org/10.1016/j.agrformet.2018.03.014

Ishfaq, M., Farooq, M., Zulfiqar, U., Hussain, S., Akbar, N., Nawaz, A., Anjum, S.A., 2020. Alternate wetting and drying: A water-saving and ecofriendly rice production system. Agricultural Water Management 241, 106363. https://doi.org/10.1016/j.agwat.2020.106363

Jiang, C., Guan, K., Pan, M., Ryu, Y., Peng, B., Wang, S., 2020. BESS-STAIR: a framework to estimate daily, 30m, and all-weather crop evapotranspiration using multi-source satellite data for the US Corn Belt. Hydrology and Earth System Sciences 24, 1251–1273. https://doi.org/10.5194/hess-24-1251-2020

Knox, S.H., Matthes, J.H., Sturtevant, C., Oikawa, P.Y., Verfaillie, J., Baldocchi, D., 2016. Biophysical controls on interannual variability in ecosystem-scale CO_2 and CH_4 exchange in a California rice paddy. Journal of Geophysical Research: Biogeosciences 121, 978–1001. https://doi.org/10.1002/2015JG003247

Knox, S.H., Sturtevant, C., Matthes, J.H., Koteen, L., Verfaillie, J., Baldocchi, D., 2015. Agricultural peatland restoration: effects of land-use change on greenhouse gas (CO_2 and CH_4) fluxes in the Sacramento-San Joaquin Delta. Global Change Biology 21, 750–765. https://doi.org/10.1111/gcb.12745

Liu, J., Zehnder, A.J.B., Yang, H., 2009. Global consumptive water use for crop production: The importance of green water and virtual water. Water Resources Research 45. https://doi.org/10.1029/2007WR006051

Liu, X., Xu, J., Yang, S., Zhang, J., 2018. Rice evapotranspiration at the field and canopy scales under water-saving irrigation. Meteorol Atmos Phys 130, 227–240. https://doi.org/10.1007/s00703-017-0507-z

Marshall, M., Tu, K., Andreo, V., 2020. On Parameterizing Soil Evaporation in a Direct Remote Sensing Model of ET: PT-JPL. Water Resources Research 56, e2019WR026290. https://doi.org/10.1029/2019WR026290

Martin, D.L., Stegman, E.C., Fereres, E., 1990. Irrigation scheduling principles. IN: Management of Farm Irrigation Systems. American Society of Agricultural Engineers, St. Joseph, MI. 1990. p 155-203, 19 fig, 9 tab, 81 ref.

Massey, J.H., Mark Stiles, C., Epting, J.W., Shane Powers, R., Kelly, D.B., Bowling, T.H., Leighton Janes, C., Pennington, D.A., 2017. Long-term measurements of agronomic crop irrigation made in the Mississippi delta portion of the lower Mississippi River Valley. Irrig Sci 35, 297–313. https://doi.org/10.1007/s00271-017-0543-y

Massey, J.H., Walker, T.W., Anders, M.M., Smith, M.C., Avila, L.A., 2014. Farmer adaptation of intermittent flooding using multiple-inlet rice irrigation in Mississippi. Agricultural Water Management 146, 297–304. https://doi.org/10.1016/j.agwat.2014.08.023

McAneney, K.J., Itier, B., 1996. Operational limits to the Priestley-Taylor formula. Irrigation Science 17, 37–43. https://doi.org/10.1007/s002710050020

Melton, F.S., Huntington, J., Grimm, R., Herring, J., Hall, M., Rollison, D., Erickson, T., Allen, R., Anderson, M., Fisher, J.B., 2021. OpenET: Filling a critical data gap in water management for the western united states. JAWRA Journal of the American Water Resources Association.

Mobe, N.T., Dzikiti, S., Dube, T., Mazvimavi, D., Ntshidi, Z., 2021. Modelling water utilization patterns in apple orchards with varying canopy sizes and different growth stages in semi-arid environments. Scientia Horticulturae 283, 110051. https://doi.org/10.1016/j.scienta.2021.110051

Moldenhauer, K., Counce, P., Hardke, J., 2013. Rice Growth and Development, in: Arkansas Rice Production Handbook. University of Arkansas Extension Service, pp. 9–20.

Monteith, J.L., 1981. Evaporation and surface temperature. Quarterly Journal of the Royal Meteorological Society 107, 1–27. https://doi.org/10.1002/qj.49710745102

Monteith, J.L., 1965. Evaporation and environment. Symposia of the Society for Experimental Biology 19, 205–234.

Mu, Q., Zhao, M., Running, S.W., 2011. Improvements to a MODIS global terrestrial evapotranspiration algorithm. Remote Sensing of Environment 115, 1781–1800. https://doi.org/10.1016/j.rse.2011.02.019

Norton, G.J., Shafaei, M., Travis, A.J., Deacon, C.M., Danku, J., Pond, D., Cochrane, N., Lockhart, K., Salt, D., Zhang, H., Dodd, I.C., Hossain, M., Islam, M.R., Price, A.H., 2017. Impact of alternate wetting and drying on rice physiology, grain production, and grain quality. Field Crops Research 205, 1–13. https://doi.org/10.1016/j.fcr.2017.01.016

Oliver, S.A., Oliver, H.R., Wallace, J.S., Roberts, A.M., 1987. Soil heat flux and temperature variation with vegetation, soil type and climate. Agricultural and Forest Meteorology 39, 257–269. https://doi.org/10.1016/0168-1923(87)90042-6

Pan, J., Liu, Y., Zhong, X., Lampayan, R.M., Singleton, G.R., Huang, N., Liang, K., Peng, B., Tian, K., 2017. Grain yield, water productivity and nitrogen use efficiency of rice under different water management and fertilizer-N inputs in South China. Agricultural Water Management 184, 191–200. https://doi.org/10.1016/j.agwat.2017.01.013

Parajuli, P.B., Jayakody, P., Ouyang, Y., 2018. Evaluation of Using Remote Sensing Evapotranspiration Data in SWAT. Water Resources Management 32, 985–996. https://doi.org/10.1007/s11269-017-1850-z

Penman, H.L., 1948. Natural evaporation from open water, bare soil and grass. Proceedings of the Royal Society of London. Series A. Mathematical and Physical Sciences 193, 120–145.

Priestley, C.H.B., 1959. Turbulent transfer in the lower atmosphere.

Priestley, C.H.B., Taylor, R.J., 1972. On the Assessment of Surface Heat Flux and Evaporation Using Large-Scale Parameters. Mon. Wea. Rev. 100, 81–92. https://doi.org/10.1175/1520-0493(1972)100<0081:OTAOSH>2.3.CO;2

Qiu, R., Liu, C., Cui, N., Wu, Y., Wang, Z., Li, G., 2019. Evapotranspiration estimation using a modified Priestley-Taylor model in a rice-wheat rotation system. Agricultural Water Management 224, 105755. https://doi.org/10.1016/j.agwat.2019.105755

Reba, M.L., Massey, J.H., Adviento-Borbe, M.A., Leslie, D., Yaeger, M.A., Anders, M., Farris, J., 2017. Aquifer Depletion in the Lower Mississippi River Basin: Challenges and Solutions. Journal of Contemporary Water Research & Education 162, 128–139. https://doi.org/10.1111/j.1936-704X.2017.03264.x

Riaz, F., Riaz, M., Arif, M.S., Yasmeen, T., Ashraf, M.A., Adil, M., Ali, S., Mahmood, R., Rizwan, M., Hussain, Q., 2020. Alternative and non-conventional soil and crop management strategies for increasing water use efficiency, in: Environment, Climate, Plant and Vegetation Growth. Springer, pp. 323–338.

Runkle, B.R.K., Suvočarev, K., Reba, M.L., Reavis, C.W., Smith, S.F., Chiu, Y.-L., Fong, B., 2019. Methane Emission Reductions from the Alternate Wetting and Drying of Rice Fields Detected Using the Eddy Covariance Method. Environ. Sci. Technol. 53, 671–681. https://doi.org/10.1021/acs.est.8b05535

Shah, S.B., Edling, R.J., 2000. Daily Evapotranspiration Prediction from Louisiana Flooded Rice Field. Journal of Irrigation and Drainage Engineering 126, 8–13. https://doi.org/10.1061/(ASCE)0733-9437(2000)126:1(8)

Shih, S., Rahi, G., Harrison, D., 1982. Evapotranspiration studies on rice in relation to water use efficiency. Transactions of the ASAE 25, 702–0707.

Stannard, D.I., 1993. Comparison of Penman-Monteith, Shuttleworth-Wallace, and Modified Priestley-Taylor Evapotranspiration Models for wildland vegetation in semiarid rangeland. Water Resources Research 29, 1379–1392. https://doi.org/10.1029/93WR00333

Stisen, S., Soltani, M., Mendiguren, G., Langkilde, H., Garcia, M., Koch, J., 2021. Spatial Patterns in Actual Evapotranspiration Climatologies for Europe. Remote Sensing 13, 2410. https://doi.org/10.3390/rs13122410

Sumner, D.M., Jacobs, J.M., 2005. Utility of Penman–Monteith, Priestley–Taylor, reference evapotranspiration, and pan evaporation methods to estimate pasture evapotranspiration. Journal of Hydrology 308, 81–104. https://doi.org/10.1016/j.jhydrol.2004.10.023

Teluguntla, P., Ryu, D., George, B., Walker, J.P., 2020. Impact of flooded rice paddy on remotely sensed evapotranspiration in the Krishna River basin, India. Hydrological Processes 34, 2190–2199. https://doi.org/10.1002/hyp.13748

Velpuri, N.M., Senay, G.B., Singh, R.K., Bohms, S., Verdin, J.P., 2013. A comprehensive evaluation of two MODIS evapotranspiration products over the conterminous United States: Using point and gridded FLUXNET and water balance ET. Remote Sensing of Environment 139, 35–49. https://doi.org/10.1016/j.rse.2013.07.013

Vinukollu, R.K., Wood, E.F., Ferguson, C.R., Fisher, J.B., 2011. Global estimates of evapotranspiration for climate studies using multi-sensor remote sensing data: Evaluation of three process-based approaches. Remote Sensing of Environment 115, 801–823. https://doi.org/10.1016/j.rse.2010.11.006

Wang, Y., Zhou, L., Jia, Q., Yu, W., 2017. Water use efficiency of a rice paddy field in Liaohe Delta, Northeast China. Agricultural Water Management 187, 222–231. https://doi.org/10.1016/j.agwat.2017.03.029

Xu, J., Bai, W., Li, Y., Wang, H., Yang, S., Wei, Z., 2019. Modeling rice development and field water balance using AquaCrop model under drying-wetting cycle condition in eastern China. Agricultural Water Management 213, 289–297. https://doi.org/10.1016/j.agwat.2018.10.028

Xue, J., Anderson, M.C., Gao, F., Hain, C., Yang, Yun, Knipper, K.R., Kustas, W.P., Yang, Yang, 2021. Mapping Daily Evapotranspiration at Field Scale Using the Harmonized Landsat and Sentinel-2 Dataset, with Sharpened VIIRS as a Sentinel-2 Thermal Proxy. Remote Sensing 13, 3420. https://doi.org/10.3390/rs13173420

Zhai, B., Fu, Q., Li, T., Liu, D., Ji, Y., Li, M., Cui, S., 2019. Rice Irrigation Schedule Optimization Based on the AquaCrop Model: Study of the Longtouqiao Irrigation District. Water 11, 1799. https://doi.org/10.3390/w11091799

Zhao, M., Heinsch, F.A., Nemani, R.R., Running, S.W., 2005. Improvements of the MODIS terrestrial gross and net primary production global data set. Remote Sensing of Environment 95, 164–176. https://doi.org/10.1016/j.rse.2004.12.011

Zhu, G., Li, X., Zhang, K., Ding, Z., Han, T., Ma, J., Huang, C., He, J., Ma, T., 2016. Multi-model ensemble prediction of terrestrial evapotranspiration across north China using Bayesian model averaging. Hydrological Processes 30, 2861–2879.

Chapter 3 Appendix:

Data Inventory by analysis:

Site-years used in growing season water use analysis:

- 2015 NF & SF
- 2016 NF & SF
- 2017 NF & SF
- 2018 NF & SF
- 2020 NF & SF

Site years used in EC vs. ECOSTRESS instantaneous and daily:

- 2018 NF & SF
- 2020 NF & SF
- 2021 SF

Site years used in EC vs. PT-JPL:

- 2018 NF & SF
- 2020 NF & SF
- 2021 SF

Comparison of ECOSTRESS pixels across different areas of the field:

Different pixel locations were sampled across both NF and SF during the growing seasons to test the variability present across the field and across different subsets (Figure A 1). The same sampling scheme was utilized across both NF and SF. Sampling locations were at the EC tower (ECT), the center of the field (C), east end of the field center (CE), west end of the field center (CW), mid-point between C and CE (MCE), and mid-point between C and CW (MCW).
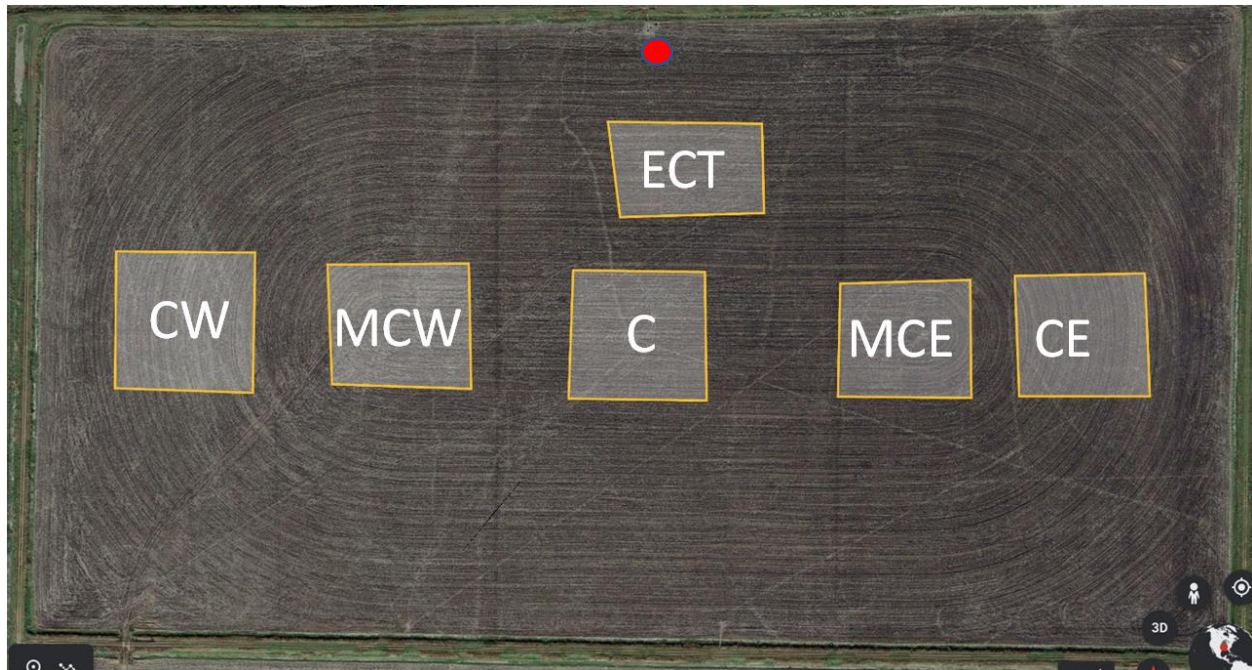
Figure A 1. Sampling scheme for ECOSTRESS used across both fields. The red circle marks the approximate location of the EC tower in both fields. The field shown is SF.

Differences in ET measured across each pixel were minimal. During the 2020 growing season in SF as an example, all points across all pixels were on or near the 1:1 line (m>0.95, R^2>0.95), indicating that sampling different portions of the field did not result in varying estimates of LE (Figure A 2).
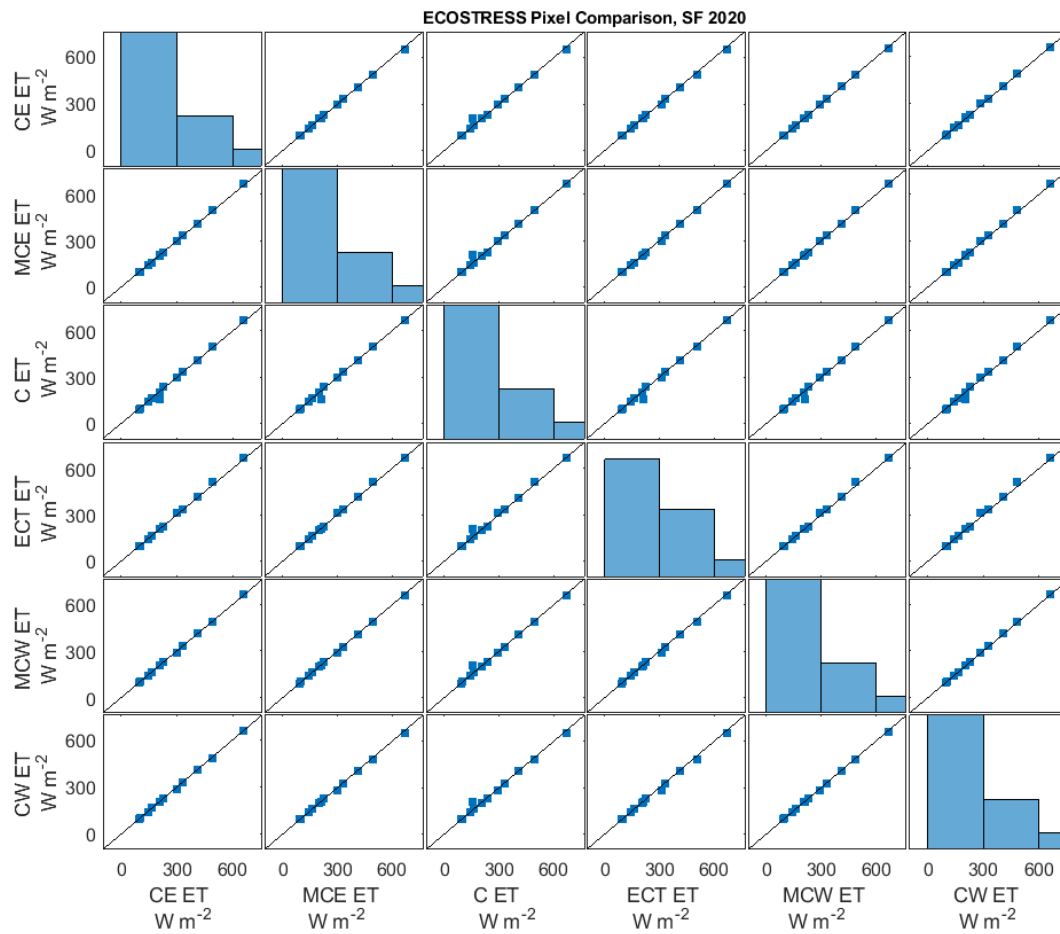
Figure A 2. Comparison of ECOSTRESS ET across selected subsets in SF during from 2020 (n=12). Solid black line is 1:1. Histograms show distribution of flux magnitudes for each pixel.

Conclusions

In our first work, we provided seasonal estimates of ET and identified no impacts of drying on ET. During the 2015-2017 growing seasons, estimated ET ranged from 551 to 628 mm during the growing season. Normalizing seasonal ET by growing season length, the mean ET rate ranged between 4.13 mm day^{-1} and 4.55 mm day^{-1}. During drying events, we observed no decreases in ET in the AWD treatment when compared to ET in a DF treated field during the same period of time. We observed a convergence of ET rates between the fields across all three growing seasons, where ET rates between fields became increasingly similar with increasing canopy development. The PMAET model estimated ET accurately during the growing season when incorporating the "big leaf" modeling approach with LAI as a scaling term. The FAO56 single crop coefficient consistently overestimated ET, but performance was acceptable when looking at periods in the mid-to-late growing season when irrigation decision making is more critical. Ultimately, we concluded that site specific crop coefficients are necessary to estimate ET accurately using the FAO56 single crop coefficient. Based on our findings, we determined that the level of AWD practiced in our study was "safe" and provides support for the adoption of AWD as a water saving technique in commercial rice production.

Using data collected in the 2015-2017 growing season, we applied an ET partitioning method to estimate T using local measurements of GPP, ET, and VPD. Estimated T, ET, and GPP were used to determine how water use changed during the growing season with respect to both drying and canopy development. Across the 2015-2017 growing seasons, transpiration accounted for 43 to 56% of ET. We found strong relationships between T:ET and LAI during the growing season, where daily LAI explained at least 73% of the variability in T:ET during the growing season. We saw similar patterns of increasing eWUE and uWUE with increasing LAI,

but mean value of tWUE did not fluctuate throughout the growing season. In a comparison of partitioning methods, we saw some similarity in estimated T:ET when looking at the mean relationship between both ET and T when data was available across all methods. However, the estimated ET and resulting T during the periods indicated greater uncertainty in both terms across methods. When observing canopy water use during the growing season, we observed a disconnect between peak GPP and a lagging peak LAI, where the individual peaks marked distinctly different developmental periods in the canopy lifecycle. The disconnect between peak LAI and GPP was further observed in the modeling portion of our paper. The uWUE and PT-JPL methods expressed differences in T:ET dynamics during the growing season because of their utilization of GPP and LAI, respectively. From our work, we concluded that the uWUE method for partitioning ET was able to generate reasonable estimates of T throughout the growing season. Using those estimates of T, we further analyzed the drying periods of AWD treatment and saw no signs of stress in GPP, ET, or T across NF and SF. The lack of stress observed in any of the terms related to water use indicates that the level of AWD presented in this study can be considered "safe". As canopy water use is not affected, we can further recommend the AWD practice as a possible solution for water conservation in commercial rice production.

Finally, we provided a survey of ET throughout the growing season using growth periods as periods of time defined by developmental stages of the canopy and irrigation management. Across 10 site-years, cumulative growing season ET ranged between 547 and 792 mm in NF and SF. Our results indicated that the vegetative period between 10 and 70 DAP accounted for between 40 and 60% of the total ET across all the defined growth periods. When translated to effective rates of ET using cumulative ET and duration within each period, the vegetative period following the first flood (VPost) and the early reproductive period marked by panicle initiation

(RPI) were the most active periods of water use across each site-year. We compared EC estimates across 5 site-years to the ECOSTRESS remote sensing platform, where we found good agreement at both the instantaneous and daily timescales. Our results indicated that ECOSTRESS overestimated ET at the daily timescale, and degree of underestimation ranged between 4 and 35% compared to daily ET estimated using EC. We also observed a significant relationship between model performance and canopy development, where ECOSTRESS increasingly overestimated ET with increasing LAI during the growing season in both NF and SF. To test the fundamental framework of the ECOSTRESS product, we adapted the PT-JPL model to provide estimates of daily ET using local measurements of microclimate and phenology. While the PT-JPL model consistently underestimated ET on average, the degree of underestimation was only a maximum of 6% when compared to EC ET estimates across both fields. Assessing the potential of the PT-JPL included running the model using field observations of LAI rather than modeled estimates, where we saw some improvement in NF, but increased bias and uncertainty in SF. Based on our findings, we concluded that both ECOSTRESS and the PT-JPL model have potential as methods to estimate ET in rice.

College of Engineering
Department of Biological and Agricultural Engineering

Chapter 1, "Impacts of alternate wetting and drying and delayed flood rice irrigation on growing season evapotranspiration" of Colby Reavis's dissertation was published in the Journal of Hydrology in 2021 with co-authors, Kosana Suvočarev, Michele L. Reba, and Benjamin R.K. Runkle.

I, Dr. Benjamin R.K. Runkle, advisor of Colby Reavis, confirm Colby Reavis is the first author and completed at least 51% of the work for this manuscript.

Benjamin Runkle
Associate Professor
University of Arkansas
Department of Biological and Agricultural Engineering

Date